
Editorial Office of *Earth's Cryosphere (Kriosfera Zemli)*
Institute of Geography, Russian Academy of Sciences
37 Vavilov str., office 22, Moscow, 117312, Russia
Editorial staff: *N.V. Arutyunyan*, *N.G. Belova, O.V. Levochkina, O.M. Lisitsyna, G.E. Oblogov*
Phone: 8(985) 957-10-01, e-mail: kriozem@gmail.com

Journal promoted by
Russian Academy of Sciences, Siberian Branch, Novosibirsk
Earth's Cryosphere Institute, Tyumen Scientific Centre SB RAS, Tyumen
Melnikov Permafrost Institute, SB RAS, Yakutsk

Editorial Manager *M.A. Trashkeeva*
Designed by *N.F. Suranova*
Typeset by *N.M. Raizvikh*

English text by *M.A. Korkka, V.A. Krutikova, V.V. Kuzovkin*

RUSSIAN ACADEMY OF SCIENCES
SIBERIAN BRANCH
EARTH'S CRYOSPHERE INSTITUTE, TYUMEN SCIENTIFIC CENTRE

EARTH'S CRYOSPHERE
SCIENTIFIC JOURNAL

Founded in January 1997	6 issues per year	Vol. XXV, No. 3	May–June 2021

CONTENTS

CRYOLITHOGENESIS

Gavrilov A.V., Pizhankova E.I. Natural environment dynamics and morpholithogenesis in shallows of the East Siberian Arctic shelf 3

GEOLOGICAL CRYOGENIC PROCESSES AND FORMATIONS

Nesterova N.V., Makarieva O.M., Fedorov A.N., Shikhov A.N. Geocryological factors of dynamics of the thermokarst lake area in Central Yakutia 19

GASES AND GAS HYDRATES IN THE EARTH'S CRYOSPHERE

Duchkov A.D., Semenov V.P., Sokolova L.S., Sivtsev A.I. Zone of stability of methane hydrates in the area of the Srednevilyuisk gas-condensate field (Vilyui syneclise) 30

SNOW COVER AND GLACIERS

Kitaev L.M. Conjugation of changes in air temperature, snow cover thickness and soil temperature of East European Plain 37

Prokhorova U.V., Terekhov A.V., Ivanov B.V., Verkulich S.R. Calculation of the heat balance components of the Aldegonda glacier (Western Spitsbergen) during the ablation period according to the observations of 2019 43

CHRONICLE

Kizyakov A.I., Streletskaya I.D., Khomutov A.V. Marina Oskarovna Leibman (*on the 70th anniversary*) 52

EARTH'S CRYOSPHERE
SCIENTIFIC JOURNAL

Kriosfera Zemli, 2021, vol. XXV, No. 3, pp. 3–18

CRYOLITHOGENESIS

NATURAL ENVIRONMENT DYNAMICS AND MORPHOLITHOGENESIS IN SHALLOWS OF THE EAST SIBERIAN ARCTIC SHELF

A.V. Gavrilov, E.I. Pizhankova

Lomonosov Moscow State University, Faculty of Geology,
Leninskie Gory, 1, Moscow, 119991, Russia; gavrilov37@bk.ru, epijankova@mail.ru

The shallows of the Laptev and East Siberian seas formed on the site of islands composed of the sediments of the Late Pleistocene Ice Complex which eroded in the 17th–20th centuries and are linked to positive morphostructures. The present article considers factors of modern sedimentation in marine shallows with the formation of islands (Yaya, Nanosny, Zatoplyaemyy, Leykina, etc.). Among these factors are a decrease in sea ice extent, an increase in the duration of the ice-free period, and the activation of destructive cryogenic processes triggered by the current climate warming. A decrease in ice coverage led to the dominance of hydrodynamic processes in sedimentation, unlike the primary role of sea ice in this process in the 17th–19th centuries. Sediment deficit in these centuries is substituted by its excess owing to the activation of cryogenic processes at the turn of the 20th and 21st centuries. As a result, the erosional shoreface profile is transforming into an accumulative one. Sedimentation is occurring parallel to a rising sea level related to a warming climate. A rise in the surface of islands and sandbanks is recorded on satellite images where there are modern positive vertical movements. The formation of islands and sandbanks is accompanied by their syngenetic freezing.

Key words: *morpholithogenesis, sedimentation, morphostructures, modern climate warming, remote sensing data, marine shallows.*

INTRODUCTION

The main direction of the development of the Laptev and East Siberian sea shelf (Fig. 1) during the Holocene is the destruction of a thick (up to 60 m) Late Neopleistocene Ice Complex (IC) sediments by destructive cryogenic processes (lake thermokarst, thermal abrasion and thermal denudation) [*Romanovskii et al., 1999; Are, 2012*]. The inability to resist heat influence is explained by the structure and composition of the IC, which includes thick syngenetic ice wedges, and its high summative volumetric ice content (70–95 %). The lake thermokarst began to develop in the negative morphostructures of the shelf of the East Siberian sector of Russia, which was drained at the time, at the end of the Late Neopleistocene (14–13 ka) [*Romanovskii et al., 1999*]. It has led to their initial flooding during the Late Neopleistocene–Holocene marine transgression. Having been land for a long time the elevations of positive morphostructures composed of the IC, were destroyed by thermal abrasion and thermal denudation, turning into peninsulas and later into IC remnant islands.

Historical data begins to trace the process of destruction of these islands from the 17th–18th centuries. The book "Noord en Oost Tartarye" by the Dutchman N. Witsen, published in 1692 and 1705, discusses an abundance of shallows on the way north from the "Ice Cape" (Cape Buor-Khaya) to an island located "opposite the mouth of the Lena River at the time" [*The history..., 1954*]. Supposedly, this was one of the islands-remnants of IC [*Gavrilov et al., 2003*]. The draft of koches (Russian Pomor sailors' vessels used in the 15th–17th centuries) was 1.0–1.5 m [https://ru.wikipedia.org/wiki/Коч]. In the second half of the 20th century there were no such depths left in these places because the sea was becoming deeper. The average rate of deepening which was determined based on the time of the disappearance of Diomede Island (between 1761 and 1811), which had existed in the Dmitry Laptev Strait, and the depth within the bank at the site of this island in 1934 (7.4 m) [*The history..., 1954*] is approximately 5 cm/year. Thus, over the course of many thousands and hundreds of years of geological and historical data, respectively, the IC islands, and later shallows and banks which remained in their place, were eroding.

In September 2013 it was discovered from a helicopter that the top of Vasil'evskaya Bank is drained in the Laptev Sea on Semyonovskaya Shallow, within which Late Pleistocene IC islands existed. The formation of the island on Vasil'evskaya Bank was confirmed by a hydrographic expedition in September 2014. Its surface area at the time was approximately 0.038 km^2, elevation above sea level was less than 1 m. The island was named Yaya [https://ru.wikipedia.org/wiki/Яя_(остров)] (Fig. 2).

Fig. 1. Research area:

1 – islands which had disappeared in the 18th–20th centuries; *2* – sandy banks; *3* – shelf edge; *4* – isobaths.

Uplands (both terrestrial and underwater) are usually an object of denudation. The formation of an island within a very short (by geological standards) period of time is an extraordinary occurrence. In addition to Yaya, islands composed of contemporary and Holocene sediments formed at the location of the Late Pleistocene IC remnants, presently and earlier.

Fig. 2. Yaya Island, which had appeared at the location of Vasil'evskaya Bank, discovered in 2013.

Breakers around the island indicate the highest parts of the shallow. P.S. Sayapin's photo.

The scientific community's interest in this phenomenon and the relevance of understanding its reasons became the driving factor in the development of ideas explaining a change in the morpholithogenetic regime and the formation of islands at the turn of the 20th and 21st centuries. The results of a study of the present phenomenon are provided below.

MATERIALS AND METHODS

The geological structure of the studied islands was not researched by drilling methods, so the main research materials were Landsat, Sentinel, and Terra/MODIS satellite images (SI) from 1973–2020, as well as a series of geological materials. The latter include maps at scales of 1:1,000,000 of the third [*State... Map..., 2014, 2016, 2017; Burguto et al., 2016*] and second generations, tectonic and neotectonic maps, seismoacoustic data of Semyonovskaya Shallow profiling by VNIIOkeangeologia [*Rekant et al., 2009*] and Pacific Oceanological Institute (POI) FEB RAS monitoring. Topographic maps at scales of 1:200,000 and various published historical data related to the given problem were also used. The synthesis and combining of temporally different remote data, the identification of new formations and suspended loads in sea water were performed using the ScanEx Image Processor program suite. Calculations for the study of coast dynamics, as well as interpreta-

tion of coastal landscapes, were performed using MapInfo Professional GIS software. Data on the ice coverage of the Laptev and East Siberian Seas were obtained from the AARI digital archive [http://www.aari.nw.ru/projects/ECIMO//?im=100, 2020].

NATURAL ENVIRONMENT

From a geologically structural perspective the studied area is related to the epi-Cimmerian platform, which occupies the Laptev and East Siberian seas' shelf. A Late Cretaceous-Cenozoic sedimentary cover and a base represented by Verkhoyansk-Kolymsk and Novosibirsk-Chukotka fold belt rock are revealed in its structure [*State... Map..., 2016*]. The distribution of the region's morphostructures is due to the areal distribution of the cover and basement rocks and the direction of the latest vertical tectonic movements. Two main morphostructures stand out on a regional level: a subsidence zone (plate) of the Epi-Cimmerian Platform (A) and an East Laptev zone of uplift where basement rock exits at its surface (B) (Fig. 3). The developing continental margin basin of the studied seas corresponds to the first. The East Laptev zone is part of the stretching Lomosov-Svyatonosskiy uplift zone [*Ivanov et al., 2004*]. The submeridional positive neotectonic structure which includes the Kotelnichesko-Lyakhovskoe Uplift on the shelf and the Chokurdakh Uplift on the continent correspond to this zone [*State... Map..., 2016*]. The zone plays the part of an ancient divide of the Laptev and East Siberian sedimentational basins [*Patyk-Kara et al., 1989*] and sharply contrasts with the shelf morphostructure of the Laptev and East Siberian Seas in megarelief.

Local morphostructures stand out on the borders of the Laptev Sea Cenozoic graben-rift system morphostructure. These are trenches and grabens on the one hand and uplifts and horsts on the other hand (Fig. 3). Within the first, the thickness of the cover reaches 5.5 km, while in the second it is typically less than 1 km. The smallest value (0.5 km) is typical for the horst where Yaya Island formed [*State... Map..., 2016*].

The East Laptev zone represents an ensemble of positive and negative local morphostructures. The first include the Islands Belkovsky, Kotelny, Stolbovoy, Maly Lyakhovsky and Bolshoy Lyakhovsky, and a series of elevated massifs on the continent: Syurekh-Tas, Khaptagay, Ulakhan-Tuguttakh, Chokurdakh,

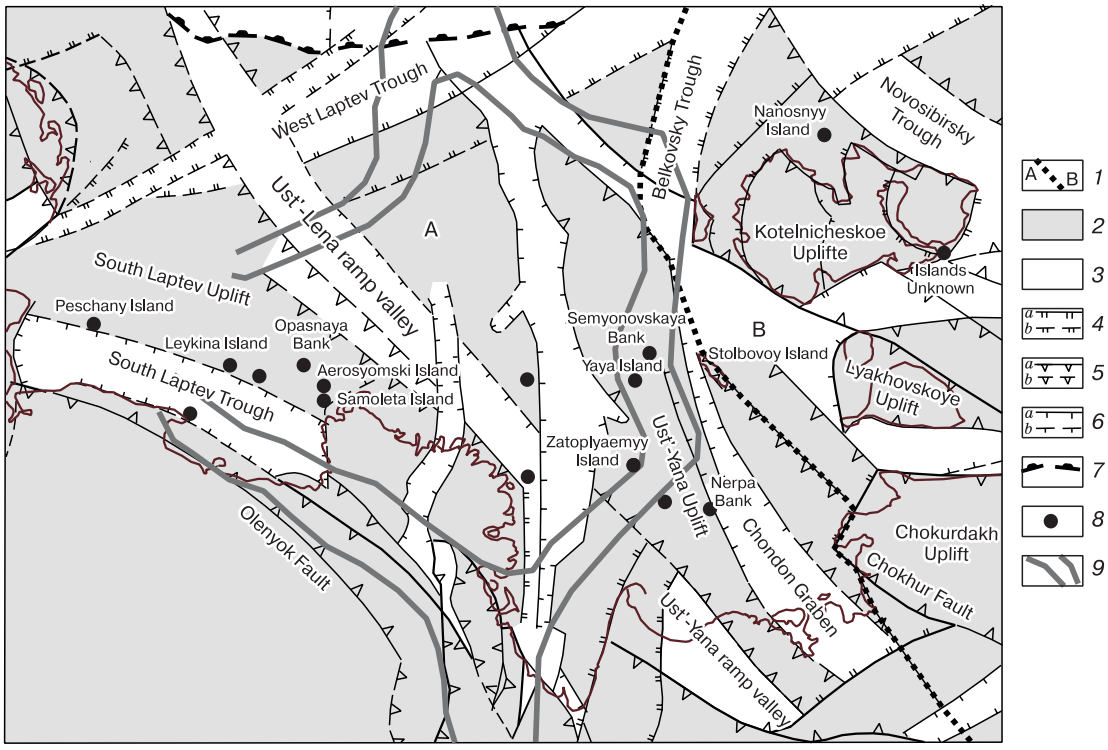

Fig. 3. Shelf morphostructures of the Laptev Sea and the western part of the East Siberian Sea [*Lukina et al., 2003; State… Map…, 2016; with changes*].

1 – regional morphostructures: A – Epicimmerian platform subsidence zone, B – East Laptev zone of uplifts. Local morphostructures: *2* – positive, corresponding to uplifts and horsts, *3* – negative, corresponding to depressions and grabens. The newest faults: *4* – normal faults (*a* – real, *b* – assumed), *5* – reverse faults (*a* – real, *b* – assumed), *6* – unspecified type (*a* – real, *b* – assumed). *7* – shelf edge, *8* – newly-formed and forming banks and islands, *9* – boundaries of earthquake distribution areas along the boundaries of the Eurasian, North American plates and the Laptev microplate [*Avetisov, 2004*].

Uryung-Khastakh, Khar-Stan and others. Negative morphostructures form the Sannikov, Eterikan, and Dmitry Laptev Straits. The sedimentary cover in this zone is discretely developed, not exceeding 500 m in thickness [*Burguto et al., 2016*].

There is permafrost on the shelf that was formed during its draining in the Late and Middle Neopleistocene. Its degradation, primarily from the bottom, is taking place presently under the influence of heat flow from the depths. Degradation from the top occurred during the Late Neopleistocene–Holocene marine transgression and continues presently owing to an increase in the mean average temperature of bottom water, which is especially significant in the coastal zone, and the salinification of bottom sediments, which lowers its freezing point. According to the results of mathematical modeling [*Fartyshev, 1993; Romanovskii et al., 2003; Dmitrenko et al., 2011; Nicolsky et al., 2012*], the permafrost is described primarily by a continuous distribution. Discontinuous and sporadic frozen thicknesses are distinguished in the outer part of the shelf. Their top can be 50–100 m deep, the thickness varies from 500 m (near the coast) to 100 m and less (on isobaths 60–80 m).

According to lithological maps of the bottom surface [*State... Map..., 2016, 2017*], the shallows within the water area are composed of pure and monogranular sands with a dominating size fraction of more than 85 % and 75 %, respectively. Freshwater and brackish water plankton communities dominate above shallows [*Dudarev, 2016*], since the waters and their sediments are desalinated. The desalination may be related to long-term existence of grounded hummocks (stamukhas) in the shallows.

The bottom of the IC on positive morphostructures usually occurs above sea level. According to seismoacoustic data Neopleistocene sediments are overlaid by a layer of Holocene marine sediments on Semyonovskaya Shallow [*Rekant et al., 2009*]. A level of cooled sediments which covers the permafrost level is distinguished in the cryolithozone structure of the shallow. Its thickness is minimal on the flat surfaces of the tops of the banks (from 1 to 5 m). Here and there, most likely where stamukhas regulary form, the top of the permafrost lies directly under the bottom surface. On lower surfaces, depending on the depths of the sea, the thickness of the cooled level varies from 5 to 15 m. Paleothermokarst basins composed of stratified cooled sediments are identified. Their appearance is related to lake thermokarst on drained parts of the shelf at the turn of the Late Neopleistocene and Holocene [*Romanovskii et al., 1999*]. Marine flooding led to the transformation of lake closed taliks into submarine ones. Within them the top of permafrost currently lies 30–60 m below the seafloor [*Rekant et al., 2009*]. Unlike frozen sediments cemented by ice, cooled sediments can be a source of material for the accumulation on the Vasil'evskaya and Semyonovskaya Banks.

DATA ON THE DYNAMICS OF ISLANDS AND BANKS

There are factual data on changes in the depth of the tops of shallows only from Semyonovskaya Bank, which is located within the eponymous shallow. In this shallow, besides the named bank, there also exists the Vasil'evskaya Bank (Fig. 4). The Vasil'evskaya and Semyonovskaya Banks formed at the location of eponymous islands, which were washed away in 1936 and 1951 [*Gakkel, 1957*]. There are also data on the cessation of the existence of Figurin Island around 1950 [*Gakkel, 1957*]. In 1952, a bank was discovered in its place using echolocation and named Figurin Bank [*Popov, 1987*].

Data on changes in sea depth within Semyonovskaya Bank. In 1955 the minimum depth of the sea within Semyonovskaya Bank was 0.1 m [*Klyuev et al., 1981; Are, 2012*]. In 1965 the top surface of Semyonovskaya Shallow was contoured with a 2 m isobath. The minimum depth of these banks was 0.8 m at the axis of the shallow [*Semenov, 1971; Klyuev et al., 1981*]. Thermal subsidence and the washing of Semyonovskaya Bank led to its deepening by 2–5 m in accordance with navigation maps from 1969–1971 [*Are, 2012*]. Detailed monitoring of changes in the depth of Semyonovskaya Bank (measurements from vessels with a small draft in 1999, 2000, 2003–2006)

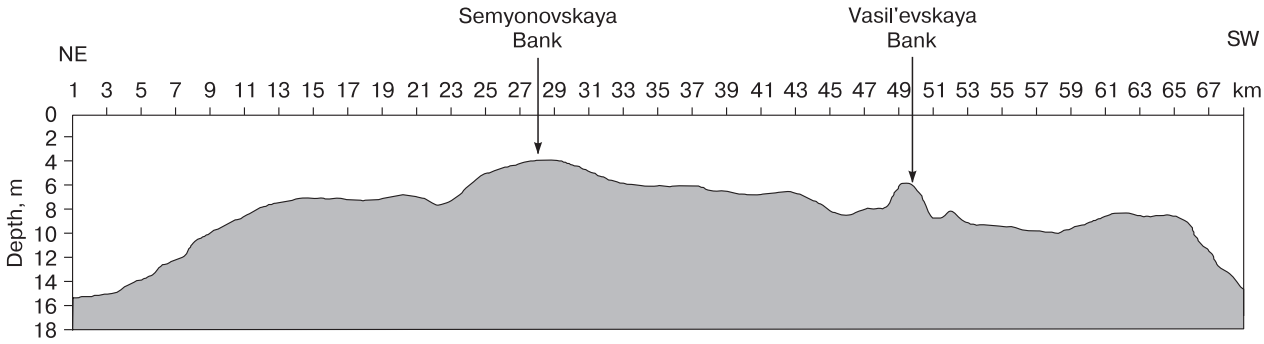

Fig. 4. Submeridianal section along the axis part of Semyonovskaya Shallow [*Charkin et al., 2007*].

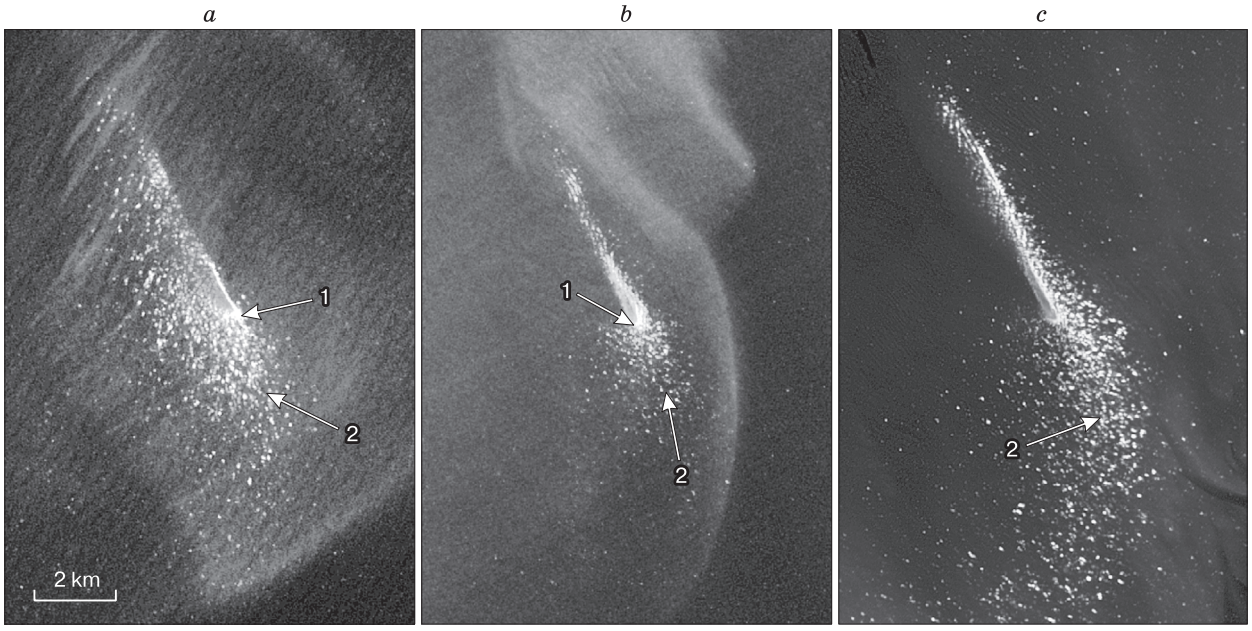

Fig. 5. Image of Vasil'evskaya Bank on Landsat-7, -8 SI, © USGS.

a – Landsat-7 (2007/08/12); *b* – Landsat-8 (2018/08/10); *c* – Landsat-8 (2020/07/19). 1 – stamukha remnants; 2 – breakers on shallows.

allowed for the description of the dynamic of its top surface in subsequent years [*Charkin et al., 2007*]. According to these data the smallest depth of Semyonovskaya Bank was 4.2 m in the beginning of the 2000s, compared to depths of 5.5 to 8.6 m within the shallow (Fig. 4). Significantly smaller minimum depths are provided in later publications [*Dudarev, 2016*] (0.8–1.0 m).

Data on shallow morphodynamics obtained using satellite images. Multitemporal satellite images (SI) provide important information about changes in shallows. Thus, based on Terra/MODIS data, the shallow at the top of Vasil'evskaya Bank was already first seen in 2003–2005 due to small breaking waves. From the end of October 2003 a stamukha forms almost yearly on this bank. Juxtaposition of Landsat-7 and -8 images from 2007, 2018 and 2020 allowed us to record the emergence of Yaya Island, the remains of stamukhas and breakers in shallows (Fig. 5). Using SI Landsat, Sentinel and MODIS from different seasons from 1973–2019 allowed us to identify a series of other banks. In periods of freeze-up and seasonal ice destruction they can be decoded based on stamukhas and hummocks' cooccurrence with them, while in the ice-free season they can be decoded by the presence of suspended matter fields above banks or breakers under wind conditions. Such are the Semyonovskaya and Nerpa Shallows, nameless shallows to the northeast and west of the Lena River delta, and the Opasnaya Bank [*Kucheiko et al., 2020*].

The rising surface of Semyonovskaya Bank on the eponymous shallow was first recorded on SI in 2004 based on the breakers above it. Later (2018) its location on SI was also determined using the breakers in the image. The results of the decoding allow us to conclude that sediments accumulate on Semyonovskaya Bank like on Vasil'evskaya, but more slowly. These facts explain the varying values of the depth of this bank in measurements from the beginning of the

Table 1. **Nanosnyy Island dynamics based on results of the measurements on Landsat -7, -8 SI**

Date of space imagery	Length of island, km	Width, km	Coastline length, km	Area, km^2
1999/07/13	2.9	0.23–0.34	6.0	0.75
2000/08/25	3.3	0.22–0.36	6.9	0.76
2002/08/20	3.2	0.18–0.49	7.1	0.84
2011/08/15	3.3	0.20–0.44	7.4	0.89
2014/08/13	3.6	0.20–0.63	8.7	1.22
2018/08/04 (upsurge)	3.5	0.16–0.35	7.7	0.76
2018/08/08	4.2	0.20–0.74	10.0	1.31
2018/08/11 (downsurge)	5.2	0.2–1.1	11.4	2.4
2019/07/19 (upsurge)	3.7	0.16–0.42	8.1	0.86
2019/08/04	4.3	0.16–0.90	10.6	1.46
2019/08/22 (downsurge)	4.8	0.2–0.9	11.0	2.0

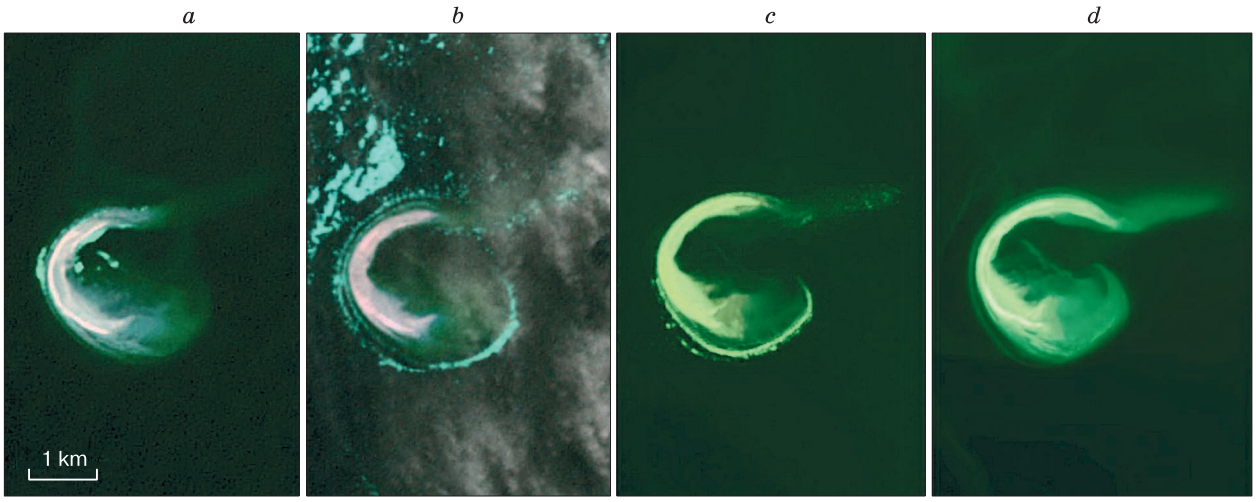

Fig. 6. Image of Nanosny Island on Landsat-7, -8 (Synthesis 543), © USGS.

a – Landsat-7 (2000/08/25); *b* – Landsat-7 (2002/08/20); *c* – Landsat-8 (2014/08/13); *d* – Landsat-8 (2018/08/08).

2000s – 4.2 m [*Charkin et al., 2007*] – and later – 0.8–1.0 m [*Dudarev, 2016*].

Banks can be exposed under wind-induced downsurges. Zatoplyaemyy Island on West Bank (117 km east of the Lena River delta) and Leykina Island (Osushnoy) (80 km northeast of Terpyai-Tumsa Peninsula) are also ascribed to formations that are exposed under downsurges and flooded under upsurges.

Newly formed islands are quite dynamic. Their configuration and surface area changes. Changes in their shapes and surface areas are recorded for Peschany, Leykina, Nanosnyy, Samoleta, Aerosyomski, Yaya Islands.

The existence of wind-driven phenomena, the amplitude of which can reach 2.0–2.5 m [*Mustafin, 1961*], complicates the precise determination of the configuration and parameters of low-lying islands. Nonetheless, for Nanosnyy Island, which had formed on Figurin Bank and is located on a shallow 33 km northeast of Cape Anisy of Kotelny Island, an increase in its length and surface area, particularly evident in recent years, has been established (Table 1, Fig. 6). The island represents a half-ring of the right shape, the convex part of which is oriented to the west, no more than 2 m in height. A shift in the island's coastline toward the east has been recorded. The products of washing from the western retreating coast are transported eastward, where they form spits which adjoin the island. From 2000 to 2014 retreat of a 1.5-km area of the western coast of Nanosnyy Island constituted 55 m on average, with a maximum of 86 m. As such, the average speed of movement from west to east was approximately 3 m/year. In the past five years the coast has retreated by the same amount, and the average speed over 18 years exceeded 5 m/year. The sea has washed away 0.21 km^2 of the western coast, and the increase in surface area in the southern and northern ends of the island has constituted 0.36 km^2.

CENTURIES-OLD CHANGES IN THE NATURAL ENVIRONMENT

Data on changes in climate and ice coverage can serve as the main indicators of centuries-old changes in the natural environment of Arctic seas. Reconstruction of the average annual air temperature (Fig. 7) demonstrates that in the 17th–beginning of 20th centuries, when the remnant islands formed by IC and the banks on their locations were washing away, the average annual air temperature was 1.5–2.0 °C lower than the contemporary temperature. The period from the warm early medieval times to the middle-end of the 19th century or a shorter interval (17th – middle of the 19th century) is called the Little Ice Age (LIA) (Fig. 7, 8).

Data on the distribution of microfossils in the surface sedimentary layer of the Laptev Sea shelf together with pollen data and data on the blockage of many-year sea ice of the coasts of Iceland can also serve as an indicator of fluctuations in climate and ice coverage of seas (Fig. 8). The coldest period (1400–1900, Fig. 8, *A*) is characterized by the disappearance of marine diatoms and minimum quantities of benthic foraminifera. Data on ice coverage near the coasts of Iceland are also quite descriptive (Fig. 8, *B*). They demonstrate that in the 17th–19th centuries it was particularly cold on the island. Migrants, of which there were already 25,000 by the year 900 (with a modern population of 150,000) – only 50 years after

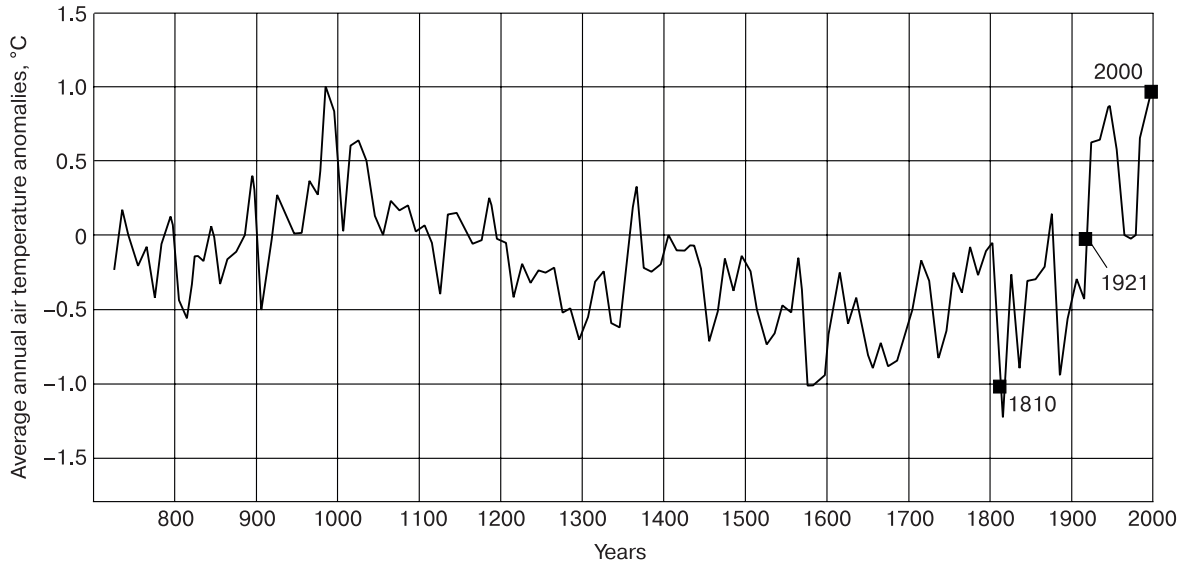

Fig. 7. Deviations of average annual air temperature in the western sector of the Russian Arctic from average values for 800–2000 as cited in [*Klimenko et al., 2013*], with simplifications.

The black squares indicate temperatures that were used to build the model of average annual temperature of bottom water in the beginning of the 1920s and 1800s.

the discovery of the island by Normans – leave the island or die [*Jones, 1964*]. Only in the beginning of the warming in 1930–1940 the sea around Iceland ceases to be icy.

Changes in ice coverage can be inferred from information about the possibility of navigation in the Arctic seas. In the warming of the Middle Ages (about 1000 years ago), the Normans reached 79° N in the strait between the Ellesmere and Greenland islands and travelled north of 80° N near Svalbard [*Jones, 1964*]. It is significant that Icelandic sagas barely mention sea ice as a barrier to sea travel.

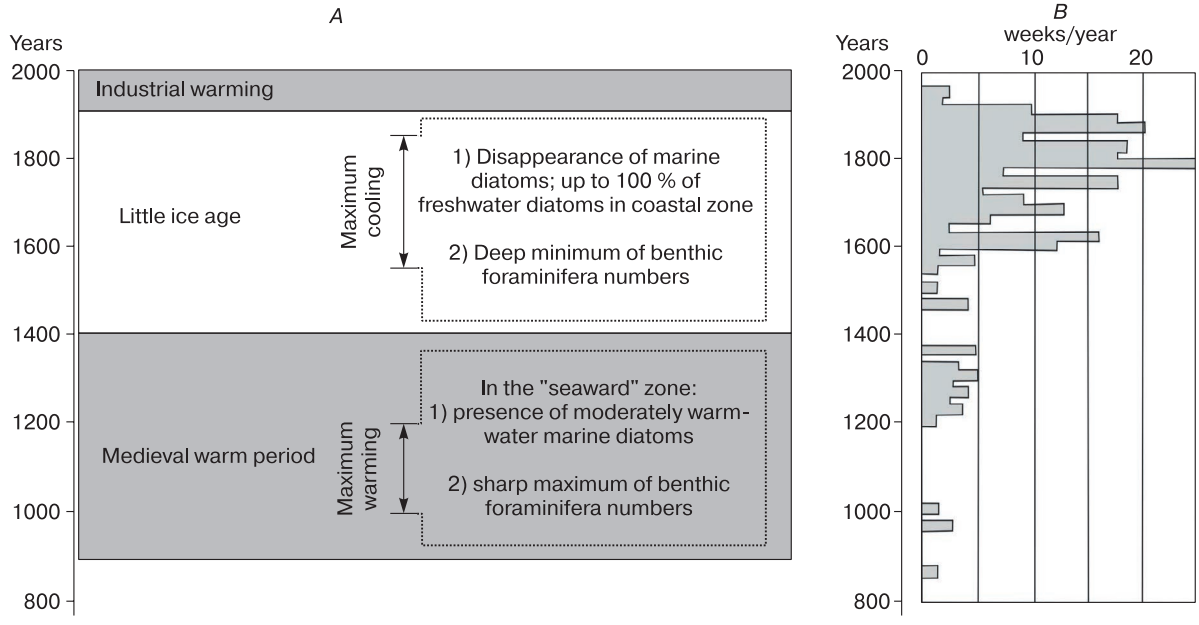

Fig. 8. Paleoclimatic reconstructions for 800–2000.

A – based on micropaleontological data on the Laptev Sea shelf [*Matul et al., 2007*]; *B* – based on the length (number of weeks per year) of blocking of the coasts of Iceland by Arctic pack ice [*Koch, 1945*].

Whale, seal and walrus hunters travelled to the coasts of Svalbard and Novaya Zemlya up to the year 1200. Expedition and fisherman travels on sea vessels among drifting ice was quite complicated in the eastern seas of the Arctic in the 17th – first half of the 19th centuries. For example, the Northeastern expedition directed by J. Billings (1787–1791) for the geographical study of the northeast with astronomical identification of geodesic control points was planned as a marine expedition, but had to be conducted on land. The study of the New Siberian Islands during this time (1770–1824) occurred exclusively by way of travel across ice [*The history..., 1954*]. In L.A. Zhigarev and V.A. Sovershaev's opinion [*1984*], sea fast ice could have been preserved or drifting ice could have existed throughout the entire summer around Semyonovskaya Shallow. Relief from ice occurred only in individual years. Based on the data in Fig. 7 and ice coverage values, the interval from the end of the 18th to the middle of the 19th centuries ought to be considered the pessimum of the LIA for the shelf part of the East Siberian seas.

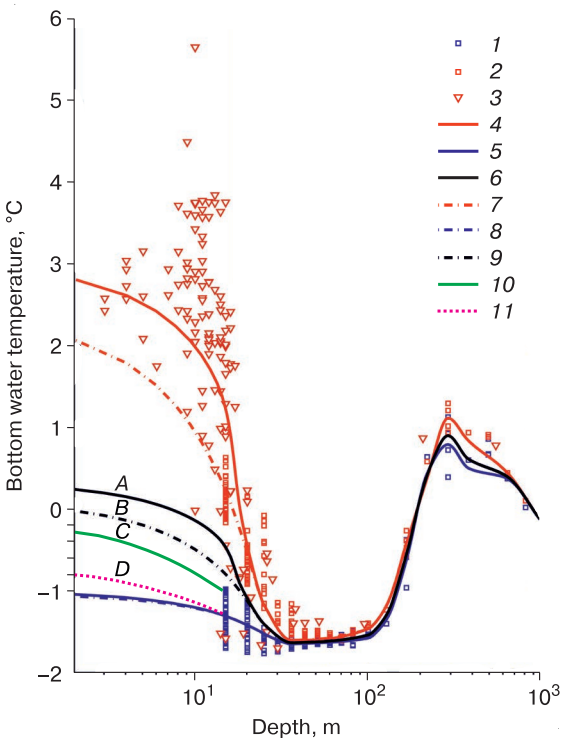

Fig. 9. Laptev and East Siberian Seas bottom water temperature data [*Nicolsky et al., 2012*] and model of century average bottom water temperature in the beginning of the 1920s and 1800s.

Average water temperature: *1* – winter temperature (AARI), *2* – summer temperature (AARI), *3* – summer temperature (International Siberian Shelf Study, ISSS). Average decadal water temperature curves for 1999–2009: *4* – summer temperature, *5* – winter temperature, *6* – average annual temperature. Average century water temperature curves for 1920–2009: *7* – summer temperature, *8* – winter temperature, *9* – average annual temperature. Model curves of medieval bottom water temperature: *10* – in the beginning of the 1920s, *11* – in the beginning of the 1800s.

The description of centuries-old dynamics of the natural environment will not be complete without the reconstruction of at least orientational values of average annual temperature of bottom water during the pessimum of the LIA. AARI has observed winter and summer bottom water temperature since 1921. For the reconstruction of its average annual values in the beginning of the 1920s the authors used the temperature data published in the work of [*Nicolsky et al., 2012*] (Fig. 9), where the temperatures of bottom water for the warmest decade (1999–2009) and its century values for the period from the beginning of the 1920s to 2009 are presented.

In order to understand what the minimum LIA temperature was in the 20th century, taking curve B (century average bottom water temperature) as the axis of symmetry we can graph a curve of minimum temperatures – curve C, symmetric to curve A, – and, using information about the amplitudes of air temperatures in the intervals 1921–2009 and 1800–1921 (Fig. 7), obtain an understanding of the minimum temperatures of bottom water in the 19th century (curve D) by creating graphs analogous to those described for the 20th century.

We will see that the average annual temperature in the beginning of the 1920s changed within the interval of the values: from –0.2...–0.3 °C near the shore to –0.8 °C at a sea depth of 10 m. During the pessimum of the LIA it changed from –0.8 °C near the shore to –1.2 °C at a depth of 10 m; in other words, it was almost identical to contemporary winter water temperature.

In conclusion to the considerations of the dynamics of the natural environment in the water area of the East Siberian Arctic it should be noted that a reconstruction (Fig. 7) based on data mainly for the western sector of the Arctic was used for the description of the average annual air temperature. It is currently higher than above the seas of the Eastern Arctic and was this way during the LIA. This is due to lesser climate continentality in the west. Because of this, the hydrodynamics, activity of cryogenic and ice processes on the shelf of Eastern Siberia in the Middle Ages was determined by even lower air and bottom water temperatures and especially greater ice coverage.

RESULTS OF THE ACTIVATION OF CRYOSPHERIC AND HYDRODYNAMIC PROCESSES INITIATED BY CLIMATE WARMING

The **climate warming** called the industrial warming and commencing in the beginning of the 20th century (Fig. 7) is most notable in 1990–2000. Warming in high latitudes (60–85° N) exceeds warm-

ing in the northern hemisphere by a factor of more than two. It is even more significant within the water areas of Arctic seas. Based on Roshydromet data the air temperature within the Laptev and East Siberian Seas in 2019 exceeded its average values in 1961–1990 by 3.9 °C and 3.3 °C, respectively. The rate of temperature increase relative to the indicated period of time exceeds that for the northern hemisphere (0.18 °C/10 years) [*The second assessment report..., 2014*] by a factor of 13 above Arctic seas (2.43 °C/10 years) [*Report..., 2020*]. In the authors' opinion, the reason for such an increase is the decrease in sea ice surface area and unabatingly decreasing surface albedo.

Decrease in ice coverage is expressed as decreasing sea ice surface area and is accompanied by an extending length of the ice-free season. The correlation coefficient of the decrease in ice surface area in September with summer air temperatures of the marine Arctic for 1979–2019 constitutes –0.92 [*Report..., 2020*]. If the degradation of sea ice in the 1980s and 1990s occurred owing to an Atlantic influence and was observed primarily only in the western sector of the Eurasian Arctic [*The second assessment report..., 2014*], in the 2000s it becomes rather palpable in the eastern sector, as well. The surface area of sea ice in the Laptev and East Siberian Seas has been steadily decreasing for the past two decades. In 2011–2020 it decreased by a factor of four compared to 1970–1989 (Fig. 10). According to AARI data, in August 2020 the Laptev Sea was entirely free of ice.

The increase in the length of the ice-free season on average for the Arctic seas of Russia in 2001–2011 relative to the cold years of 1965–1975 constituted 40 days [*The second assessment report..., 2014*]. According to data from Kigilyakh and Ayon stations it equates to 36 and 47 days, respectively. This length is significantly less only in bays (Tiksi Station – 7 days).

Hydrodynamic processes. An increase in the duration of the ice-free season means an increase in the dynamically active period, which was estimated at only 10–20 % of the year in the 1970s [*Sovershaev, 1981*], while in 2001–2011 it increased to 20–30 %. Seasonal ice boundaries retreating to the north and an increase in the duration of the dynamically active season significantly increase the length of wave fetch and wave activity in general. In the 1970s and 1980s the wave fetch length in the Laptev Sea varied from 90 km in July to 600 km in October, and the maximum wave height at the maximum fetch was 3 m [*Kaplin et al., 1991*]. Waves 3 m tall carry approximately 100 kW of energy per 1 m of the wave crest [*Safyanov, 1996, p. 17*]. Storm waves 5 m tall and 100 m long are now considered average. These waves are beginning to be recorded in seas where they were significantly smaller in the beginning of the 20th century: for example, in Beaufort Sea [*Thomson, Rogers, 2014*]. With such waves, for each square kilometer of the wave-covered water surface there are 3 billion kW of energy [*Safyanov, 1996*]. Even in the 1940s through 1960s waves affected the bottom in such a way during storms that sludge and sand were thrown onto the decks of vessels in the shallow Laptev and East Siberian Seas hundreds of kilometers from the coasts [*Klyuev, 1965*].

The presented quantitative data allow us to conclude that contemporary warming and decreasing sea ice coverage significantly increase the potential of morpholithogenesis. However, the specified potential is just a possibility of its manifestation. For the implementation of accumulation sediment material is necessary. Given its sufficient amount the energy of waves is spent on transport and accumulation of material, given its deficit it is spent on the washing of sediments. The formation of sediment material during contemporary warming is tightly related to the activation of cryogenic processes.

The activation of destructive cryogenic processes determines the annual arrival of 62 and 90 million tons of sediments to the bottom of the Laptev

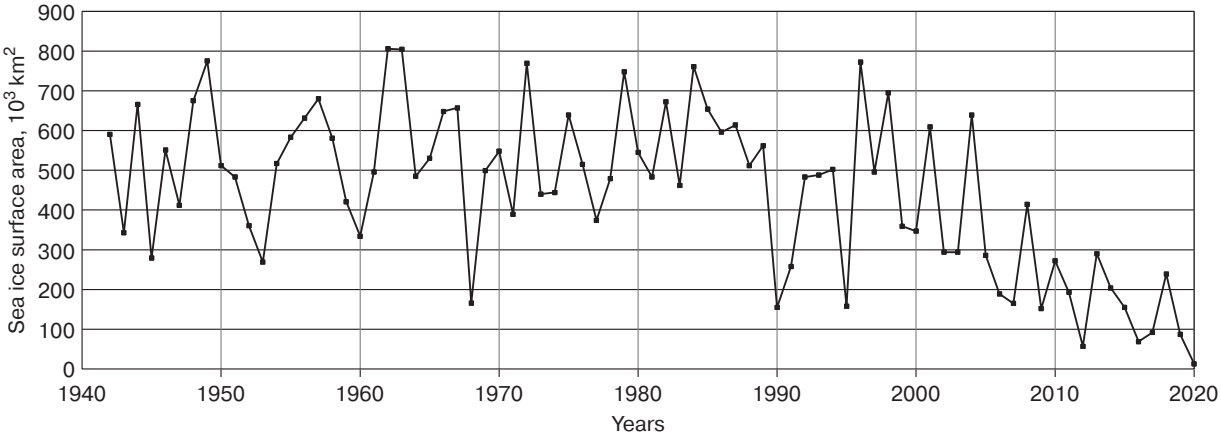

Fig. 10. Average sea ice area (ice coverage) in August in the Laptev Sea and the western part of the East Siberian Sea for 1940–2020 based on AARI data [http://www.aari.ru/projects/ECIMO/?im=100].

and East Siberian Seas, respectively [*Grigoriev, 2017*]. It occurs by way of the effect of these processes not only on coasts, but also on the bottom. The results of the juxtaposition of multitemporal different aerial and satellite images demonstrated that for Bolshoy Lyakhovsky Island and the southern coast of the Dmitry Laptev Strait 27 km^2 of the surface area of Bolshoy Lyakhovsky Island and 12.4 km^2 of the continental coast were washed away under the influence of thermal abrasion and thermal denudation from 1951 to 2000. In the period from 2000–2013 these values constituted 12.2 and 6.5 km^2, respectively. The rates of retreat of shores constituted 3.2 m/year for 1951–2000 and 6.4 m/year for 2000–2013 on average [*Pizhankova, Dobrynina, 2010; Pizhankova, 2016*]. A twofold increase in the rate of coastal retreat is a consequence of climate warming, which has particularly activated since the mid-1990s.

Thermal subsidence of the bottom is an equally widespread process. Widely known data from repeated (1940–1960) hydrographic imaging in the coastal zone 6–8 km wide along the 160-km Anabaro-Olenek coast composed of IC sediments [*Klyuev, 1970*] can serve as an example of their manifestation. Depression from subsidence of bottom sediments with high ice content constituted 0.4–1.0 m here. As a result, isobaths shifted 0.3–1.0 km toward the coast. According to F.E. Are's [*1998*] calculations 3.4 million tons of sediments entered the sea every year in the 1940s–1960s owing to thermal subsidence, as well as thermal abrasion and thermal denudation of these coasts. Currently, considering the scale of contemporary warming and shrinking ice coverage, the volume of sediments entering the sea should be even larger.

The degradation of permafrost in the Laptev and East Siberian Seas, as noted above, occurs not only from the bottom of the permafrost, but also from the surface, from their top. Unlike the LIA, during industrial warming it is actualized not only owing to sediment salinization, but, mainly, as a result of increasing bottom water temperature. It becomes particularly significant during periods of warming when the sum of summer positive temperatures of bottom water begins to exceed the sum of negative winter temperatures and its average annual temperature becomes positive.

In the first half of the 20th century published data on the existence of positive average annual temperature of bottom water based on data from instrumental observations were related only to the warming of the 1930s–1940s [*Geography..., 1949*]. In the 1970s the same temperatures, as well as bottom sediment temperatures above 0 °C, were recorded as a result of geocryological research completed near Muostakh Island [*Molochushkin, 1969*] and in Van'kina Bay [*Zhigarev, Plakht, 1974*]. Such temperatures were observed in the isobath interval from 2 to 7 m. In both cases they were related to the zone of heat influence of Lena River runoff. Temperatures above 0 °C were also known near mouths of large rivers and in numerous shallow bays. In other locations water temperatures in shallows were negative [*Are, 2012*].

Water temperature has been rising significantly since 1985 [*Dmitrenko et al., 2011; Nicolsky et al., 2012*]. Based on published data, the highest bottom water temperatures occurred in 1999–2009. It is quite significant that in surface area, up to 76° N, and in depth (up to depths of 9–10 m), the area of their distribution significantly expands. Positive water temperatures cause thawing of permafrost. Thawing eases the transport of sediments and their accumulation.

Newly formed above-surface and underwater landforms are currently freezing. The freezing of newly formed landforms occurs from the surface in the fast ice zone (isobath interval 0–2 m), where deep conductive cooling of bottom sediments occurs by way of ice freezing to the bottom. It is so significant that average annual temperatures of submarine permafrost near the water edge are characterized by values as low as in subaerial permafrost. In the 1970s they constituted –10...–12 °C in Van'kina Bay 72° N [*Katasonov, Pudov, 1972*]. Perennial freezing facilitates the conservation of newly formed landforms by complicating their erosion.

In conclusion it should be said that the activation of destructive cryogenic processes is first and foremost provided by shrinking ice coverage, an increase in the length of the dynamically active season and subsequently increasing power of hydrodynamic processes. During the LIA there were also areas where the permafrost layer was overlaid by a layer of cooled sediments. However, a small length of the wave fetch under conditions of widespread drifting ice and a short ice-free season did not contribute to the transport and accumulation of bottom sediments. The transport of the latter occurred mainly owing to ice processes.

The particle-size distribution of the sediments is quite an informative data for the identification of the conditions of sediment accumulation. The fraction composition of bottom sediments and its lateral variability within the area captured by sheets S-53; 54 of the geological map are shown in Fig. 11.

The contents of Fig. 11 show that contemporary sand-sized sediments are predominant near the coasts of the continent and the New Siberian Islands, as well as at the top parts of shallows. One such extensive shallow, which includes the Semyonovskaya Bank with Yaya Island, West Bank with Zatoplyaemyy Island and Nerpa Bank, is presented in Fig. 11, *a*. Monogranular sands transition into monogranular pure sands, where the sand fraction content exceeds 85 %, reaching 94 % in individual samples, in elevated areas of Semyonovskaya Shallow, West and Nerpa

Banks. It has equivalent values within two other sheets of the geological map (S-51; 52 and S-50) [*State... Map..., 2014, 2017*]. These are shallows, the tops of which are represented by Peschany, Leykina, Aerosyomki, Samolet Islands and nameless banks. In the authors' opinion, a similar process also occurs in the vicinity of Nanosnyy Island. In the location of the relict Figurin Bank the process of accumulation of modern sand sediments has been underway since the second half of the 20th century. This process is accompanied by their syncryogenesis.

The sand is of a local origin, it formed as a result of rewash of sands which were present as mixtures in the composition of primarily aleuritic IC ground blocks in the Late Neopleistocene. On the geological map [*State... Map..., 2014, 2016*] they are ascribed to palimpsest sediments. These are relict sediments which have been intensely reprocessed by contemporary hydrodynamic processes [*Geological Dictionary, 2011*]. In the modern genetic classification, they are ascribed to perluvium. Particles of the finer fraction are washed out and transported to deeper regions of the water area. Aleurites are predominant on the slopes of the banks, the role of sand particles in their composition decreases down the slope (Fig. 11, *b*). Pelite size particles accumulate in negative landforms of the bottom, including in the paleovalley of the eastern branch of the Yana River (Fig. 11, *c*).

In Semyonovskaya Shallow sands are not only rewashed but also used for sedimentation within Vasil'evskaya and Semyonovskaya Banks. On Vasil'evskaya Bank this process already became notice-

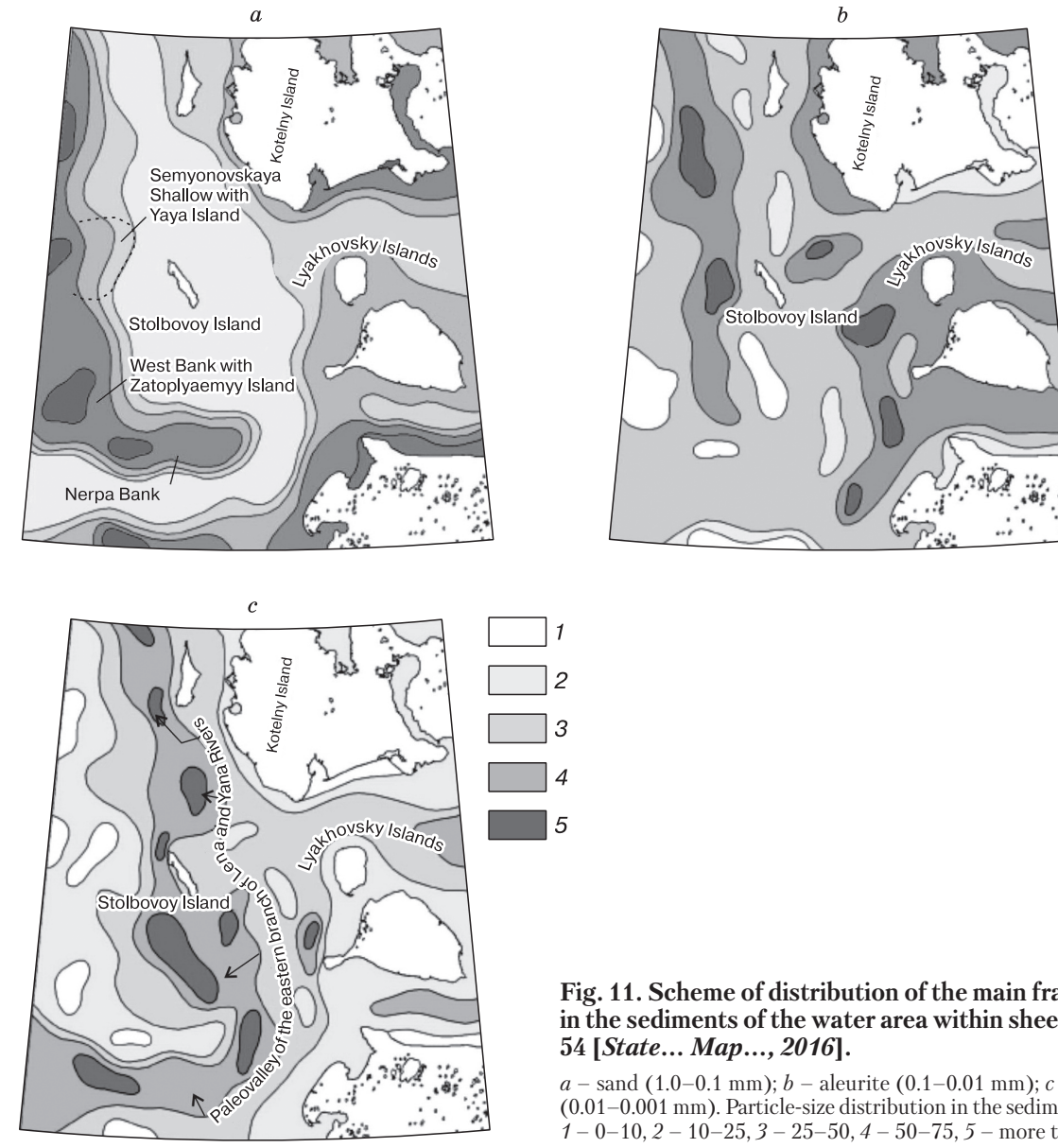

Fig. 11. Scheme of distribution of the main fractions in the sediments of the water area within sheet S-53; 54 [*State... Map..., 2016*].

a – sand (1.0–0.1 mm); *b* – aleurite (0.1–0.01 mm); *c* – pelite (0.01–0.001 mm). Particle-size distribution in the sediment (%): *1* – 0–10, *2* – 10–25, *3* – 25–50, *4* – 50–75, *5* – more than 75.

able from breaking waves in 2003–2005 and 2007, as mentioned above. Particle-size distribution of sediments within Semyonovskaya Shallow demonstrates that it currently represents an abrasion-accumulative form. Abrasion areas are mainly lower near-top parts of the shallow, while accumulative areas are the top surface of Vasil'evskaya Bank with Yaya Island, Semyonovskaya Bank and the underwater plain surrounding the shallow. Elevated parts of the shallow consist of fine- and, less commonly, medium-grained sands which formed as a result of the washing of IC sediments of the Late Neopleistocene. Currently they are reprocessed by the sea. Over the period of washing the particle-size composition of the IC, according to O.V. Dudarev's calculations [*Dudarev et al., 2015; Dudarev, 2016*], has been impoverished of its fraction of less than 0.01 mm by a factor of three, while there have become, on the contrary, approximately 70 times more particles of the sand fraction.

Despite the loss of fine-grained material as a result of washing, Semyonovskaya Shallow, according to O.V. Dudarev, still remains its source. The main ranges of suspended matter which are often recorded using SI are confined to this region. According to the data of marine monitoring expeditions its concentration reaches 26.3 mg/L during storms, while in the Vasil'evskaya Bank area it is 4–5 mg/L due to the increased content of the sand fraction in sediments (average content is 50.1 %) [*Dudarev et al., 2015*].

POI FEB RAS sea monitoring with sonar, bottom grab and CTD probe (which measures electrical conductivity, temperature and sea water density) application allowed us to obtain data on the spacial distribution of the particle-size composition of bottom sediments on the NE–SW profile, which is 140 km long (Table 2).

Drift current 35–50 cm/s was recorded during sea monitoring, which, according to V.V. Longinov [*1973*], is sufficient for detachment and transport of particles up to 0.5–1.0 mm in size. Thus, not only removal and transport into depressions of suspended particles are recorded, but also the possibility of sand particle transport. The latter demonstrates that even storms are not necessary for the accumulation of sands on Vasil'evskaya and Semyonovskaya Banks and the formation of Yaya Island.

Normal, as well as stronger, sea roughness forms poorly sorted sediments (for example, aleuritic mictite (Table 2)) by tranforming the lithodynamic regime. On the slope of Vasil'evskaya Bank with a sea depth of 7–9 m there are moderately sorted fine-grained sands with an average 69.1 % modal fraction group content (63.0 % median subfraction). The sediment belt of Semyonovskaya Bank with a 69 % sand fraction content does not descend lower than a 15-meter depth. Near the foot of the shallow at sea depths of 17 m the zone of pelitic aleurite accumulation begins (Table 2).

In summary, it should be noted that the particle-size distribution of bottom sediments corresponds to the contemporary hydrodynamic regime. The latter, in turn, is justified by the expansion of the sea ice-free water area, an extension by a factor of 1.5 of the dynamically active time and the existence of a large volume of thawed sediments which are available for transport and accumulation.

However, why is sediment accumulation is observed primarily on Semyonovskaya Shallow and Figurin Bank (Nanosnyy Island)? To answer this question we must look to data on the contemporary rise in the sea level and the vertical movement of Earth's crust.

Contemporary vertical movement of Earth's crust. The formation in the second half of the 20th and beginning of the 21st centuries of Nanosnyy and Yaya Islands and a rise in the surface of Semyonovskaya Bank occur despite a rise in the sea level. In the second half of the 20th century it was estimated to be 1.7 mm/year, in 1993–2010 it was estimated to be 3.2 mm/year [*IPCC, 2014*]. In relation to this the estimate of contemporary vertical tectonic movements is deemed absolutely essential. Among these are movements which currently take place or took place several hundred years ago, which are identified based on quantitative data [*Nikonov, 2006*], specifically geodesical, level measuring, historical, archaeological, geophysical, as well as data obtained with the help of measurements by multitemporal satellite images and maps using space geodesy methods. The rate of vertical movements within platform plains varies from 0.1 to 4 mm/year [*Nikonov, 2006; Zakharov, 2006*].

Table 2. **Particle-size composition of the deposits of the NE–SW profile through Semyonovskaya Shallow [*Dudarev et al., 2015*]**

Region	Depth, m	Fraction content, %			Lithological type of sediment
		1–0.1 mm	0.1–0.01 mm	<0.01 mm	
Vasil'evskaya Bank slope	7–9	69.1	27.5	3.4	Fine-grained sand
Middle part of the shallow	7	43.5	47.0	9.5	Aleuritic mictite
Semyonovskaya Bank slope	10	37.9	56.9	5.2	Sandy aleurite
Foot of the shallow	17	15.2	67.8	17.0	Pelitic aleurite
Accumulative plain north of the shallow	27	4.2	28.6	67.2	Aleuritic pelite
Accumulative plain south of the shallow	25	0.0	6.5	93.5	Pelite

The authors attempted to identify and estimate the rate of vertical movements in the region. For the Nanosnyy Island area, which is ascribed to the Eastern-Laptev uplift zone (regional morphostructure B), such an estimate was made based on an analysis of the results of observations of perennial sea level dynamics (Table 3). It was completed using data from the polar stations Kigilyakh and Sannikov Strait. The former is located on Cape Kigilyakh of Bolshoy Lyakhovsky Island; the latter is located in the southwestern end of Kotelny Island. Given the aforementioned trends of rise in the sea level (+1.7 mm/year during 1950s–1980s and +3.2 mm/year during 1993–2010) the change in level in the Dmitry Laptev Strait based on average readings from Kigilyakh Station was characterized by the following values for the same periods: –0.85 mm/year during the first of the indicated periods and –1.38 mm/year during the second (Table 3). Negative values of the readings indicate that not only does the sea level rise, but also the coast where the station is located, and the rise of the coast precedes the rise of the sea level. Data on Sannikov Strait Station demonstrate that during 1950s–1980s the rate of the rise of the southwestern coast of Kotelny Island exceeded the rate of the rise of the level of the ocean by 0.33 mm/year and was 0.20 mm/year behind it during 1993–2010.

Contemporary uplift is established for Semyonovskaya Shallow and Yaya Island based on the results of juxtaposition of seismological data and data on contemporary movements of Earth's crust [*Avetisov, 2004*]. The shallow is located within the submeridianal zone of earthquakes, which stretches through the entire shelf (Fig. 3). The rate of vertical movements as compared to other Arctic seismically active sites can be estimated to be no less than 2–3 mm/year.

The obtained data allow us to conclude that both positive structures of the Eastern-Laptev zone and the earthquake epicenter zone stand out in the similarity or slight exceeding of their rate of vertical movements as compared to that of the sea level rise. Data on the formation of Yaya and Nanosnyy Islands and measurements from SI allow us to quantitatively characterize the sedimentation (Table 1). Nanosnyy Island, which is composed of contemporary sediments, is already marked on the topographic map of 1986, which records the condition of the region in 1973. Yaya Island was first recorded only in 2013. The sedimentation rates of Nanosnyy and Yaya Islands can be characterized as rather fast, considering that it occurs upward on the underwater slope, against the pull of gravity. Such transport of sediments occurs as a result of the transformation of the thermal abrasion profile of the underwater slope into an accumulative one. The transformation is justified by increased power of hydrodynamic processes which, in turn, is provided by an early cleansing of the water area of ice and an increase in the length of the dynamically active period.

Other islands (Leykina, Zatoplyaemyy, Aerosyomki, Samoleta) and banks are characterized using SI only by changes in their shapes. Their surface areas remain almost unchanged. Sedimentation on elevated areas of the sea bottom are a very rare occurrence. In East Siberian seas, like in all seas, it is mainly related to negative structures, the bulk of sediments is directed specifically there. This is pelite-sized material (Fig. 11). However, the presence of palimpsest sands on the indicated islands and banks [*State... Map..., 2014, 2016*] indicates their replacement of sandy sediments, which had formed as a result of IC thermal abrasion in these areas: i.e., sedimentation. Here, however, as in Semyonovskaya Shallow and the vicinity of Nanosnyy Island, sand fraction particles accumulate in elevated areas of the shallows, while finer particles are carried to negative bottom landforms. We will note again that this is indicative of an accumulative profile of equilibrium on the underwater slope of shallows. The rate of sedimentation under conditions of sea level rise is apparently insufficient for its identification using SI.

The question about Peschany Island stands on its own. It is marked on the geological map [*State... Map..., 2017*] as consisting of Late Holocene sea wave sediments. The pedestal of the island in the diameter exceeds its size by a factor of 2–2.5. The top of the pedestal with the island, the height of which constitutes 1 m, rises more than 10–15 m above the surrounding underwater plain [*State... Map..., 2017*]. This height can apparently be attributed to the existence of its significantly more ancient formation. Ring-shaped bars, which are the location of stamukha concentration, deciphered by the ice remains on SI,

Table 3. **The magnitude of the linear trend of sea level change based on observation data at Kigilyakh and Sannikov Strait stations for the periods 1950–1980 and 1980–2016 [*Merkulov et al., 2017*] and its correlation with the rate of contemporary coast rise in the region of observation stations**

Stations	Observation period	Trend magnitude (mm/year)		Coast rise rate in relation to the sea level trend
		Before 1980s	After 1980s	
Kigilyakh	1951–2016	–0.85	–1.38	Over the trend
Sannikov Strait	1950–2016	–0.33	+0.20	Almost identical

Note. A minus signifies a lowering of the sea level in relation to the coast, a plus signifies its rise.

Fig. 12. Gravel-pebble material and drift-wood, pushed by drifting ice onto the coast of Kotelny Island [*Are, 2012*].

reliably protect it from erosion and determine the long existence of the island in a little-changing form.

Ice processes. Even if litho- and morphogenetic sea ice activity changed in shallows in the contemporary warming, it changed quite insignificantly. The role of ice in sedimentation occurs in several ways. This is accumulation as a result of transport activity of frazil and cloudy ice, i.e. containing a large amount of mineral and organic inclusions. Bulldozing of bottom sediments up the underwater slope by drifting ice under pressure from onsetting wind plays a rather significant morphogenetic role [*Barnes et al., 1988; Kempema et al., 1989*]. It is thought that bulldozing is one of the main processes which contributed to the formation of barrier islands near Alaska's coasts. During warming it occurs closer to the coast [*Ogorodov, 2011*] and continues to be an efficient geomorphological factor in the water area of the Laptev and East Siberian Seas (Fig. 12). In many cases sedimentation can occur in the wave or wind shadow of stamukhas, as well as around the latter during storms, which, according to A.Yu. Gukov [*2014*], happened during the formation of Yaya Island.

In cold periods or years burial of surface ice (remains of fast ice, stamukhas, icebergs) by marine sediments also apparently takes place. Their subsequent thawing may be the cause of the formation of arc-like spits and bars which form lagoons adjoined to preexisting islands. There are particularly many of them in the northern part of the Kara Sea, where the connection between lagoons with icebergs buried earlier is especially likely.

Shallows are the location of concentration of stamukhas which freeze to the bottom. As mentioned above, they protect newly formed landforms, assuming storm-caused unrest and ice loads from the sea. The formation of thick grounded hummocked many-rowed barriers at sea depths of 4–5 m along the fast ice border takes place each year in the autumn and spring during its formation and destruction [*Ogorodov, 2011*].

On hummocked areas, after thawing of stamukhas, sediments can be desalinized, which eases their freezing, if they were not frozen. Within areas of their regular yearly formation this circumstance contributes to the stabilization of the frozen condition of the ground, which, inarguably, facilitates sedimentation.

CONCLUSIONS

1. Within the Laptev and East Siberian Seas, during the course of the 17th–20th centuries, island-remnants of the Late Neopleistocene Ice Complex were washed, as later were the shallows and banks which had formed in their place. At the turn of the 20th and 21st centuries sedimentation with island formation begins in these shallows.

2. Shallows are attributed to positive morphostructures which correspond to raised tectonic blocks in the rift system of the Laptev Sea. Sedimentation in shallows occurs together with sedimentation in negative morphostructures and river paleovalleys.

3. The main reason for contemporary sedimentation in shallows is a decrease in the surface area of sea ice in East Siberian seas and an increase by a factor of 1.5–2 (compared to the 1970s) of the length of the ice-free season in relation to climate warming.

The priority role of sedimentation in shallows currently belongs to hydrodynamic processes, while earlier it occurred mainly by way of sea ice.

4. A deficit of sedimentary material in the 17th–20th centuries is replaced by its excess at the turn of the 20th and 21st centuries in relation to the activation of cryogenic processes – thermal abrasion and thermal denudation of coasts, thermal subsidence and bottom thermal abrasion, degradation of permafrost from the top. As a result, the thermal abrasion profile of the underwater coastal slope in shallows transforms into an accumulative one. Coarser material (sandy) is given the opportunity to move upward, forming and growing banks and islands, finer material is carried into the deep into paleovalleys and negative morphostructures.

5. Sedimentation in shallows occurs under conditions of a rising sea level, which takes place at a rate of 3 mm/year. Because of this it becomes noticeable and is seen in satellite images for morphostructures subjected to tectonic uplift, the rate of which is commensurable with or beyond the rate of the rising sea level. This is the Nanosnyy Island region in the East Siberian uplift zone and Semyonovskaya Shallow, which is ascribed to the seismically active zone of the Laptev Sea.

6. Ice processes also play an important role. They stimulate sedimentation owing to transport of bottom sediments by drifting ice, contribute to freezing

by desalinating sediments in locations of stamukha formation and provide protection from storms for newly formed islands and banks.

7. Archives of satellite images and modern technologies for their processing play a significant role in the study of morphogenesis on the shallows of Arctic Seas.

Acknowledgements. *The authors express their gratitude to A.A. Kucheiko for useful information obtained from Sentinel and Terra/MODIS satellite images, for the suggestions and advice, to V.E. Tumskoy for the remarks that made it possible to substantially improve the original version of the article.*

References

Are, F.E., 1998. The thermoabrasion of Laptev Sea shores and its input into sediment balance of the sea. Kriosfera Zemli [Earth's Cryosphere], II (1), 55–61 (in Russian).

Are, F.E., 2012. Coastal Erosion of the Arctic Lowlands. Academic Publishing House "Geo", Novosibirsk, 291 pp. (in Russian).

Avetisov, G.P., 2004. Seismicity of the Russian Arctic continental margin. Geology and mineral resources of Russia. Six volumes. Volume 5. Arctic and Far East Seas. Book 1. Arctic seas. VSEGEI, St. Petersburg, pp. 31–43 (in Russian).

Barnes, P.W., Rawlinson, S.E., Reimnitz, E., 1988. Coastal geomorphology of Arctic Alaska. In: Arctic Coastal Processes and Slope Protection Design. A.T. Chen, C.B. Leidersdorf (Eds.). American Society of Civil Engineers, New York, pp. 3–30.

Burguto, A.G., Dorofeev, V.K., Rekant, P.V., et al., 2016. State Geological Map of the Russian Federation. Scale of 1:1 000 000 (third generation). Laptev-Siberian Sea series. Sheet S-53. Stolbovoy Island; S-54 Lyakhovsky Islands. Explanatory letter. Cartographic factory VSEGEI, St. Petersburg, 300 pp. + 9 tabs. (in Russian).

Charkin, A.N., Dudarev, O.V., Semiletov, I.P., Shilo, I.N., 2007. The Current State of Relict Banks on the shelf of the East Siberian Seas. In: Cryogenic Resources of Polar Regions. Materials of the International Conf. (Salekhard, June 2007). ONTI of the Pushchino Scientific Center of the Russian Academy of Sciences, Pushchino, vol. 1, pp. 184–186 (in Russian).

Dmitrenko, I.A., Kirillov, S.A., Tremblay, B., et al., 2011. Recent changes in shelf hydrography in the Siberian Arctic: potential for subsea permafrost instability. J. Geophysical Research, vol. 116, C10027, DOI: 10.1029/2011JC007218.

Dudarev, O.V., 2016. Recent lithomorphogenesis on the East Arctic shelf of Russia. Abstract... doc. g-m. n., Vladivostok, 49 pp. (in Russian).

Dudarev, O.V., Charkin, A.N., Semiletov, I.P., et al., 2015. Peculiarities of the present-day morpholithogenesis on the Laptev Sea Shelf: Semenovskaya Shoal (Vasema Land). In: Proceedings of the Academy of Sciences, 462 (1), 510–516 (in Russian).

Fartyshev, A.I., 1993. Features of the Coastal Shelf Cryolithozone of the Laptev Sea. Nauka, Novosibirsk, 136 pp. (in Russian).

Gakkel, Ya.Ya., 1957. Science and development of the Arctic. Morskoy transport, Leningrad, 132 pp. (in Russian).

Gavrilov, A.V., Romanovskii, N.N., Hubberten, H.-W., Romanovsky, V.E., 2013. Distribution of islands – ice complex remnants on the East Siberian arctic shelf. Kriosfera Zemli [Earth's Cryosphere], VII (1), 18–32 (in Russian).

Geography of the Soviet Arctic Seas, 1949. Proceedings of the AARI, vol. 8. No. 2. The Laptev Sea. Glavsevmorput, Moscow; Leningrad, 484 pp. (in Russian).

Geological Dictionary, 2011. In three volumes. Third edition, revised and additional. O.V. Petrov (Ed.). Vol. 2, VSEGEI, St. Petersburg, 446 pp. (in Russian).

Grigoriev, M.N., 2017. Study of permafrost formations degradation in East Siberia coastal zone (subsequent to the results of expeditions of 2014–2016). Arctic and Antarctic Research, issue 1, 89–96 (in Russian).

Gukov, A.Yu., 2014. Revival of Vasilievsky Island. Priroda [Nature], No. 5, 70–73 (in Russian).

IPCC, 2014: Climate Change, 2014: Synthesis Report. Contribution of Working Groups I, II and III to the Fifth Assessment Report of the Intergovernmental Panel on Climate Change [main group of authors, R.K. Pachauri and L.A. Meyer (Eds.)]. Geneva, Switzerland, IPCC, 163 pp.

Ivanov, V.L., Kim, B.I., Kos'ko, M.K., Ivanova, N.M., 2004. Geological structure and development history of the basin. Laptev sedimentary basin. In: Geology and mineral resources of Russia. Six volumes. Vol. 5. Arctic and Far East Seas. Book 1. Arctic seas. VSEGEI, St. Petersburg, pp. 274–310 (in Russian).

Jones, G., 1964. The Norse Atlantic Saga. Being the Norse Voyages of Discovery and Seetlement to Iceland, Greenland, America. Oxford University Press, London, 246 pp.

Kaplin, P.A., Leontiev, O.K., Lukyanova, S.A., Nikiforov, L.G., 1991. Shores (Nature of the World). Mysl, Moscow, 479 pp. (in Russian).

Katasonov, E.M., Pudov, G.G., 1972. Cryolithological studies in the area of Vankina Bay of the Laptev Sea. In: Permafrost research, vol. XII. Moscow State University Publishing House, Moscow, pp. 130–136 (in Russian).

Kempema, E.W., Reimnitz, E., Barnes, P.W., 1989. Sea ice sediment entrainment and rafting in the Arctic. J. Sediment. Petrol. 59 (2), 308–317.

Klimenko, V.V., Matskovsky, V.V., Dalmann, D., 2013. Comprehesive reconstruction of the temperature of the Russian Arctic over the past two millennia. Arktika: ekologiya i ekonomika [Arctic: Ecology and Economy], No. 4 (12), 84–95 (in Russian).

Klyuev, E.V., 1965. The role of permafrost factors in the dynamics of the bottom topography of the polar seas. Okeanologiya [Oceanology], 5 (5), 863–869 (in Russian).

Klyuev, E.V., 1970. Thermal abrasion of the polar seas coastal strip. Izvestiya VGO, 102 (2), 129–135 (in Russian).

Klyuev, E.V., Kotyukh, A.A., Olenina, N.V., 1981. Cartographic and hydrographic interpretation of the disappearance of Semyonovsky and Vasilievsky Islands in the Laptev Sea. Izvestiya VGO, 113 (6), pp. 485–492 (in Russian).

Koch, L., 1945. The East Greenland Ice. Meddelelser om Grőnland, Copenhagen, Bd. 130, No. 3, 373 pp.

Kucheiko, A.A., Ivanov, A.Yu., Ainov, K.V., Lisachenko, E.S., 2020. Detection of shallows and small islands in the southern part of the Laptev Sea using satellite data. Earth from Space, issue 27, 50–60 (in Russian).

Longinov, V.V., 1973. Sketches of Oceanic Lithodynamics. Nauka, Moscow, 244 pp. (in Russian).

Lukina, N.V., Patyk-Kara, N.G., Sokolov, S.Yu., 2003. Russian Arctic Seas. Neotectonic structures and active faults. In: Atlas: Geology and mineral resources of the Russian shelf areas. M.N. Alekseev (Ed.). Scientific World, Moscow, sheet 3–4 (in Russian).

Matul, A.G., Khusid, T.A., Mukhina, V.V., et al., 2007. Recent and Late Holocene environments on the southeastern shelf of the Laptev Sea as inferred from microfossil data. Oceanology 47 (1), 90–101 (in Russian).

Merkulov, V.A., Ashik, I.M., Timokhov, L.A., 2017. Tendencies of multi-year variability of the sea level at the coastal stations of the Arctic Ocean. Arctic and Antarctic Research, No. 3 (113), 51–65 (in Russian).

Molochushkin, E.N., 1969. On the nature of heat transfer between water and bottom sediments in the coastal zone of the Laptev Sea. In: Questions of the geography of Yakutia. Yakut book Publishing House, Yakutsk, issue 5, pp. 121–126 (in Russian).

Mustafin, N.F., 1961. On catastrophic surges in the southeastern part of the Laptev Sea. Arctic and Antarctic Research, No. 7, 59–65 (in Russian).

Nicolsky, D.J., Romanovsky, V.E., Romanovskii, N.N., et al., 2012. Modeling sub-sea permafrost in the East Siberian Arctic Shelf: The Laptev Sea region. J. Geophysical Research, vol. 117, F03028.

Nikonov, A.A., 2006. Modern movements of the Earth's crust. Ed. 2nd, sup., Editorial URSS, Moscow, 192 pp. (in Russian).

Ogorodov, S.A., 2011. The Role of Sea Ice in Coastal Dynamics. Publishing House MSU, Moscow, 173 pp. (in Russian).

Patyk-Kara, N.G., Arkhangelov, A.A., Plakht, I.R., 1989. Regional geomorphological benchmarks in the Cenozoic history of the Eastern Arctic. Geomorphology, No. 4, 96–104 (in Russian).

Pizhankova, E.I., 2016. Modern climate change at high latitudes and its influence on the coastal dynamics of the Dmitriy Laptev Strait area. Earth's Cryosphere XX (1), 46–59.

Pizhankova, E.I., Dobrynina, M.S., 2010. The dynamics of the Lyakhovsky Islands coastline (results of aerospace image interpretation). Kriosfera Zemli [Earth's Cryosphere], XVI (4), 66–79 (in Russian).

Popov, S.V., 1987. Marine names of Yakutia. Essays on the toponymy of the Laptev and East Siberian Seas. Book Publishing House, Yakutsk, 163 pp. (in Russian).

Rekant, P.V., Tumskoy, V.E., Gusev, E.A., et al., 2009. Distribution and peculiarity of bedding of the sub-sea permafrost near Semenovskoe and Vasilievskoe Shallows (Laptev Sea) revealed by high-resolution seismic profiling. In: System of the Laptev Sea and the Adjacent Arctic Seas: Modern and Past Environments. Moscow University Press, Moscow, pp. 332–348 (in Russian).

Report on the peculiarities of the climate in the territory of the Russian Federation for 2019, 2020. Roshydromet, Moscow, 97 pp. – http://www.meteorf.ru/press/news/20626/

Romanovskii, N.N., Gavrilov, A.V., Tumskoy, V.E., et al., 1999. Thermokarst and its role in the formation of the near shore zone of the Laptev Sea shelf. Kriosfera Zemli [Earth's Cryosphere], III (3), 79–91 (in Russian)

Romanovskii, N.N., Hubberten, H.-W., Gavrilov, A.V., et al., 2003. Permafrost and gas hydrate stability zone evolution on the eastern part of the Eurasia Arctic Sea shelf in the Middle Pleistocene–Holocene. Kriosfera Zemli [Earth's Cryosphere], VII (4), 51–64 (in Russian)

Safyanov, G.A., 1996. Coastal Geomorphology. Moscow University Press, Moscow, 400 pp. (in Russian).

Semenov, Yu.P., 1971. Conditions for the formation of bottom sediments in the Laptev Sea. In: Sea Geology. Publishing house of Research Institute of Arctic Geology, Leningrad, vol. 1, p. 47–53 (in Russian).

Sovershaev, V.A., 1981. Influence of Sea Ice on the Development of the Arctic Shelf Permafrost Zone (on the example of the Eastern Arctic Seas). In: Permafrost zone of the Arctic Shelf. Publishing House of the Institute of Permafrost Science of the Siberian Branch of the USSR Academy of Sciences, Yakutsk, pp. 70–83 (in Russian).

State Geological Map of the Russian Federation, 2014. Scale of 1:1 000 000 (third generation). Sheet S-51. Olenek Bay. S-52 Lena River Delta. Lithological map of the water area bottom surface. Cartographic factory VSEGEI, St. Petersburg (in Russian).

State Geological Map of the Russian Federation, 2016. Scale of 1:1 000 000 (third generation). Sheet S-53, 54 – Stolbovoy Island – Lyakhovsky Islands. Lithological map of the water area bottom surface. Cartographic factory VSEGEI, St. Petersburg (in Russian).

State Geological Map of the Russian Federation, 2017. Scale of 1:1 000 000 (third generation). Sheet S-50 – Ust-Olenek. Lithological map of the water area bottom surface. Cartographic factory VSEGEI, St. Petersburg (in Russian).

The history of the discovery and development of the northern sea route, 1954. Vol. 1. Morskoy transport, Moscow, 475 pp. (in Russian).

The second assessment report of Roshydromet on climate changes and their consequences on the Russian Federation territory. General summary, 2014. Roshydromet, Moscow. – URL: https://cc.voeikovmgo.ru/images/dokumenty/2016/od2/od2.pdf

Thomson, J., Rogers, W.E., 2014. Swell and sea in the emerging Arctic Ocean. Geophysical Research Letters, No. 41, 3136–3140.

Zakharov, V.S., 2006. Modern vertical movements of the Earth's crust. In: Modern global changes in the natural environment. In 2 volumes. Vol. 1. Scientific World, Moscow, pp. 626–643 (in Russian).

Zhigarev, L.A., Plakht, I.R., 1974. Features of the structure, distribution and formation of subaqueous cryogenic strata. In: Problems of Cryolithology. Moscow State University, Moscow, vol. IV, pp. 115–124 (in Russian).

Zhigarev, L.A., Sovershaev, V.A., 1984. Thermoabrasive destruction of the Arctic islands. In: Coastal Processes in Cryolithozone. Nauka, Novosibirsk, pp. 31–38 (in Russian).

URL: https://ru.wikipedia.org/wiki/Я_(остров) (last visited: 12.11.2019).

URL: https://ru.wikipedia.org/wiki/Коч (last visited: 05.02.2020).

URL: http://www.aari.ru/projects/ECIMO/?im=100 (last visited: 23.12.2020).

Received March 27, 2021
Revised version received January 17, 2021
Accepted February 3, 2021

EARTH'S CRYOSPHERE
SCIENTIFIC JOURNAL

Kriosfera Zemli, 2021, vol. XXV, No. 3, pp. 19–29

GEOLOGICAL CRYOGENIC PROCESSES AND FORMATIONS

GEOCRYOLOGICAL FACTORS OF DYNAMICS OF THE THERMOKARST LAKE AREA IN CENTRAL YAKUTIA

N.V. Nesterova[1,2], O.M. Makarieva[1,2], A.N. Fedorov[3], A.N. Shikhov[4]

[1] *St. Petersburg State University, Institute of Earth Sciences, Department of land hydrology, Universitetskaya nab. 7-9, St. Petersburg, 199034, Russia*
[2] *North-Eastern Permafrost Station of Melnikov Permafrost Institute, SB RAS, Portovaya str. 16, Magadan, 685000, Russia; nnesterova1994@gmail.com*
[3] *Melnikov Permafrost Institute, SB RAS, Merzlotnaya str. 36, Yakutsk, 677010, Russia*
[4] *Perm State University, Bukireva str. 15, Perm, 614068, Russia*

The analysis of Landsat satellite images revealed a significant increase in the area of thermokarst lakes in Central Yakutia over the period 2000–2019. The lake area increased twice in the Suola and Taatta River basins and by 25 % in the Tanda River basin. It has been established that, despite the presence of a general linear trend, the increase in the area of lakes occurs abruptly. Qualitative relationship between the changes in the state of the upper layer of permafrost and the dramatical increase in the area of thermokarst lakes has been revealed. The main factor leading to disruption of a stable state of thermokarst forms are short-term (1–3 years) periods of sudden changes in temperature of seasonally thawed layer from below-average to anomalously high values. These periods can be caused by a rare combination of hydrometeorological conditions, such as anomalously high values of snow water equivalent, increased annual precipitation, and an increased water content of soils of the seasonally thawed layer.

Key words: *thermokarst lakes, permafrost, Landsat images, Central Yakutia, temperature and water content of a seasonally thawed layer, precipitation, snow cover, Spasskaya Pad'.*

INTRODUCTION

Central Yakutia is characterized by the widespread occurrence of thermokarst formations [*Soloviev, 1959; Bosikov, 1991*]. Their most evident manifestation is thermokarst lakes, which occupy 80 % of the total number of lakes in Yakutia [*Nestereva, 2012*]. Such lakes have a significant influence on the formation of the water balance of the territory [*Karlsson et al., 2012; Fedorov et al., 2014; Swanson, 2019*] and the development of economic activity [*Crate et al., 2017*]. The study of the conditions, under which thermokarst processes are activated, is extremely relevant against the background of the forecasted significant climate warming in Central Yakutia [*Streletskiy et al., 2019*].

Changes in the number and the area of thermokarst lakes in different Russian regions and worldwide have been observed under the conditions of modern climate warming. For example, a significant decrease in the area of thermokarst lakes in the northwestern part of Alaska has been noted due to an increase in the intensity of thermoerosion processes [*Jones, Arp, 2015; Swanson, 2019*]. In the Northwestern Territories of Canada, the total area of thermokarst lakes generally increased between 1978 and 1992 and decreased between 1992 and 2001 [*Plug et al., 2008*]. In Russia, multidirectional changes in the area of thermokarst lakes have been revealed only in 8 out of 20 reference areas located in different parts of the cryolithozone; however, no unambiguous relationship between the dynamics of lakes and geocryological conditions has been derived [*Kravtsova, Bystrova, 2009*]. In the work of S.N. Kirpotin [*Kirpotin et al., 2008*], it was established that the total area of lakes in the zone of the continuous permafrost increases, while in the zone of the discontinuous permafrost, on the contrary, it decreases. The modern estimates of changes in the area and number of thermokarst lakes in Central Yakutia are presented in many works. For example, J. Boike [*Boike et al., 2016*], I. Nitze [*Nitze et al., 2017*], and M. Ulrich [*Ulrich et al., 2017*] point to a growth in the area of lakes in this region. According to T.V. Rodionova, V.I. Kravtsova, and T.V. Tarasenko, the total area and number of thermokarst lakes expanded by two to three times for different sites over the period from 1980 to 2009 [*Kravtsova, Tarasenko, 2011; Rodionova, 2013*].

The purpose of this work is to study the conditions leading to the nonlinear dynamics of the increase in the number and the area of thermokarst lakes in Central Yakutia on the basis of the remote sensing data and observations of a state of a seasonally thawed layer. The study accomplished two basic

tasks: 1) the changes in the area of thermokarst lakes in the basins of three rivers of Central Yakutia have been assessed on the basis of the Landsat satellite images in period 2000–2019; 2) the qualitative relationship between the state of the seasonally thawed layer of permafrost deposits, climatic factors, and the increase in the area of thermokarst lakes in Central Yakutia has been revealed.

THE STUDY AREA

The study area is located within the Lena–Amga interfluve in the southeastern part of the Central Yakutia lowland. Geocryological studies of this region were previously conducted by many authors, e.g., V.G. Zolnikov [*1954*], P.A. Soloviev [*1959*], M.S. Ivanov [*1984*], and N.P. Bosikov [*1991*].

The average absolute elevation of the lowland is 250 m with the maximum values up to 400 m. The Paleozoic, Mesozoic, and Cenozoic rocks form the geological structure of the territory. Deep faults played an important role in the history of its development. During the Cenozoic, tectonic activity in such zones had an influence on the formation of main geomorphological levels, structure, thickness, ice content of permafrost deposits and on the development of thermokarst [*Ivanov, 1984*].

The region has a severely continental climate. Over the period 1966–2018, the mean annual air temperature at the Yakutsk weather station was –8.8 °C. The maximum mean monthly temperature is observed in July and reaches +19.5 °C, the minimum mean monthly temperature is recorded in January and drops down to –38.6 °C. The mean annual amount of precipitation is 237 mm, 75–85 % of precipitation falls in summer [*Bosikov, 1991*]. The snow cover forms in October, breaks up in the first days of May; by the beginning of snowmelt, its depth is 36 cm on average (w/s Yakutsk, 1966–2018).

Central Yakutia belongs to the area of the continuous permafrost. The permafrost thickness varies from 10 to 50 m in a low floodplain, from 50 to 300 m in middle and high floodplains; it increases on terraces, exceeding 400 m in some areas [*Ivanov, 1984*]. The depth of seasonal thawing varies from 0.5 m in waterlogged areas to 4 m in pine forests [*Ivanov, 1984*]. The study area is located in the zone, where there are the Late Pleistocene deposits of the ice complex, the high ice content of which is a factor of thermokarst development both in the past and in the modern climatic conditions. Taliks are common in river valleys and under large thermokarst lakes.

The predominant landscape of the area is herb-cowberry larch forest on permafrost-taiga pale, sod-forest, and alluvial meadow soils [*Ivanov, 1984*].

One of the main features of the region is the poorly developed river network and the widespread erosion-thermokarst depressions [*Zolnikov, 1954*]. The most mature thermokarst forms, alas depressions with the flattened and sodded sides are covered with meadow-steppe vegetation on saline soils.

The study area involves the basins of three rivers (Suola, Tanda, and Taatta) with areas from 1270 to 8290 km^2 with the widespread alas depressions (Table 1, Fig. 1). The basins of these rivers were chosen as the objects of the study due to the availability of hydrological gauges with data on the river discharge observations in the period 1960–2017. These data are necessary for the next stage of the work related to the assessment and modeling of the role of thermokarst lakes in the hydrological regime of the Central Yakutia rivers. The alas area percentage of the watershed area was estimated on the basis of the works of J.I. Torgovkin and A.A. Shestakova [*Torgovkin et al., 2018; Torgovkin, Shestakova, 2018*]. It varies from 4.9 % within the Tanda River watershed to 9.7 % in the Suola River watershed, upstream the hydrological gauge (h/g) of Bedeme village.

Table 1. **The distribution of alases and thermokarst lakes in the river basins (2000–2019)**

Name of the basin	Code of the hydrological gauge	Watershed area, km^2	Alas area		Number of images	The minimum area of lakes			The maximum area of lakes			The changes in the area of lakes		The area of lakes, 09.06.2019	
			km^2	%		km^2	%	year	km^2	%	year	km^2	% of the initial value	km^2	%
Suola River–Byuteidakh settlement	3217	1270	81.7	6.4	58	8.9	0.7	2003	19.4	1.5	2018	10.5	117	17.9	1.4
Tanda River–Byariya village	3306	2000	97.9	4.9	11	23.4	1.2	2001	29.4	1.4	2018	6.0	25	27.7	1.4
Taatta River–Uolba village	3628	8290	776.0	9.4	7	118.0	1.4	2001	225.0	2.7	2018	107.0	90	213.3	2.6
Suola River–Bedeme village	3659	3380	326.0	9.7	27	34.0	1.0	2004	70.8	2.0	2008	36.8	108	66.1	1.9

Note: Relative values of the area are given as a percentage of the watershed area.

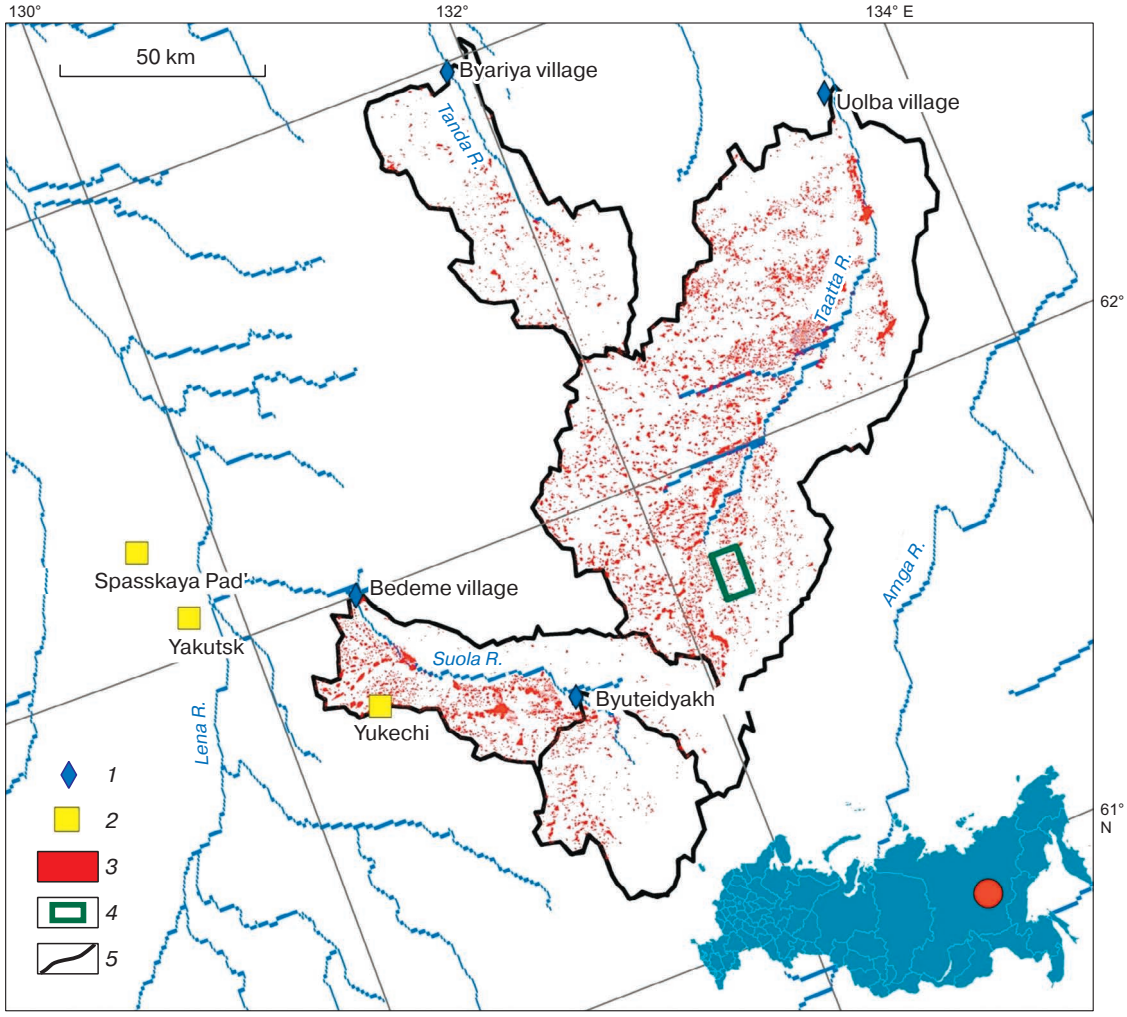

Fig. 1. The map of the study area.

1 – hydrological gauge, *2* – monitoring site/weather station, *3* – alases, *4* – reference site, *5* – boundary of watershed.

MATERIALS OF THE STUDY

Remote sensing data. Different types of the remote sensing data are used to study the long-term dynamics of thermokarst lakes. The aerial survey data or ultrahigh resolution (1 m and more) satellite images were used in some works [*Sannel, Brown, 2010; Jones et al., 2011*]. Until recently, their disadvantage has been rare repeatability of survey. As a result, anomalous meteorological conditions (e.g., heavy precipitation), that might occur shortly before the survey, could lead to improper conclusions about the changes in the area of thermokarst lakes [*Olthof et al., 2015*]. Only in 2017, after the launch of nanosatellite from the Planet Labs, it became possible to monitor the area of thermokarst lakes with a high spatial resolution (3 m) in the daily mode [*Cooley et al., 2017*].

The Landsat satellite images (TM, ETM+ and OLI sensors) with a spatial resolution of 30 m remain the main data source for estimating the changes in the area of thermokarst lakes over long periods of time (more than 10 years). Estimation of the areas of lakes using these data is less accurate than estimation on the basis of super-resolution images. However, the most important advantage is the availability of the homogeneous series of observations for the period since 1984 (since 1999 for some regions of Russia, including Central Yakutia). In addition to the spatial resolution, the Landsat data is limited by a high share of cloudy images. The frequency of cloud-free images turns out to be several times lower than the nominal temporal resolution (16 days).

To distinguish the water surface from satellite data, the mid-infrared (SWIR) spectral range [*Frazier, Page, 2000*] or spectral indices, based on it, are used. The most effective of the indices is considered to be the normalized difference water index mNDWI [*Xu, 2006*]. When identifying thermokarst lakes,

there is the problem related to the fact that the area of most of the lakes is comparable with the area of one pixel of Landsat image (0.09 ha). Thus, more than 50 % of the pixels, falling within the limits of thermokarst lakes, are not fully occupied by water. To estimate accurately the area of thermokarst lakes, it is recommended to determine the percentage of water area in each pixel on the basis of the spectral mixture analysis [*Olthof et al., 2015*], or consider only relatively large lakes (with the area over 0.5–1.0 ha), which will give a lesser error.

In this study, 54 Landsat images (sensors TM, ETM+, OLI) for the period from 2000 to 2019, were used. They were obtained from the web-service of the USGS [*USGS..., 2020*] to determine the area of thermokarst lakes in Central Yakutia. We considered the images of the summer season (from June to September). The choice of images for the entire summer season (and not only for its second half, when the lake area reaches the seasonal minimum) was due to the scarcity of cloud-free data. It is also important to note that in most cases, the intra-annual variability of the water surface area is less than the interannual variability. To minimize the errors in determining the area of lakes, the cutoff threshold for the minimum area was taken to be 1 ha (which corresponds to 11 pixels of the Landsat imaging system). To reduce the estimation errors for each particular lake, we chose the threshold equal to 1 ha for the assessment of the minimum area of lakes. When the threshold value equal to 0.4 ha is chosen, such errors can be very significant, because image pixels do not fall completely within the limits of the water surface of a lake.

The methodology of identification of the lakes included the following stages:

1) the recalculation of values of brightness in spectral channels from initial values (Digital Numbers, DN) into reflectance and the atmospheric correction by Dark Object Subtraction (DOS). This operation was performed using the "Semi-automated image classifier" software module of the QGIS geoinformation system [*Congedo, 2016*], which is used for loading, preprocessing, and classification of images from the satellites of Landsat series, Sentinel-2, and Terra/Aqua MODIS;

2) the water surface distinguishing by the threshold value of the Modified Normalized Difference Water Index (MNDWI), which is assumed to be 0.3. The author of this index [*Xu, 2006*] proposed the lower threshold (0.09). In this work, an increase in the threshold value allowed us to separate partially the water surfaces and the shadows from clouds;

3) the conversion data to a vector format, calculation of areas, and removal of the objects smaller than 1 ha in area. The capabilities of the ArcGis Model Builder were used to automate calculations at 2–3 stages. The area of the lakes was calculated for each image separately, with subsequent removal of duplicate objects in overlapping areas of the images.

In addition to removal of lakes with a small area, the data are basically restricted by the presence of shadows from clouds in most of the images. Shaded areas also have low brightness in the SWIR range and can be mistakenly attributed to water objects. Most of the obtained images contained the cumulus clouds and shadows from them, which occupied 1–5 % of the area. In this regard, we have been able to estimate the area of thermokarst lakes on all 54 images only for the basin of the Suola River–Byuteidyakh settlement, which has the minimum area, but is representative for the selected territory. The total area of the lakes in the basin of the Suola River–Byuteidyakh settlement has the significant correlation with the total area of the lakes in the neighboring watersheds, obtained for the same dates with the use of the images without cloud cover. The coefficient of determination of the total area of thermokarst lakes in the upper and lower parts of the Suola River basin is 0.79. For the other basins, the number of completely cloudless scenes ranged from 7 to 25.

Additionally, in this work, we have studied dynamics of thermokarst lakes in the territory of Yukechi monitoring site on the area of 113 ha (similar to the area presented in [*Fedorov et al., 2014; Ulrich et al., 2017*]) over the period 2000–2019. Using the abovementioned method, 44 images were analyzed, from which 27 images were taken in the same dates as the images of the watershed of the Suola River–Byuteidyakh settlement. In doing so, we considered a lake area of less than 1 ha as an area of a whole pixel, in which the lake was included.

Ground-based observation data. To assess the relationship between the characteristics of the seasonally thawed layer and snow cover and dynamics of the development of thermokarst lakes, we used the data of observations from the Spasskaya Pad' monitoring site, which is located on the flat inter-alas plain with the indigenous larch forest growing on fine-grained sands. Materials included daily data on the soil water content at depths of 0.1, 0.2, 0.4, 0.6, and 0.8 m and the temperature at a depth of 1.2 m over the period 1998–2010 [*GAME–Siberia..., 2003; Iijima et al., 2010*], as well as the data on the soil water content (up to 1.5 m) and the soil temperature (up to 3.2 m), which were measured 1–2 times a month over the period 1998–2018 (data provided by A.N. Fedorov, Melnikov Permafrost Institute, SB RAS). In the work [*Iijima et al., 2010*], it was demonstrated that the data from Spasskaya Pad' site are representative of the typical landscape conditions of Central Yakutia. The data on the snow cover (1996–2018) and the soil temperature (1964–2017) at a depth of 1.6 m at the Yakutsk weather station were also used for the analysis (Fig. 1).

RESULTS OF THE DATA ANALYSIS

Dynamics of thermokarst lake area. In the basins of the Suola and Taatta rivers, the area of thermokarst lakes doubled in the period 2000–2019. In the basin of the Tanda River–Byariya village, the area of the lakes increased only by 25 % (6 km^2) (Table 1). Its basin is characterized by the smallest area of the distribution of alas depressions (4.9 %, Table 1). This is most likely related to the sporadic (more limited compared to other considered basins) distribution of the Ice Complex on the Emil terrace of the Lena–Amga interfluve [*Soloviev, 1959; Zakharova et al., 2018*]. Despite the fact that this part of the ancient terrace of the Lena River represents the widespread surface with small lakes (0.018–0.075 km^2) [*Zakharova et al., 2018*], the threshold of the minimum area of lakes (1 ha), used in this study, allows us to trace their dynamics.

Figure 2 demonstrates the increase in the total area (both residual and primary) of thermokarst lakes from 2001 to 2019 at the most representative site (Fig. 1) in the western part of the Taatta River basin. On July 17, 2001 (Fig. 2, *a*), there were 20 lakes with the total area of 93 ha at the site. Over 18 years, the total number of lakes and their area have almost increased fourfold (76 lakes with the total area of 323 ha were recorded on July 27, 2019) (Fig. 2, *b*).

Figure 3 represents a plot of the changes and a diagram of the range of changes in the area of lakes in the basin of the Suola River–Byuteidyakh settlement in the period 2000–2019. The maximum area of the lakes was observed in 2008 and 2018, and the minimum area – in the period 2001–2004. There is a proportional increase in the area of both residual and primary thermokarst lakes. For the watershed of the Suola River–Byuteidyakh settlement, the area of primary thermokarst lakes, not intersected by alases, was 1.1 km^2 (or 11.8 % of the total area of lakes of 9.3 km^2) on 17.07.2001, and 3.0 km^2 (or 17.0 % of the total area of lakes of 17.9 km^2) on 07.08.2020. A similar situation is observed in the basin of the Tanda River–Bariya village: the area of primary thermokarst lakes increased by 1.8 km^2 from 2001 to 2019 (4.6 km^2 or 19.7 % of the total area of lakes of 23.3 km^2 and 6.4 km^2 or 22.7 % of the total area of lakes of 28.2 km^2, respectively).

The increase in the number of primary thermokarst lakes is confirmed by the observations at Yukechi site [*Ulrich et al., 2017*]. Between 1944 and 2014, 15 new primary thermokarst lakes with the total area

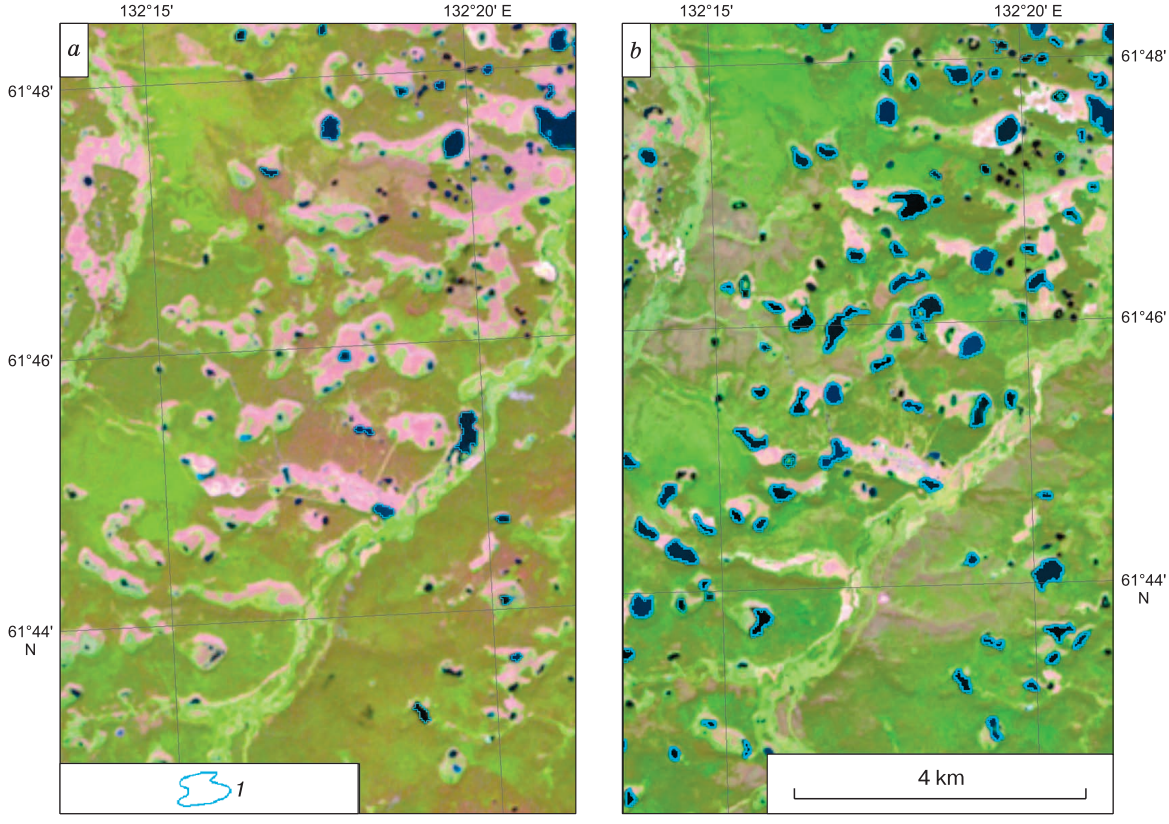

Fig. 2. Increase in quantity and the area of the residual thermokarst lakes by the example of the western part of the Taatta River basin, revealed on the basis the Landsat images taken at different times:

a – 17.07.2001, *b* – 27.07.2019. *1* – thermokarst lakes.

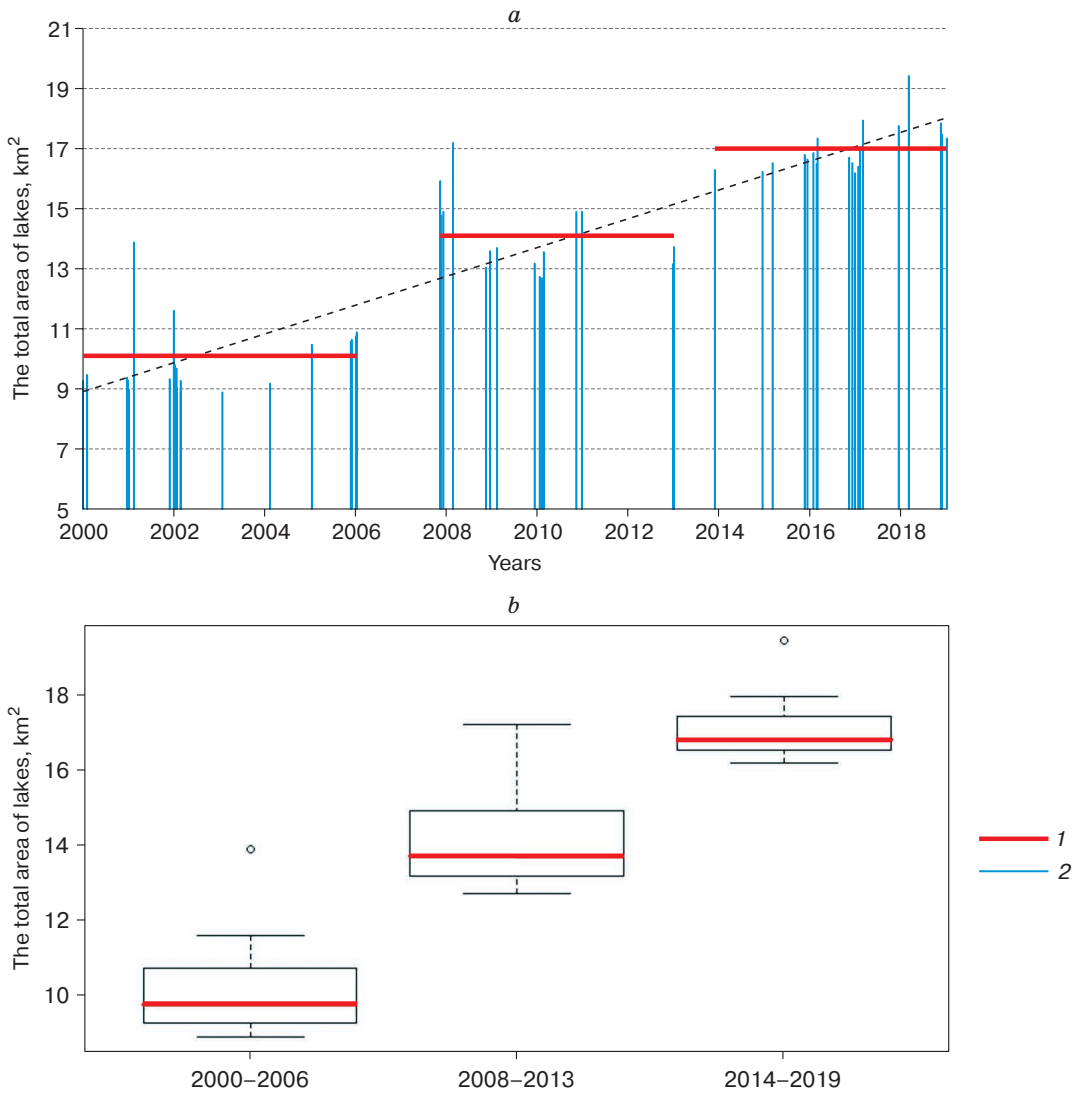

Fig. 3. The trend of changes (*a*) and the diagram of the spread of the area (*b*) of thermokarst lakes in the watershed of the Suola River–Byuteidyakh settlement over the period 2000–2019.

1 – the average area of lakes over the periods 2000–2006, 2008–2013, and 2014–2019; *2* – the area of lakes on specific dates. Data with omissions in 2007 and 2012.

of 0.7 ha (an increase from 0.04 to 0.6 % of the site area) were formed at the site. During the same period of time the area of residual lakes increased from 0.4 to 1.4 ha (from 0.4 to 1.2 %). In total, the area of residual and primary thermokarst lakes of Yukechi site increased more than fourfold (from 0.5 ha to 2.1 ha or from 0.4 to 1.9 %) over the period 1944–2014.

The comparison of the area of lakes at the watershed of the Suola River–Byuteidyakh settlement and the total area of the lakes at Yukechi site points to the unidirectional tendency of their increase with the *R*-squared value of 0.79 (Fig. 4). Thus, we can assume that the observations at Yukechi site are representative for the study area. On the basis of the established relationship (Fig. 4) and historical data on the area of lakes at Yukechi site, which have been recorded since 1944 [*Ulrich et al., 2017*], we assumed that the total lake area increased more than 2.5-fold (from 6.8 km^2 in 1944 to 17.6 km^2 in 2019) in the watershed basin of the Suola River–Byuteidyakh settlement over the period 1944–2019; the main increase occurred between 2000 and 2019 (2-fold).

Despite the presence of the general linear trend of increase in the area of lakes, the changes occur abruptly. For example, in 2007 and 2014 there was dramatical expansion in the area of lakes, determining its dynamics in subsequent years (Fig. 3). An average area of the lakes in the Suola River basin–Byu-

teidyakh settlement was 10.1 km^2 in the period 2000–2006, 14.1 km^2 in the period 2008–2013, and 17.0 km^2 in the period 2014–2019.

This is proved by the work [*Ulrich et al., 2017*], in which the authors identified the trend of significant short-term increases in the lake areas over short periods of time, e.g., 1965–1967, 1992–2010 (with the largest increase between 2007–2008), and 2012–2014. The authors point to both the increase in the residual lakes and the active appearance of new primary thermokarst lakes in recent years. The rates of expansion of the residual and primary thermokarst lakes reach, on average, 1.6 and 1.2 m/year for the period 1944–2014, respectively.

Geocryological factors affecting thermokarst processes in Central Yakutia. To identify the relationship between the changes in a thickness of a seasonally thawed layer and the increase in the area of thermokarst lakes in Central Yakutia, we analyzed data of the ground-based observations.

In the work [*Rodionova, 2013*], dynamics of the thermokarst processes in Central Yakutia is associated with changes in the precipitation regime. Indeed, the dramatical increase in the lake area in 2007–2008 was preceded by the period 2005–2008 with anomalously snowy winters and with the total annual precipitation exceeding the norm by 20–43 %. While the average value of snow water equivalent was 59 mm by the beginning of snowmelt according to the snow survey at the Yakutsk weather station (1966–2018), in 2005–2007 this value was 88, 86 and 78 mm exceeding the norm by 49, 46 and 32 %, respectively [*Bulygina et al., 2020*]. The average annual amount of precipitation for the period 2005–2008 was 303 mm (while the norm was 237 mm). However, there is no direct functional relationship between the area of thermokarst lakes and the amount of solid or total precipitation.

In the work [*Iijima et al., 2010*], the geocryological consequences of heavy precipitation in the study

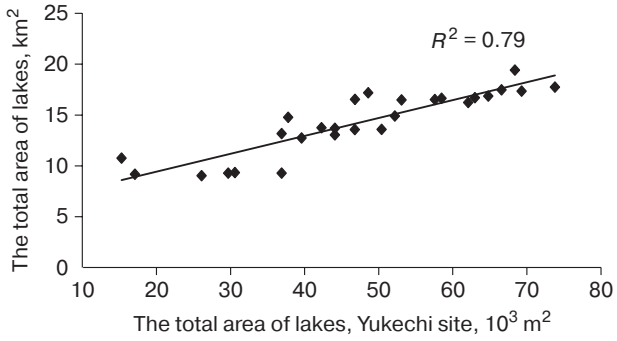

Fig. 4. Dependence of the total area of lakes in the watershed of the Suola River–Byuteidyakh settlement on the total area of lakes at Yukechi site lakes on the basis of the Landsat images for the same dates, 2000–2019.

period were considered in detail. Anomalously high values of snow water equivalent and liquid precipitation in the pre-winter period resulted in a prolonged period of the increased soil water content in the seasonally thawed layer in Central Yakutia. Thus, in 2006, according to the data from Spasskaya Pad' site, the average soil water content of the upper 80-cm layer was 24 % during the warm period (May–September) compared to 11 % in 2003. On October 1, 2006, before the beginning of freezing, soil was in a state of complete water saturation (the soil moisture content was 50 % in the upper 10-cm layer and 46 % in the 80-cm layer). Thus, by the beginning of snowmelt in 2007, the soil was frozen and, probably, the ice content was even higher due to water migration to the freezing front. The maximum measured soil water content in the 1-meter layer was up to 34 % in 2006, and only 14 % in 2003.

Figure 5 demonstrates, that the maximum area of thermokarst lakes in the basin of the Suola River–Byuteidyakh settlement is related to the average (for the warm period) and the maximum daily soil water content for the layer of 1 m and 0.8 m thick in the previous year. The correlation coefficient is 0.63 and 0.80, respectively. Obviously, the identified dependences have the qualitative nature, because they can be built only for a short period of time, characterized by a dramatical change in the study values. In the future, in dry years, when the soil water content will be minimal, the area of lakes most likely will not decrease to the level of the 2000s.

As a result of the combined effect of two interrelated factors – the significant soil water and ab-

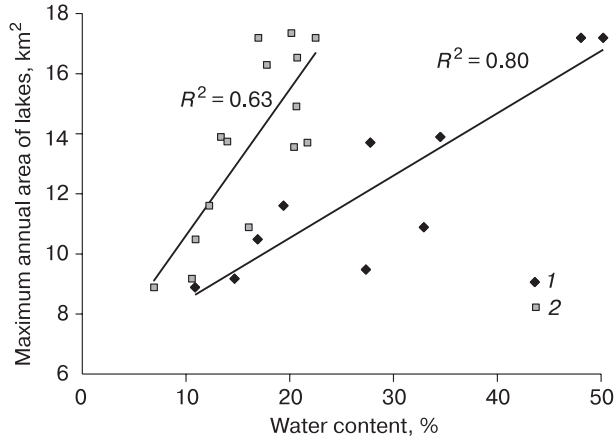

Fig. 5. Dependence of the maximum total area of lakes in the watershed of the Suola River–Byuteidyakh settlement of soil water content at Spasskaya Pad' site in the preceding year.

1 – maximum for the year daily soil water content of the top layer 0.8 m thick (1999–2008); *2* – mean annual soil water content of the layer 1 m thick during the warm period (2000–2015).

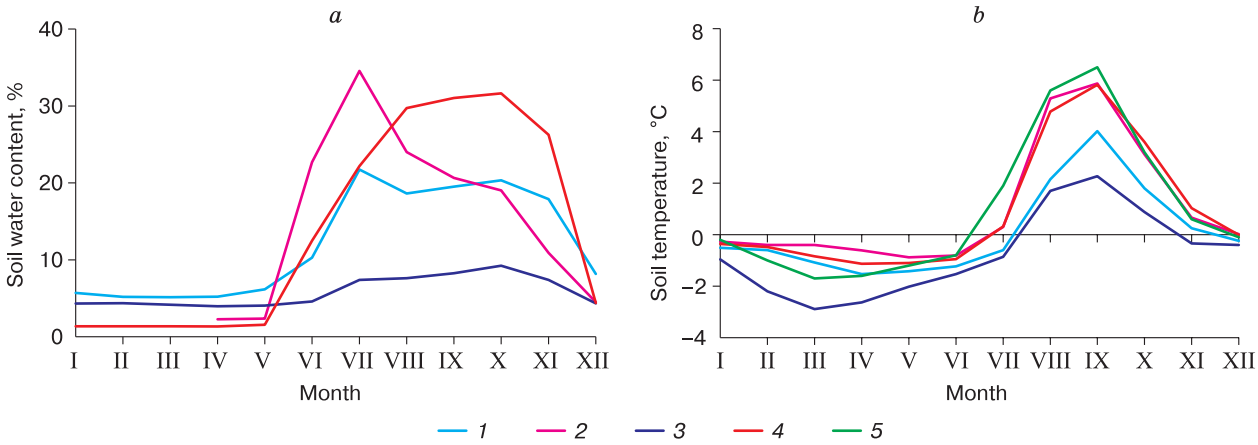

Fig. 6. Mean monthly values of the soil water content at a depth of 0.8 m at Spasskaya Pad' site (*a*) and the soil temperature at a depth of 1.6 m according to data from Yakutsk weather station (*b*).

1 – 1998–1999; *2* – 2000; *3* – 2003–2004; *4* – 2005–2007; *5* – 2014.

normally high values of snow water equivalent – the thermal regime of soil changes. Figure 6 represents the plots of changes in the mean monthly values of the soil water content of the 0.8-m layer and the soil temperature at a depth of 1.6 m. It is seen that the periods of increased soil temperature correspond to the periods of increased soil water. For example, the increased soil water content in 2005 due to high values of snow water equivalent in winter and heavy precipitation in summer, as well as the snow cover depth in the next winter season, prevented soil freezing, which resulted in the increase in soil temperature at a depth of 1.6 m in 2006. The winter period between 2006 and 2007 was also characterized by the snow cover with the above normal thickness, which again resulted in the increase in the soil temperature in 2007. The maximum depth of thawing before 2004 varied from 1.37 to 1.57 cm; in 2007 it was 1.67 cm [*Iijima et al., 2010*]. The periods, when the considered values changed, also coincide with the main periods of abrupt change in the area of lakes.

We plotted changes in the average total area of lakes in the basin of the Suola River–Byuteidyakh settlement and the mean monthly minimum (March–April) and maximum (September) soil temperatures at a depth of 1.6 m at the Yakutsk weather station (Fig. 7). Comparison of the data of the lake area with the data from w/s Yakutsk is due to the fact that, unlike Spasskaya Pad' site, where data are available only for the individual, not always comparable, dates, at the weather station, the daily data are available for the entire year. Nevertheless, the relationship between the values of the soil temperature at the two sites has a high correlation (0.77).

The coefficient of determination between the total area of lakes and the soil temperature at a depth of 1.6 m with a shift of 1 year is 0.12, but Fig. 7 clearly illustrates that the tendency of changes in the area of lakes repeats the variations of the soil temperature with a 1-year delay. The increase in the soil temperature in 2005–2007 is followed by the dramatical expansion in the area of lakes from 8.9 to 15.7 km^2 in 2007–2008. A similar situation is observed in 1999–2000: the dramatical increase in the soil temperature by 0.8 °C in March–April and by 1.9 °C in September in 1999–2000 is followed by a jump in the area of lakes from 9.4 to 10.4 km^2 in 2000–2001. In 2014, the high values of the maximum temperature (6.5 °C in September) were also accompanied by an increase in the area of lakes (Fig. 7).

According to the data from Yukechi site [*Ulrich et al., 2017*], the maximum change in the lake area occurred in 1966–1967, when the total lake area dramatically increased from 0.5 ha (1965) to 1.2 ha (1967). In August 1966–1967, mean monthly values of the maximum soil temperatures at 1.6-m depth were 4.1 °C in 1966 and 5.0 °C in 1967, significantly exceeding the mean annual temperature of 3.2 °C (1964–1980).

One of the possible mechanisms for the fast expansion in the area of primary thermokarst lakes may be cryogenic landslides on the shores of lake depressions, which indicate the activation of thermokarst processes [*Leibman, 2005; Pelletier, 2005; Smith et al., 2005; Sannel, Kuhry, 2011*]. Small thermokarst forms – byllars – are often formed along the lakeshores [*Brouchkov et al., 2004; Séjourné et al., 2015*].

When the soil temperature increases, the depth of thawing increases, the soil is saturated with thawed ice and the soil blocks move down the slope. As a result, these blocks are accumulated and the process attenuates until the time of a new onset of a certain combination of extreme hydrometeorological conditions. An example is the coastal retreat in 2011–2013,

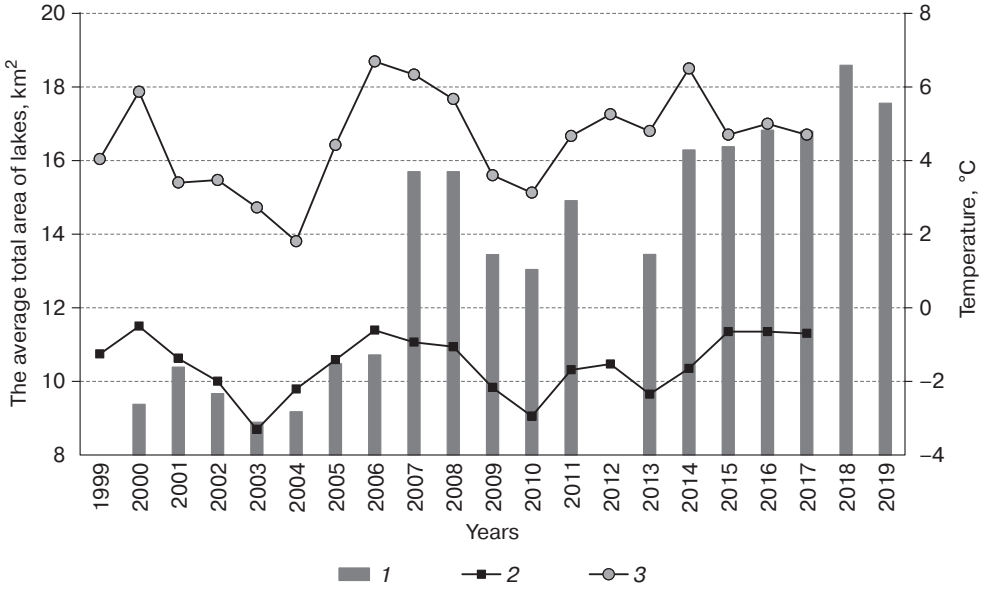

Fig. 7. Changes in the average total area of lakes and the mean soil temperature in March–April and in September at a depth of 1.6 m at Yakutsk weather station.

1 – mean area of lakes, Suola River–Byuteydyakh settlement; *2* – the mean soil temperature at a depth of 1.6 m for March–April; *3* – the mean soil temperature at a depth of 1.6 m for September. Assuming that the area of lakes in 2007 is not less than the area of lakes in 2008.

demonstrated in the work of A. Sejourné et al. [*Séjourné et al., 2015*], the rate of which varied from 0.5 to 3.16 m/year.

When the amount of atmospheric precipitation increases and, as a consequence, the level of lakes rises, additional erosion of the shores takes place. Under conditions of highwater levels, maintaining for 1–2 years, and due to the impact of new thermal impulse, the thawed sediments are oversaturated with water and collapse, thus increasing the area of the lake basin [*Leibman, 2005; Séjourné et al., 2015*].

In spite of the leading role of rainfall or snowmelt, which form the short-lived maximums of the lake areas, the lakes do not return to their initial state after their abrupt increase in area. This is confirmed by the data of [*Zakharova et al., 2018*], satellite altimetry pointing to the initial rise in the water levels of thermokarst lakes in 2006 with the maximum areas of lakes in 2007 and 2008. The average level rise between 2006 and 2009 was 130 cm with the maximum values up to 230 cm. After 2009, the water level began to drop and, over the period 2013–2016, decreased only by 70 cm on average with the maximum decrease of 120 cm [*Zakharova et al., 2018*].

Geocryological conditions have a direct impact on the development and the increase in the area of thermokarst lakes in Central Yakutia in the long term. It is evident, that the local conditions significantly determine dynamics of the temperature and the soil water content of the seasonally thawed layer. The limited point data of observations, which we are forced to use as indicators for large areas, allows us to establish only qualitative relations between the area of lakes and changes in the characteristics of permafrost deposits. The trend of the changes in these values (observed or forecasted) may serve as the indicator of the tendencies in the development of thermokarst processes in Central Yakutia.

CONCLUSIONS

On the basis of the Landsat satellite images, it has been revealed that the total area of the lakes in the basins of the Suola, Tanda, and Taatta rivers in the eastern part of Central Yakutia increased over the period 2000–2019. The development of the lakes occurs at different rates in different areas, with proportional growth for both the residual lakes and the primary thermokarst lakes. In the basins of the Suola and Taatta rivers, the area of the lakes doubled over the 20-year period; in one of the sites of the Taatta River basin, the number of lakes and their area increased almost 4 times over 18 years, and in the basin of the Tanda River – by 25 %, which is most likely due to the more limited distribution of the Ice Complex compared to other considered basins.

Using the identified relationship between the area of the lakes in the Suola River basin and dynamics of the area of the lakes at Yukechi site, we assumed that the total area of the lakes during the period 1944–2019 in the basin of the watershed of the Suola River–Byuteidyakh settlement increased more than

2.5-fold, with the main increase between 2000 and 2019 (2-fold).

It has been established that despite the presence of the general linear trend of increase in the area of the lakes, it occurs abruptly. The periods 1965–1967, 1999–2001, 2006–2008, and 2014–2015 are the examples, when there were dramatical expansion in the lake area, which caused the development of the lakes in subsequent periods. This is proved by the work of other authors [*Brouchkov et al., 2004; Ulrich et al., 2017*]. Some authors point to the short duration of the active phase of the thermokarst development and even consider it as a catastrophic event [*Brouchkov et al., 2004*].

The correlation between the characteristics of the seasonally thawed layer and the dramatical increase in the area of thermokarst lakes in Central Yakutia has been revealed. The main factor leading to disturbance of the stable state of the thermokarst lakes is the short-term (1–3 years) periods of the anomalous increase in the temperature of the seasonally thawed layer. These periods may be caused by a combination of hydrometeorological conditions, such as anomalous high values of snow water equivalent and annual precipitation, and the increased water content of the seasonally thawed layer.

In the work [*Kravtsova, Bystrova, 2009*], it is emphasized that a joint analysis of the remote sensing data and materials of hydrometeorological and geocryological observations is necessary for understanding the reasons of the nonlinear development of thermokarst lakes. The results of our study demonstrate that the combination of hydrometeorological factors (e.g., a high-water period) may lead to the nonlinear changes in the thickness of the seasonally thawed layer and the "explosive" development of thermokarst lakes. The established relationship may be used to forecast the development of thermokarst lakes in the future, both on the basis of the observational data on the state of permafrost and the model calculations.

Acknowledgements. *The research was supported by the Russian Foundation for Basic Research within the framework of scientific projects No. 19-35-50030 mol_nr, No. 19-35-90090_aspirants and with the support of St. Petersburg State University (Action 6, Project ID: 38360634).*

References

Boike, J., Grau, T., Heim, B., et al., 2016. Satellite-derived changes in the permafrost landscapes of Central Yakutia, 2000–2011: Wetting, drying, and fires. Global Planet Change 139, 116–127.

Bosikov, N.P., 1991. Evolution of the alas of Central Yakutia. IMZ SB RAS, Yakutsk, 128 pp. (in Russian).

Brouchkov, A., Fukuda, M., Fedorov, A., et al., 2004. Thermokarst as a Short-term Permafrost Disturbance, Central Yakutia. Permafrost and Periglacial Processes 15, 81–87.

Bulygina, O.N., Razuvaev, V.N., Alexandrova, T.M., 2020. Description of the data set "Route snow surveys", Certificate of state registration of the database No. 2013620279. – http://meteo.ru/data/166-snow-surveys#описание-массива-данных (in Russian) (last visited: 09.01.2020).

Congedo, L., 2016. Semi-Automatic Classification Plugin Documentation, 274 pp. – https://semiautomaticclassificationmanual-v5.readthedocs.io/en/latest/ (last visited: 10.12.2018).

Cooley, S.W., Smith, L.C., Stepan, L., Mascaro, J., 2017. Tracking dynamic northern surface water changes with high-frequency planet CubeSat imagery. Remote Sensing 9 (12), Art. No. 1306.

Crate, S., Ulrich, M., Habeck, J.O., et al., 2017. Permafrost livelihoods: A transdisciplinary review and analysis of thermokarst-based systems of indigenous land use. Anthropocene 18, 89–104.

Fedorov, A.N., Gavriliev, P.P., Konstantinov, P.Y., et al., 2014. Estimating the water balance of a thermokarst lake in the middle of the Lena River basin, eastern Siberia. Ecohydrology 7 (2), 188–196.

Frazier, P.S., Page, K.J., 2000. Water body detection and delineation with Landsat TM data. Photogrammetric Engineering and Remote Sensing 66 (12), 1461–1467.

GAME–Siberia and Frontier Observational Research System for Global Change. Dataset for Water and Energy Cycle in Siberia (Version 1), 2003. – http://192.244.231.21/iorgc/hcorp/data/database/cdc/siberia/sub1.html (last visited: 01.09.2018).

Iijima, Y., Fedorov, A.N., Park, H., et al., 2010. Abrupt increases in soil temperatures following increased precipitation in a permafrost region, central Lena River basin, Russia. Permafrost and Periglacial Processes 21, 30–41.

Ivanov, M.S., 1984. Cryogenic structure of Quaternary deposits of the Leno-Aldan depression. Nauka, Novosibirsk, 125 pp. (in Russian).

Jones, B.M., Arp, C.D., 2015. Observing a Catastrophic Thermokarst Lake Drainage in Northern Alaska. Permafrost and Periglacial Processes 26 (2), 119–128.

Jones, B.M., Grosse, G., Arp, C.D., et al., 2011. Modern thermokarst lake dynamics in the continuous permafrost zone, northern Seward Peninsula, Alaska. J. Geophysical Research, Biogeosciences 116 (G2), p. G00M03.

Karlsson, J.M., Lyon, S.W., Destouni, G., 2012. Thermokarst lake, hydrological flow and water balance indicators of permafrost change in Western Siberia. J. Hydrology 464, 459–466.

Kirpotin, S.N., Polnschuk, Yu.M., Bryksina, N.A., 2008. Dynamics of thermokarst lake areas in continuous and discontinuous permafrost zones of Western Siberia under global warming. Vestnik Tomskogo gosudarstvennogo universiteta [Tomsk State University Bulletin], 311, pp. 185–190 (in Russian).

Kravtsova, V.I., Bystrova, A.G., 2009. Changes in the size of thermokarst lakes in various regions of Russia over the past 30 years. Kriosfera Zemli [Earth's Cryosphere], XIII (2), 16–26 (in Russian).

Kravtsova, V.I., Tarasenko, T.V., 2011. Dynamics of thermokarst lakes of Central Yakutia under climate changes since 1950. Kriosfera Zemli [Earth's Cryosphere], XV (3), 31–42 (in Russian).

Leibman, M.O., 2005. Cryogenic slope processes and their geoecological consequences in the conditions of ice propagation formation. Prof. Thesis, Institute of Earth's Cryosphere, SB RAS, Tyumen, 262 pp. (in Russian).

Nestereva, M.I., 2012. Occurrence and distribution of thermokarst lakes on the territory of Yakutia. Molodoy uchenyy [Young Scientist], No. 9, 79–82 (in Russian).

Nitze, I., Grosse, G., Jones, B., et al., 2017. Landsat-based trend analysis of lake dynamics across Northern permafrost regions. Remote Sensing 9 (7), 640.

Olthof, I., Fraser, R.H., Schmitt, C., 2015. Landsat-based mapping of thermokarst lake dynamics on the Tuktoyaktuk Coastal Plain, Northwest Territories, Canada since 1985. Remote Sensing of Environment 168, 194–204.

Pelletier, J.D., 2005. Formation of oriented thaw lakes by thaw slumping. J. Geophysical Research 110, p. F02018.

Plug, L.J., Walls, C., Scott, B.M., 2008. Tundra lake changes from 1978 to 2001 on the Tuktoyaktuk Peninsula, western Canadian Arctic. Geophysical Research Letters 35 (3), p. L03502.

Rodionova, T.V., 2013. Studies of the thermokarst lakes dynamics in various areas of the permafrost zone of Russia from space images. PhD Thesis, Moscow, 196 pp. (in Russian).

Sannel, A.B.K., Brown, I.A., 2010. High-resolution remote sensing identification of thermokarst lake dynamics in a subarctic peat plateau complex. Canadian J. Remote Sensing 36 (S1), pp. S26–S40.

Sannel, A.B.K., Kuhry, P., 2011. Warming-induced destabilization of peat plateau/thermokarst lake complexes. J. Geophysical Research 116, p. G03035.

Séjourné, A., Costard, F., Fedorov, A., et al., 2015. Evolution of the banks of thermokarst lakes in Central Yakutia (Central Siberia) due to retrogressive thaw slump activity controlled by insolation. Geomorphology 241, 31–40.

Smith, L.C., Sheng, Y., MacDonald, G.M., Hinzman, L.D., 2005. Disappearing Arctic lakes. Science 308 (5727), p. 1429.

Soloviev, P.A., 1959. Cryolithozone of the northern part of the Lena-Amga interfluves. Publishing House of the Academy of Sciences of the USSR, Moscow, 141 pp. (in Russian).

Streletskiy, D.A., Suter, L.J., Shiklomanov, N.I., et al., 2019. Assessment of climate change impacts on buildings, structures and infrastructure in the Russian regions on permafrost. Environmental Research Letters 14 (2), p. 025003.

Swanson, D.K., 2019. Thermokarst and precipitation drive changes in the area of lakes and ponds in the National Parks of northwestern Alaska, 1984–2018. Arctic, Antarctic, and Alpine Research 51 (1), 265–279.

Torgovkin, Ya.I., Shestakova, A.A., 2018. GIS "Alasy Meginо-Kangalassky district (ulus)". Geoinformatika [Geoinformatics], No. 4, 33–40 (in Russian).

Torgovkin, Ya.I., Shestakova, A.A., Vasiliev, A.I., 2018. Spatial analysis of alas of Central Yakutia using GIS technologies. Problemy regional'noy ekologii [Problems of Regional Ecology], No. 6, 138–140 (in Russian).

Ulrich, M., Matthes, H., Schirrmeister, L., et al., 2017. Differences in behavior and distribution of permafrost-related lakes in Central Yakutia and their response to climatic drivers. Water Resources Research 53 (2), 1167–1188.

USGS: United States Geological Survey, Earth Explorer., 2020. – https://earthexplorer.usgs.gov/ (last visited: 10.01.2020).

Xu, H.Q., 2006. Modification of normalized difference water index (NDWI) to enhance open water features in remotely sensed imagery. International J. Remote Sensing 27 (14), 3025–3033.

Zakharova, E.A., Kouraev, A.V., Stephane, G., et al., 2018. Recent dynamics of hydro-ecosystems in thermokarst depressions in Central Siberia from satellite and in situ observations: Importance for agriculture and human life. Science of the Total Environment 615, 1290–1304.

Zolnikov, V.G., 1954. Relief and soil-forming rocks of the Eastern half of Central Yakutia. In: Materials on natural conditions in agriculture of Central Yakutia. Publishing house of the USSR Academy of Sciences, Moscow, vol. 1, pp. 7–54 (in Russian).

Received January 9, 2020
Revised version received February 7, 2021
Accepted February 10, 2021

EARTH'S CRYOSPHERE
SCIENTIFIC JOURNAL

Kriosfera Zemli, 2021, vol. XXV, No. 3, pp. 30–36

GASES AND GAS HYDRATES IN THE EARTH'S CRYOSPHERE

ZONE OF STABILITY OF METHANE HYDRATES IN THE AREA OF THE SREDNEVILYUISK GAS-CONDENSATE FIELD (VILYUI SYNECLISE)

A.D. Duchkov[1], V.P. Semenov[2], L.S. Sokolova[1], A.I. Sivtsev[3]

[1]*Trofimuk Institute of Petroleum Geology and Geophysics, SB RAS, Akademika Koptyuga prsp. 3, Novosibirsk, 630090, Russia; duchkovad@ipgg.sbras.ru*
[2]*Melnikov Permafrost Institute, SB RAS, Permafrost str. 36, Yakutsk, 677010, Russia; semenov.vp@rambler.ru*
[3]*TAAS-Yuryakh Neftegazodobycha LLC, Ammosova str. 18, Yakutsk, 677018, Russia; sivtsevai@tyngd.rosneft.ru*

The results of determining the lower boundary of the methane hydrate stability zone based on geothermal measurements in 22 wells of the Srednevilyuisk gas-condensate field have been presented. A graphical method has been applied, which consisted in comparing the thermograms with a phase diagram characterizing the equilibrium conditions of formation for the methane gas hydrates contained in the upper deposits of the field. At present, the upper gas deposits of the field (depths of 1035 and 1057 m) are located only 60–70 m below the stability zone. An approximate assessment of changes in the location of the lower boundary of the stability zone of methane hydrates in the Late Neopleistocene–Holocene has been made. It has been revealed that during the cold periods (~130 and 15 thousand years ago), the stability zone could fall below the upper gas deposits of the Srednevilyuisk field by 20–50 m.

Key words: *Vilyui syneclise, Srednevilyuisk gas-condensate field, permafrost, methane natural gas hydrate stability zone, boundaries of the zone, Late Pleistocene–Holocene.*

INTRODUCTION

Natural gas hydrates can form and persist only in those layers of sediments (zones of hydrate stability) in which there are favorable thermobaric (*PT*) conditions [*Istomin, Yakushev, 1992*]. Current zones of stability of gas hydrates in the deposits of the Northern Hemisphere had been formed during the cooling of the climate in the Pleistocene and the origin of the cryolithozone. The formation and development of the zones of gas-hydrates stability on the continents as a whole repeat the evolution of permafrost [*Romanovskii, 1993*].

In a recent work by the authors [*Duchkov et al., 2019*], the current location of the boundaries of the methane hydrate stability zones (MHSZ) in the deposits of the sedimentary cover of the Vilyui Syneclise, overlain from the surface by a cryogenic stratum having a thickness of 480 to 650 m, has been determined. The MHSZ of the syneclise include huge massifs of the frozen and thawed Cretaceous and Upper Jurassic deposits, occurring on average at the depths of 200 to 1200 m. Multi-storey gas and gas condensate fields have been discovered in the region [*Sitnikov et al., 2017*], the upper deposits of which approach the lower boundary of the MHSZ. Of greatest interest in that regard is the Srednevilyuisk gas-condensate field (GCF), where the lower boundary of the MHSZ is located, according to our calculations, only a hundred meters above the upper gas accumulation [*Duchkov et al., 2019*]. To clarify the relative position of the methane hydrate stability zone and the upper gas accumulation, the authors have carried out a more detailed study of the MHSZ parameters in the deposits of that field. Relatively recently, a similar study has been carried out for the neighboring Mastakh gas-condensate field [*Sivtsev, Rozhin, 2011*].

It is known that in the Late Neopleistocene–Holocene, the climate of Siberia underwent significant changes, there were frequent alternations of warm and glacial epochs, during which the mean-annual temperature dropped below the current one by 8–15 °C [*Derevyanko, 2008; Fotiev, 2020*]. Those climate variations inevitably had to cause corresponding changes in the thickness of the permafrost and the methane hydrate stability zones. In [*Bondarev et al., 2019*], for the first time, mathematical modeling of possible changes in the permafrost thickness in the Vilyui Syneclise regions in the Late Neopleistocene–Holocene (in the period from 200 thousand years ago up to the present) has been carried out. The authors have used the results obtained at the same time to roughly estimate the dynamics of displacements of the lower boundary of the MHSZ in the Vilyui Syneclise in the Late Neopleistocene–Holocene and the probability that the upper gas deposits of the Srednevilyuisk GCF will ever enter the MHSZ during that period (with their constant location through the depth). The results of those studies are presented in this article.

Srednevilyuisk gas-condensate field

The Srednevilyuisk gas-condensate field is located 60 km east of the city of Vilyuisk of the Sakha Republic (Yakutia), on the right and left banks of the Vilyui River (Fig. 1).

Tectonically, the field is confined to the double-plunging anticline of the same name on the Srednevilyuisk–Tolonsk dome-shaped uplift of the western slope of the Khapchagai mega-swell. The field is multi-accumulation one. The Permian, Triassic and Jurassic deposits are gas-bearing. The main accumulations are located in the Lower Triassic deposits at depths of 2332–2590 m. The section along the I–I latitudinal profile (Fig. 2) demonstrates that the upper portion of the section, in which the permafrost and MHSZ are located, is composed of terrigenous deposits (sandstones with interlayers of siltstones and mudstones) of the Upper Jurassic–Cretaceous age, which are saturated with fresh or brackish waters [*Kontorovich et al., 1981*]. The work [*Grubov, Slavin, 1971*] presents the results of the study of groundwater directly in the Srednevilyuisk region. They indicate that the Upper Jurassic and Cretaceous deposits are saturated with fresh and slightly brackish waters, the salinity of which is on average 0.5–2.2 g/L. The water abundance of deposits is determined by the porosity, reaching 27–33 %, the water is saturated with gas of methane composition (up to 95–99 %).

The upper-strata arched accumulation (J_3–I) of the Srednevilyuisk gas-condensate field is confined to the lower part of the Upper Jurassic Marykchan Formation, composed of sandstones with interlayers of siltstones and mudstones. The geological model of the reservoir has been built based on the results of drilling and geophysical data. According to that model, the gas-water contact (GWC) of the accumulation is located at a depth of ~1035 m (at absolute depth of –918 m), the height of the deposit is 18.4 m, the depth of its upper boundary is ~1016 m, and the gas-bearing area is 10.9 km^2. The spatial position of the upper accumulation (a projection onto the earth's surface of the gas-water contact) is demonstrated in Fig. 1. The contour of the accumulation is also demonstrated in the section along the I–I profile (Fig. 2). Approximately 20 m lower, in the Lower Vilyui Formation, a second Upper Jurassic accumulation (J_3–II) has been revealed, the GWC of which has been fixed at a depth of ~1057 m (at absolute depth of –940 m). The rest of the accumulations of the Srednevilyuisk gas condensate field are located at depths of more than 1400 m.

Temperature distribution in the upper part of the Srednevilyuisk gas-condensate field section

The temperature regime of sedimentary rocks of the Srednevilyuisk field has been studied in sufficient detail as a result of many years of geothermal studies carried out here by employees of the Melnikov Permafrost Institute (IMZ), SB RAS [*Semenov, Zheleznyak, 2013; Zheleznyak, Semenov, 2020*]. Table 1 shows the values of the permafrost thickness and rock

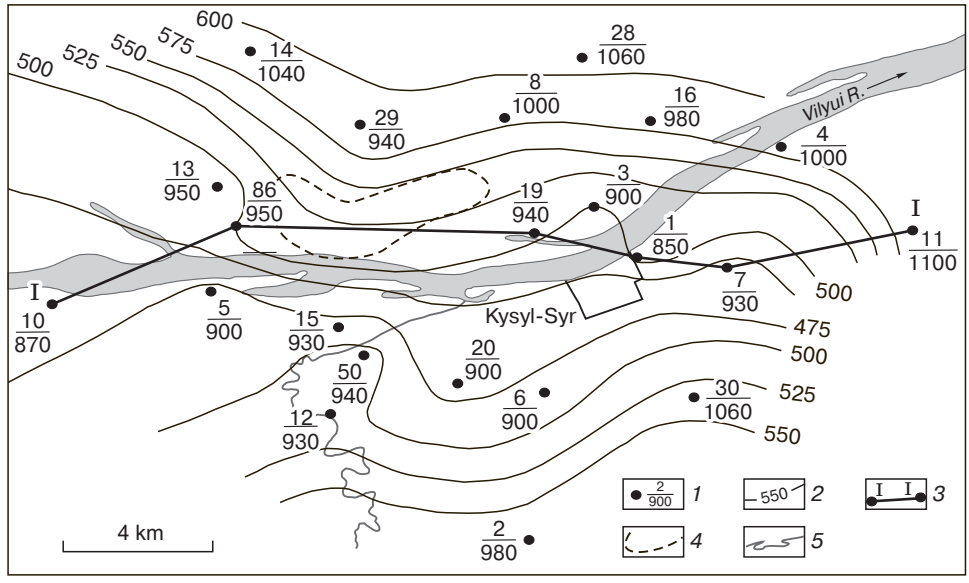

Fig. 1. Scheme of the lower boundaries of cryolithozone and methane hydrate stability zone in the sediments of the Srednevilyuisk gas-condensate field.

1 – the wells used for an estimation of the depth of the MHSZ lower boundary (in the numerator – the number of the well, in the denominator – the depth of the MHSZ lower boundary, m); *2* – isolines of the cryolithozone thickness, m; *3* – geological-geophysical section I–I; *4* – projection of the gas-water contact of the Upper Jurassic accumulation (J_3–I) of the field on the earth's surface; *5* – surface watercourses.

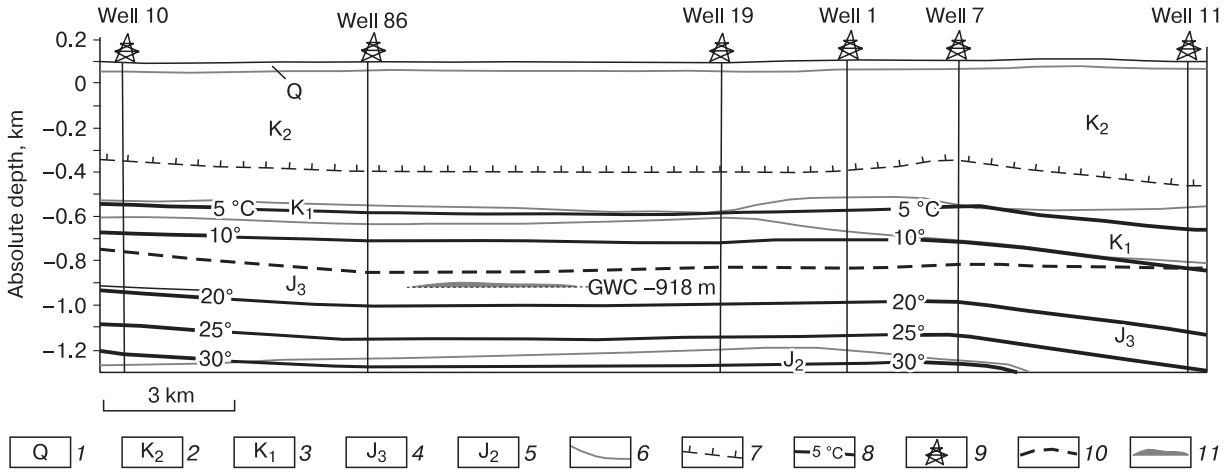

Fig. 2. Latitudinal geological-geophysical section of the Srednevilyuisk gas-condensate field.

1 – Q, Quaternary deposits; *2* – K_2, sands and sandstones with interlayers of siltstones and clays; *3* – K_1, interbedding of gray-colored sandstones with siltstones, mudstones and clays; *4* – J_3, sandstones interbedded with mudstones and siltstones; *5* – J_2, sandstones with subordinate alternation of mudstones and siltstones; *6* – boundaries of geological complexes; *7* – the permafrost lower boundary; *8* – isotherms, °C; *9* – well and its number; *10* – the MHSZ lower boundary; *11* – location of the gas-water contact (GWC) of the Upper Jurassic gas accumulation (J_3–I).

temperature at a depth of 1 km for 22 wells in the field (Fig. 1).

Based on those data, a diagram of the depth of lower boundary (H_p) of permafrost within the Srednevilyuisk gas-condensate field has been compiled (Fig. 1). The section (Fig. 2) demonstrates the location of the H_p and the temperature distribution in the sediments below the permafrost. In the studied area, the thickness of the permafrost varies from 450 to 630 m with an average value of 520 m. In the central part of the area, it is 460–520 m; its increase has been recorded in the northern, eastern and southern directions up to 570–630 m.

The H_p of permafrost was mainly determined by the location of the zero geoisotherm on the well thermograms. That method is confirmed by numerous experimental data indicating that freezing (or thawing) of fresh formation waters occurs when the temperature reaches 0 °C. For several wells (No. 4, 8, 20), when estimating the H_p, standard logging data were used.

Temperature values at a depth of 1 km (T_1) have been determined for 19 wells using thermograms from the archive of the Melnikov Permafrost Institute, SB RAS. Within the Srednevilyuisk gas-condensate field, the temperature at that depth varies from 13.8 to 19.0 °C, its average value is 16.3 °C. In the subpermafrost layer, the sediment temperature increases rapidly with depth (Fig. 2): the zero geotherm is located along the profile approximately at a depth of 0.5 km below the surface, the 5 °C and 30 °C isotherms lie at the depths of 0.7 km and 1.4 km. At a depth of 2 and 3 km, the average temperatures are: T_2 = 49 °C and T_3 = 83 °C; the average geothermal gradient in subpermafrost sediments is estimated at 3.38 °C/100 m, and the average heat flux within the gas-condensate field is about 60 mW/m^2 [*Zheleznyak, Semenov, 2020*].

The methane hydrate stability zone in sedimentary rocks of the Srednevilyuisk gas-condensate field

To assess the H_h position in the sediments of the Srednevilyuisk gas-condensate field, a graphical method was used, which consists in comparing the thermograms with the equilibrium curve of hydrate formation (phase diagram) for the actual composition of gas in the upper gas accumulation and fresh water. The intersection points of the thermograms and the phase diagram, plotted in the same coordinate system (depth and temperature) and on the same scale, give estimates of the depth of the location of the upper and lower boundaries of the stability zone. When carrying out the calculations, a hydrostatic model of the pressure change with depth was being adopted.

In this study, the authors are mainly interested in the location of the lower boundary of MHSZ, since it has been previously demonstrated [*Duchkov et al., 2019*] that within the Vilyui Syneclise, the upper boundary of the MHSZ is everywhere at depths of 180–200 m.

According to the archival data, the gas of the upper accumulation of the Srednevilyuisk gas-condensate field consists of CH_4 (97.05 %) and other components, the set of which is almost similar to the gas composition of the Mastakh gas-condensate field, for which the equilibrium conditions of hydrate formation have been estimated in [*Sivtsev, Rozhin, 2011*]. The corresponding phase diagram is shown in Fig. 3.

Table 1. **The thickness of cryolithozone and the depth of lower boundary of the MHSZ for the wells of the Srednevilyuisk gas-condensate field**

Well numbers	H_p, m	T_1, °C	H_h, m	Well numbers	H_p, m	T_1, °C	H_h, m
1	500	17	930	14	570	14.5	1040
2	580	16	980	15	480	17	930
3	500	18.2	900	16	560	16	980
4	560	–	1000*	19	510	17	940
5	480	18	900	20	460	–	900*
6	480	18	900	28	630	13.8	1060
7	460	17	930	29	590	15	940
8	560	–	1000*	30	540	14	1060
10	450	19	870	50	510	17	940
11	560	12	1100	86	500	16.6	950
12	510	17.5	930	Mean	520	16.3	960
13	480	16.5	950				

*The values have been determined by the formula $H_h = 470 + 0.94H_p$.

Note: H_p – thickness of the cryolithozone (depth of the zero isotherm) [*Zheleznyak, Semenov, 2020*]; T_1 – sediment temperature at a depth of 1 km; H_h – depth of the MHSZ lower boundary.

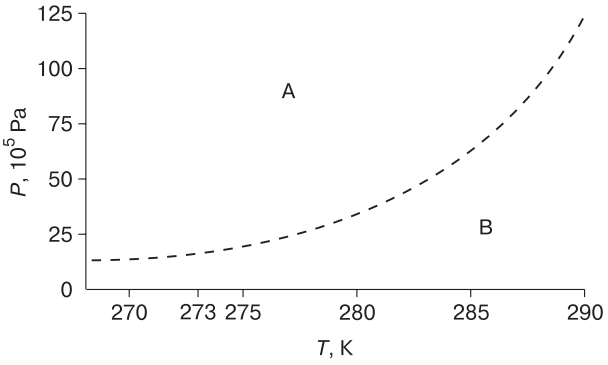

Fig. 3. Equilibrium conditions of hydrate formation (phase diagram) for the gas of the following composition (mol %): CH_4 – 96.69; C_2H_6 – 2.01; C_3H_8 – 0.27; C_4H_{10} – 0.14; CO_2 – 0.2; N_2 – 0.64 [*Sivtsev, Rozhin, 2011*].

Calculations have been made for fresh water according to the method presented in [*Sloan, 1997*]. In the figure: above the equilibrium curve is the area of methane-hydrate formation (A), and below it is the area of the two-phase 'water–gas' or 'ice–gas' state (B).

Calculations have been made for fresh water according to the method presented in [*Sloan, 1997*].

With the help of that phase diagram, as well as the H_p and T_1 values indicated in Table 1, estimates of the depth of the lower boundary of the MHSZ have been done for 19 wells. Comparison of the H_p and H_h values has revealed a good correlation between those values: $H_h = 470 + 0.94\ H_p$ ($R^2 = 0.54$). The resulting ratio was used to estimate H_h for three wells (No. 4, 8, 20), in which it was not possible to perform temperature measurements. The H_h values for all wells are summarized in Table 1 and demonstrated in Fig. 1. Figure 2 demonstrates that the lower boundary of the MHSZ is located in subpermafrost sediments along the I–I profile from west to east at depths of 870–1100 m, practically occupying the position of the 15 °C geoisotherm. The average depth of the H_h is about 960 m. The zone of methane-hydrate stability includes the frozen and thawed Cretaceous sandy-silty sediments. The highest position (up to 900–950 m), H_h achieves in the central part of the field (the thickness of the MHSZ decreases there up to 700–750 m). To the north, east and south, the lower boundary of the MHSZ drops to 1000–1100 m. Within the contour of the upper gas accumulation, it is located at depths of 940–950 m. From the upper boundary of the accumulation (at a depth of about 1016 m), the MHSZ is separated by a strata only 70–80 m thick.

Thus, a more detailed study of the MHSZ parameters in the sediments of the Srednevilyuisk gas-condensate field has confirmed that at present the upper gas accumulation of that field is located deeper than the lower boundary of the MHSZ.

It can be assumed that in the preceding colder (glacial) epochs, the thickness of the MHSZ was greater than the present-day one, and it could be closer to the upper accumulation of the Srednevilyuisk gas-condensate field or even capture it. We tried to assess that possibility using the results of the modeling of changes in thickness of the cryogenic strata in past epochs in the Vilyui Syneclise, carried out at the Institute of Oil and Gas Problems SB RAS [*Bondarev et al., 2019*].

Approximate assessment of changes in the boundaries of the MHSZ in the sediments of the Srednevilyuisk GCF in the Late Neopleistocene–Holocene

Mathematical modeling of possible changes in the permafrost parameters of the Vilyui Syneclise in past epochs has been carried out in [*Bondarev et al., 2019*] for a sediment massif with a thickness of 3 km and various conditions. At the upper boundary of the massif, as boundary conditions, in one case, the changes in air temperature deviations from the current temperature at the boundary of ice formation in Antarctica have been used [*Kotlyakov, Lorius, 2000*]. In the other one, for the same purpose, the temperature changes obtained as a result of geocryological interpretation of the paleoclimatic record based on comprehensive studies of the valve content of diatoms and biogenic silica in bottom sediments of Baikal Lake [*Fotiev, 2009*] have been applied. Two different conditions were also assumed at the lower boundary of the massif: either a constant temperature equal

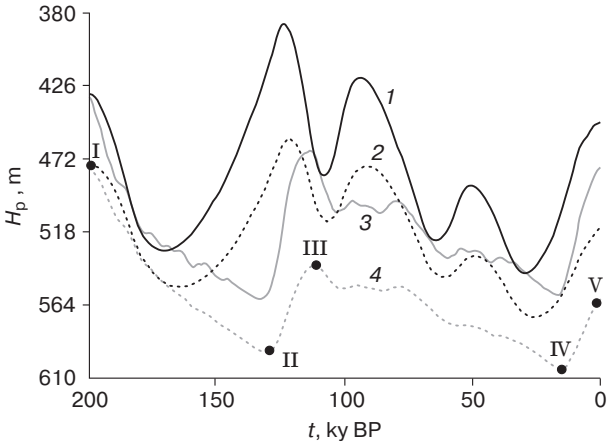

Fig. 4. Dynamics of changes in the location of the lower boundary of permafrost (H_p) in the Srednevilyuisk region under various scenarios of climate change and temperature conditions at the lower boundary of the model massif [*Bondarev et al., 2019*].

Graphs *1*, *2* – temperature of sediments at the upper boundary of the massif according to the Baikal Chronicle [*Fotiev, 2009*]; graphs *3*, *4* – temperature of sediments at the upper boundary of the massif according to the study of the ice core of the Antarctica [*Kotlyakov, Lorius, 2000*]; graphs *1*, *3* – at the lower boundary of the massif (3000 m), a constant temperature of sediments (83 °C) is maintained; graphs *2*, *4* – a constant heat flux (60 mW/m^2) remains at the lower boundary; I–V – points on graph *4*, for which the location of the MHSZ lower boundary have been estimated.

to 83 °C, or a constant intraterrestrial heat flux equal to 60 mW/m^2. Both of those conditions mean the temperature distribution in the subpermafrost rocks of the massiv during the entire modeling period corresponded to the current one. The calculation results (changes in H_p under different conditions in the period of from 200 ky BP up to the present) are shown in Fig. 4.

The calculations for the area of Srednevilyuisk gas-condensate field, where temperatures, heat fluxes and thermal properties of rocks were measured, have been performed. Modeling has revealed that in the Srednevilyuisk GCF area (and, apparently, in the entire Vilyui Syneclise) in the Late Neopleistocene–Holocene there was a cryolithozone close to the current one in thickness. It had been formed more than 200 ky BP and existed not only in cold epochs, but also in warm ones. Different conditions for setting the temperature at the boundaries of the massif lead to significant differences in the location of the cryolithozone lower boundary, although in each case H_p for 200 thousand years moved by no more than 100–140 m. The H_p position is more influenced by the temperature at the lower boundary of the massif, and to a lesser extent it depends on the chosen climate change scenario. More severe conditions (thicker permafrost) are predicted when a constant value of the heat flow is set at the lower boundary of the massif.

Table 2. **Position of the MHSZ lower boundary in the sediments of the Srednevilyuisk gas-condensate field**

Number of point (Fig. 4)	t, ky BP	H_p, m	T_1, °C	H_h, m
I	200	480	17.7	910
II	130	595	13.7	1060
III	112	538	15.6	990
IV	15	610	13.3	1080
V	0	560	14.8	1010

Note: H_p – temperature of sediments at a depth of 1 km has been calculated by the formula $T_1 = 0.0338\ (1000 - H_p)$.

The assessment of the location of the lower boundary of the MHSZ in the sediments during that period can be performed for each of the H_p graphs. However, it is preferable to choose the most realistic schedule for further work. The selection criterion can be, for example, the ratio of current measured and the calculated values of average permafrost thickness. According to various estimates, at present, the average thickness of permafrost within the Srednevilyuisk gas-condensate field is estimated at 520–550 m (Table 1 [*Duchkov et al., 2019*]). From Fig. 4 it follows that the *2* and *4* graphs are closest to the average measured H_p values (H_p = 518 and 560 m, respectively). The *1* and *3* graphs demonstrate lower values of H_p. From the *2* and *4* graphs, it follows that the *4* graph predicts the deepest freezing of sediments in past epochs. The authors have chosen it to assess possible changes in the MHSZ parameters within the field. For simplicity, it has been decided to evaluate the position of H_h only at the extreme and terminal points of the *4* graph, that is, at 5 points (I–V), the parameters of which (t and H_p) are shown in Table 2. That approach allows us to determine the most interesting information on the maximum displacements of the H_h border in time.

To assess changes in the depth of the lower boundary (H_h) of the methane hydrate stability zone in the period under consideration, it is sufficient to know the location of the zero isotherm (H_p) and the temperature value at a depth of 1 km (T_1). Estimates of the T_1 values have been made according to the previously mentioned average value of the geothermal gradient in the subpermafrost sediments of the Srednevilyuisk gas-condensate field equal to 3.38 °C/100 m. That choice of the gradient is justified by the condition adopted in the modeling at the lower boundary (3 km) of the rock massif, namely, preservation of a heat flow equal to the current one during the entire time period (200 ky). That condition presupposes that the temperature field of the permafrost sediments practically remains unchanged in the same period. The T_1 (°C) values were determined by the for-

mula $T_1 = 0.0338\ (1000 - H_p)$. When assessing the location of the lower boundary of the MHSZ (H_p), a graphical method has been used – geothermal data (H_p and T_1) were compared with the phase diagram presented in Fig. 3. The results of calculations for T_1 and H_h are shown in Table 2. Graphs of possible maximum displacements of H_p and H_h in the Neopleistocene–Holocene are demonstrated in Fig. 5.

200 ky BP, the lower boundaries of the permafrost and the MHSZ were located at depths of 480 and 910 m, respectively, i.e. occupied the highest position. Subsequently, the thickness of permafrost and the methane hydrates stability zone as a whole increased under the influence of several cold snaps. The deepest H_p (up to 595–610 m) and H_h (up to 1060–1080 m) deepened 130 and 15 ky BP. In both cases, the MHSZ could capture both Upper Jurassic accumulations of the Srednevilyuisk GCF, the gas-water contacts of which are located at depths of 1035 and 1057 m. In the last cold period, H_h could sink 20 m below the second Upper Jurassic (J_3–II) accumulation.

It should be noted that the used graphical method makes it possible to solve the main problem posed – to assess the change dynamics in the depth of the lower boundary of the MHSZ in the Neopleistocene–Holocene without taking into account the time lag of the H_h displacements relative to H_p. Further development of the method for modeling the dynamics of changes in the permafrost and MHSZ parameters may, in our opinion, lead to a refinement of the obtained estimates.

Comparison of the calculation results with geological information on climate change

It is of interest to compare the information obtained on possible changes in the position in the section of the lower boundaries of the permafrost and the MHSZ (Table 2, Fig. 5) with the description of the main climatic events in the Late Neopleistocene–Holocene [*Derevyanko, 2008; Fotiev, 2020*]. Those studies demonstrate that global paleoclimatic events in the Late Neopleistocene–Holocene, established by the ratio of oxygen isotopes in the core of marine sediments, by the content of biogenic silica in the sediments of Lake Baikal, by the study of the ice core of Antarctica and by the properties of soil sections of Siberia, are in good agreement with each other.

In the future, we will compare the H_p and H_h values obtained as a result of the analysis of graph 4 (Fig. 4) with the characteristics of the alternating warm and cold periods of the Earth's paleoclimate, determined by the materials of deep-sea drilling (each period is characterized by a separate MIS – marine oxygen isotope stage) and recorded in the climatic history of the West Siberian region [*Derevyanko, 2008*], as well as in the geocryological annals of the

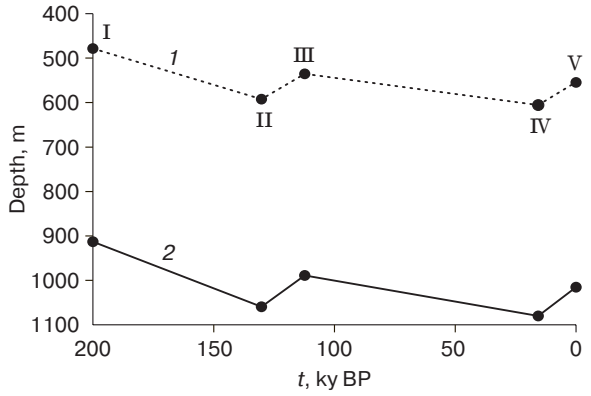

Fig. 5. Location of the lower boundary of permafrost and the methane hydrates stability zone in the sediments of the Srednevilyuisk region at separate time points I–V of the Late Neopleistocene–Holocene (period of 200 ky BP – the present).

1 – the lower boundary of permafrost [*Bondarev et al., 2019*]; *2* – the MHSZ lower boundary.

Siberian Neopleistocene (thermochrones – warm periods, cryochrones – cold ones) [*Fotiev, 2009, 2020*].

The minimum values H_p and H_h have been determined for the moment of 200 ky BP. At that time, the warm climatic period ended (MIS 7, Shirtinsky thermochron) and a long cold stage began (MIS 6, Taz cryochron), which lasted from 187 to 130–128 ky BP. During that stage, the H_p and H_h boundaries gradually subsided up to the maximum values reached about 130 ky BP. The cooling was replaced by a warm period (MIS 5, Kazantsevo Interglacial in Western Siberia, Kazantsevo thermochron), which lasted from 128 to 70 ky BP. During that warm period, first there was a sharp rise in the H_p and H_h (112 ky BP), and then stabilization and slow subsidence of the boundaries occurred due to a gradual decrease in average surface temperatures. Approximately 70 ky BP, the H_p and H_h had reached the current values and continued to submerge under the influence of a decrease in surface temperatures during cold periods that occurred 70–58 ky BP (MIS 4, Ermakovo Glaciation in Western Siberia, the beginning of the Zyryanka-Sartan cryochron) and 32–11 ky BP (MIS 2, Sartan Glaciation). The maximum values of the H_p and H_h had been reached 15 ky BP, approximately by the end of the Sartan Ice Age. Subsequently, the rise of the H_p and H_h boundaries to the present level began under the influence of climate warming in the Holocene (11–0 ky BP, MIS 1).

CONCLUSION

As a result of the carried-out studies, the MHSZ parameters in the sediments of the Srednevilyuisk gas-condensate field of the Vilyui Syneclise have been

determined. It has been revealed that there are very favorable conditions for the formation of accumulations of methane hydrates: the presence of sandy reservoirs, an increased content of methane dissolved in water throughout the section [*Sitnikov et al., 2017*], and a thick zone of hydrate stability. For the first time, for the conditions of the Vilyui Syneclise, it has been managed to make an approximate assessment of possible changes in the location of the MHSZ lower boundary in the Late Neopleistocene–Holocene, using the most probable, from our point of view, scenario for the evolution of the permafrost zone out of those published in [*Bondarev et al., 2019*]. Calculations have demonstrated that during the cold periods, about 130 and 15 ky BP, the MHSZ lower boundary could deepen below two Upper Jurassic accumulations (gas-water contact depths of 1035 and 1057 m) of the Srednevilyuisk GCF. To refine the obtained estimates, it is necessary to further develop methods for predicting changes in the parameters of both the MHSZ and permafrost zone under the influence of the climatic factor.

In conclusion, it can be noted that the estimates obtained by the authors for changes in the Neopleistocene–Holocene of the MHSZ and permafrost lower boundaries (graph *4* in Fig. 4, Fig. 5) generally correlate well with the known data on global paleoclimatic events in that time period. The same conclusion can be made regarding the scenario illustrated by graph *3* (Fig. 4). At the same time, it is obvious that the nature of changes in the permafrost lower boundary, demonstrated by graphs *1* and *2* (Fig. 4), does not correspond to the described climatic events. That makes it possible to suggests that the closest-to-reality results, when modeling the dynamics of changes in the cryolithozone thickness in past epochs, have been obtained in [*Bondarev et al., 2019*] using the changes in relative temperature at the ice formation boundary in Antarctica as the upper boundary condition [*Kotlyakov, Lorius, 2000*].

Acknowledgments. *The research has been supported in 2018–2019 by Integration project No. 6 "Paleoreconstruction of the thermal field and cryolithozone of the Vilyui Syneclise in the Late Pleistocene–Holocene" of the Comprehensive Program of Basic Research of the SB RAS "Interdisciplinary Integration Research" for 2018–2020.*

References

Bondarev, E.A., Rozhin, I.I., Argunova, K.K., 2019. Modeling of the geotemperature field and the power of the cryogenic layer in various areas of the Vilyui Syneclise. In: Proceeding of Conference "Thermophysics and power engineering of the Arctic and subarctic territories" (Yakutsk, June 24–27, 2019). Publishing house of the Melnikov Permafrost Institute of SB RAS, Yakutsk, pp. 11–16 (in Russian).

Derevyanko, A.P. (Ed.), 2008. Global climate and natural environment changes of the late Cenozoic in Siberia. Publishing house of SB RAS, Novosibirsk, 511 pp. (in Russian).

Duchkov, A.D., Zhleznyak, M.N., Sokolova, L.S., Semenov, V.P., 2019. Methane and carbon dioxide hydrate stability zones in the sedimentary cover of the Vilyui sineclise. Earth's Cryosphere XXIII (6), 16–22.

Fotiev, S.M., 2009. Siberian geocryological chronicle. Kriosfera Zemli [Earth's Cryosphere], XIII (3), 3–16 (in Russian).

Fotiev, S.M., 2020. Debatable problems of geocryology: review of achievement. Earth's Cryosphere XXIV (3), 3–15.

Grubov, L.A., Slavin, V.I., 1971. Comparative assessment of hydrogeological conditions of various regions of the Yakut artesian basin in relation to oil and gas potential. In: Hydrogeological research in oil and gas bearing areas. VNIGRI Publishing House, Leningrad, pp. 184–202 (in Russian).

Istomin, V.A., Yakushev, V.S., 1992. Gas Hydrates in Natural Conditions. Nedra, Moscow, 235 pp. (in Russian).

Kontorovich, A.E., Surkov, V.C., Trofimuk, A.A. (Eds.), 1981. Geology of Oil and Gas of the Siberian Platform. Nedra, Moscow, 376 pp. (in Russian).

Kotlyakov, V.M., Lorius, K., 2000. Four climate cycles based on ice core data from a deep well at Vostok station in Antarctica. Izvestiya RAN [Proceeding of RAN], Geographical series, No. 1, 7–19 (in Russian).

Romanovskii, N.N., 1993. The basics of cryogenesis lithosphere. MSU Publishing House, Moscow, 336 pp. (in Russian).

Semenov, V.P., Zheleznyak, M.N., 2013. Geothermal conditions of the Vilyuy Syneclise. Kriosfera Zemli [Earth´s Cryosphere], XVII (3), 3–10 (in Russian).

Sitnikov, V.S., Alekseev, N.N., Pavlova, K.A., et al., 2017. The latest forecast and updating of development of oil and gas facilities of Vilyui syneclise. Neftegazovaya geologiya. Teoriya i praktika [Oil and Gas Geology. Theory and Practice], 12 (1), 20 pp. (in Russian).

Sivtsev, A.I., Rozhin, I.I., 2011. Validation of the potential of gas accumulations under permafrost-hydrate with a fluid-shed. In: Problems of engineering permafrost. In: Proceedings of the IX International Symposium (Mirny, 3–7 Sept. 2011). Publishing House of Melnikov Permafrost Institute SB RAS, Yakutsk, pp. 422–428 (in Russian).

Sloan, E.D., 1997. Clathrate Hydrates of Natural Gases. Marcel Dekker, Inc., N.Y., Basel, Hong-Kong, 705 pp.

Zheleznyak, M.N., Semenov, V.P., 2020. Geotemperature field and cryolithozone of the Vilyui Syneclise. Publishing House SB RAS, Novosibirsk, 123 pp. (in Russian).

Received September 15, 2020
Revised version received January 7, 2021
Accepted January 11, 2021

EARTH'S CRYOSPHERE
SCIENTIFIC JOURNAL

Kriosfera Zemli, 2021, vol. XXV, No. 3, pp. 37–42

SNOW COVER AND GLACIERS

CONJUGATION OF CHANGES IN AIR TEMPERATURE, SNOW COVER THICKNESS AND SOIL TEMPERATURE OF EAST EUROPEAN PLAIN

L.M. Kitaev

Institute of Geography, RAS,
Staromonetny per. 29, Moscow, 119017, Russia; lkitaev@mail.ru

The main goal of the research is to assess the nature of the spatio-temporal changes in the temperature regime of the soil of the East European Plain (Russian part) under the conditions of changes in snow cover and soil temperature in recent decades – at the local and regional levels. The phases of changes in soil temperature, snow thickness, and surface air temperature, typical for the study area, have been identified. Significant long-term tendencies in the progress of in soil temperature are characteristic of low-snow autumn and spring periods, as well as a significant correlation between soil temperature and air temperature during those periods in the absence of statistical relationships during the snow season. A sharp decrease in the seasonal and inter-annual variability of soil temperature in the period with stable snow cover has been revealed – by 3–5 times relative to the variability of the surface air temperature, and by 1.3–2.5 times relative to the variability of soil temperature in the pre-winter and spring periods with a progress of changes. Thus, the appearance of stable snow cover in the winter season determines the progress of soil temperature within a narrow corridor of near-zero values, low or insignificant coefficients of the linear trend, low seasonal and inter-annual variability, the absence of statistical relationships with the course of changes in snow thickness and surface air temperature – both at the local, and at the regional levels of the East European Plain.

Key words: *snow thickness, surface air temperature, soil temperature, spatial distribution, multiyear progress.*

INTRODUCTION

Snow cover, which occupies a significant area in the Northern Hemisphere during the cold season, plays there the role of a link between climate variability and the state of the land surface. Being dependent on atmospheric phenomena, the snow cover has a significant effect on hydrological processes [*Lvovich, 1963, 1986*], on the state of soil and vegetation [*Vaganov et al., 1996; Nikolaev, Skachkov, 2012*]. On the other hand, the spatial heterogeneity of the snow cover and its low albedo define the features of the radiation balance and meteorological regime. The relationship between thermal conditions of upper soil layers and snow mass largely determines the overland runoff in spring and the state of the biota, in connection with which, already in 1954, V.A. Kudryavtsev proposed a system of equations describing the process of heat transfer in the soil–snow cover–atmosphere chain [*Kudryavtsev, 1954*]. Similar work has been carried out both for the zone of seasonal freezing of soils [*Sokratov et al., 2001; Sokratov, Barry, 2002; Osokin, Sosnovsky, 2015*], and, to a greater extent, for the permafrost territories [*Pavlov, 2008; Aalstad et al., 2018*], as a result of which the mechanism of soil freezing in the conditions of warming in the second half of the 20th up to early 21st centuries has been clarified.

At the same time, the ratio of the seasonal variation of the surface air temperature, snow thickness and soil temperature is ambiguous and insufficiently assessed, especially at the level of regional spatial-temporal generalizations, although that issue is of great importance, in particular, in model calculations of snow reserves using satellite data [*Kitaev et al., 2012; Aalstad et al., 2018*]. The closest interaction of the studied parameters at the beginning of the snow period has been revealed [*Pavlov, 2008; Osokin, Sosnovsky, 2015*]. I. Sleptsov and coauthors have proposed an algorithm for calculating the number of freezing and thawing cycles of frozen soils in connection with changes in air temperature, but only for the little-snowy autumn and spring periods in Central Yakutia [*Sleptsov et al., 2012*], with clearly insufficient knowledge of regional differences in the entailing of the characteristic progress.

The main purpose of the research is to assess the nature of the spatial-temporal changes in the temperature regime of soil under the conditions of changes in snow cover and surface air temperature in recent decades at the local and regional levels of the East European Plain.

METHODICAL APPROACHES

Previously, the authors have analyzed the results of observations of the seasonal surface-air-tempera-

ture variability, snow cover thickness and soil temperature in the Prioksko-Terrasny Nature Reserve (Moscow Oblast) and Central Forest Nature Reserve (Tver Oblast) for the cold period of 2013/14, 2014/15 and 2015/16 [*Kitaev et al., 2017*]. So, according to the observations on experimental sites in forest areas with a predominance of deciduous and coniferous species, as well as in open spaces in the autumn-winter-spring period of the year, the same type of phases of soil temperature changes under the conditions of the seasonal surface-air-temperature variation and snow thickness have been identified. Low variability of soil temperature at a depth of up to 4 cm in the period with stable snow cover (within the range of +1.0...–1.0 °C) has been revealed, which, possibly, indicates a decrease in the dependence of soil temperature on changes in snow thickness and fluctuations in the surface air temperature during that period due to heat-insulating properties of snow. Similar results have been obtained from the observations of the Velikiye Luki and Tula meteorological stations. The distances between them and the reserves are, respectively, 150 km to the south and 100 km to the north, and the distance between the extreme objects of observation is about 750 km from north to south.

A logical continuation of the carried-out work can be considered the transition from the local spatial level to the regional one – to the study of the relationship between spatial-temporal changes in soil temperature, snow cover thickness and surface air temperature in various climatic conditions of the East European Plain. In that case, the territories to south of the 50° latitude have not been considered due to the possible occurrence of errors in the statistical analysis of small snow reserves on the plain and the very uneven distribution of snow cover and soil freezing in the mountains. As input information, daily data have been used: surface air temperature, snow cover thickness, soil temperature and degree of snow cover on a 10-point scale, based on observations of 75 meteorological stations of the Roshydromet [www.meteo.ru] with the longest synchronous series studied characteristics (1989–2015). The period of the year, combining winter time with a stable snow cover (December–March), little-snowy pre-winter (October–November) and spring (April–May), is being investigated. The continuity of the results of previously conducted local studies and the generalizations of the regional level presented here is based on the use of unified Roshydromet methods for measuring surface air temperature and snow thickness [*Manual..., 1985*].

Observations of the soil temperature progress in the reserves have been carried out using automatic sensors (loggers) at depths of 10, 20 and 40 cm, the same at meteorological stations have been performed by means of exhaust thermometers at depths of 20, 40 and 80 cm. The analysis of observational data in the reserves and at the Velikiye Luki and Tula meteorological stations have demonstrated the absence of significant differences in measurements by automatic sensors and exhaust thermometers for soil temperatures up to a depth of 40 cm [*Kitaev et al., 2017*]. The data from meteorological stations on soil temperature at a depth of 80 cm are used as additional information for analysis. As a result, a decision on the possibility of generalizing the results of local (data from the reserves) and regional (data from the meteorological stations) observations has been taken.

SEASONAL VARIABILITY OF SOIL TEMPERATURE, SNOW COVER AND SURFACE AIR TEMPERATURE

As is revealed by the results of experimental work, in characteristic sites of the Prioksko-Terrasny Nature Reserve and Central Forest Nature Reserve (Moscow and Tver Oblasts, 2014–2016), the progress of soil temperature at a depth of up to 40 cm during the period with a stable snow cover occurs within the range of –1.0...+1.0 °C with small differences in mean values and standard deviation (Table 1) [*Kitaev et al., 2017*].

Similar ratios of changes in parameters are demonstrated by the daily average data for 75 meteorological stations of the East European Plain. As an example, the author considers the averaged over the period of 1989–2015 daily values of the characteristics for meteorological stations located in different climatic zones: Naryan-Mar (forest-tundra), Syktyvkar (taiga) and Valuiki (forest-steppe). The graphs of the seasonal progress in the characteristics of every of three stations presented in Figure 1, obtained by averaging daily values for the period of 1989–2015 generally corresponds to the previously obtained patterns for the Prioksko-Terrasny and Central Forest Reserves (the central portion of the East European Plain). The same phase change is traced in the seasonal progress: a slow, synchronous with the surface air temperature, decrease in soil temperature during the setting of snow cover; mirror-reverse transformation of the temperature profile of the soil (the lower layers of the soil become warmer in relation to the upper ones); low variability of soil temperature with stable snow cover; in the process of destruction of the snow cover, the upper layers again become warmer than the lower ones; the increase in soil temperature synchronously with the surface air temperature during the destruction of the snow cover and its final coming-off.

Similar to the previously obtained results [*Kitaev et al., 2017*], all the studied points are characterized by (similar to the variations of surface temperature) a relatively slow decrease in soil temperature in autumn and a faster increase in temperature in spring (Fig. 1), which corresponds to the conclusion of

Table 1. **Local variability of soil temperature, snow cover thickness and surface air temperature during the period with stable snow cover**

Site	Year	Air temperature, °C	Soil temperature, °C	Snow thickness, cm
Central Forest Nature Reserve				
Forested area with a predominance of deciduous species	2014/15	–4.1/7.4	0.1/0.6	11/3
	2015/16	–2.1/5.3	0.7/0.4	37/18
	2016/17	–4.9/7.2	0.5/0.5	30/13
Open space	2014/15	– 4.1/7.4	–0.1/0.6	14/5
	2015/16	–2.1/5.3	–0.5/0.6	29/20
	2016/17	–4.9/7.2	0.5/0.4	29/3
Forested area with a predominance of coniferous species	2014/15	– 4.1/7.4	–0.4/0.6	9/3
	2015/16	–2.1/5.3	0.5/0.5	32/16
	2016/17	–4.9/7.2	0.6/0.3	35/11
Prioksko-Terrasny Nature Reserve				
Forested area with a predominance of deciduous species	2014/15	–3.7/9.1	0.0/0.5	20/6
	2015/16	–3.1/5.4	–0.2/0.6	21/7
	2016/17	–2.7/5.6	0.1/0.3	27/8
Open space	2014/15	–3.7/9.1	–0.2/0.5	12/8
	2015/16	–3.1/5.4	0.0/0.3	12/6
	2016/17	–2.7/5.6	–0.2/0.4	21/9
Forested area with a predominance of coniferous species	2014/15	–3.7/9.1	0.6/0.6	7/ 4
	2015/16	–3.1/5.4	0.1/0.4	13/6
	2016/17	–2.7/5.0	0.2/0.6	21/7

A.I. Voeikov that warming effect of the snow mass exceeds the cooling effect in terms of the time of influence [*Voeikov, 1957*].

During the period with stable snow cover, the soil temperature at a depth of up to 40 cm also has slight fluctuations within the range of 2.0–3.0 °C in the near-zero zone with a slow increase in soil temperature from –5.0...–2.0 °C in the north (Naryan-Mar) to –1.5...0 °C in the south (Valuyki). At the same time, the average surface air temperature for the period with stable snow cover varies from –14 to –2 °C, and the thickness of the snow cover changes from 50 to 28 cm.

An analysis of the previously obtained patterns [*Kitaev et al., 2017*] has revealed that, in general for the region, the range of spatial differences in soil temperature at a depth of 40 cm during the snow period is small (from –1.5 to +1.5 °C), with a larger (several

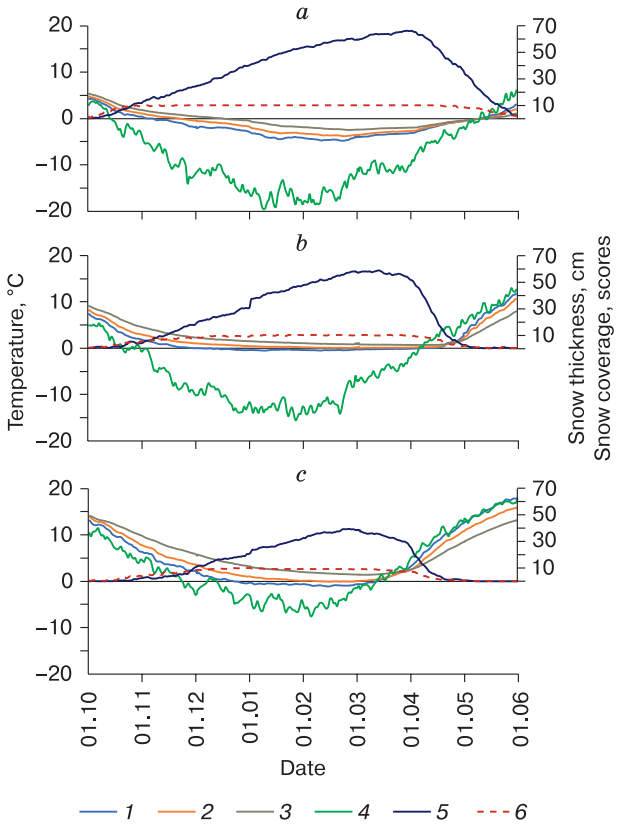

Fig. 1. Seasonal variation of the soil temperatures averaged for 1989–2015 at depths of 20 cm (*1*), 40 cm (*2*) and 80 cm (*3*), surface air temperature (*4*), snow thickness (*5*) and the degree of snow cover of the territory (*6*).

a – Naryan-Mar (forest-tundra); *b* – Syktyvkar (taiga); *c* – Valuyki (forest-steppe).

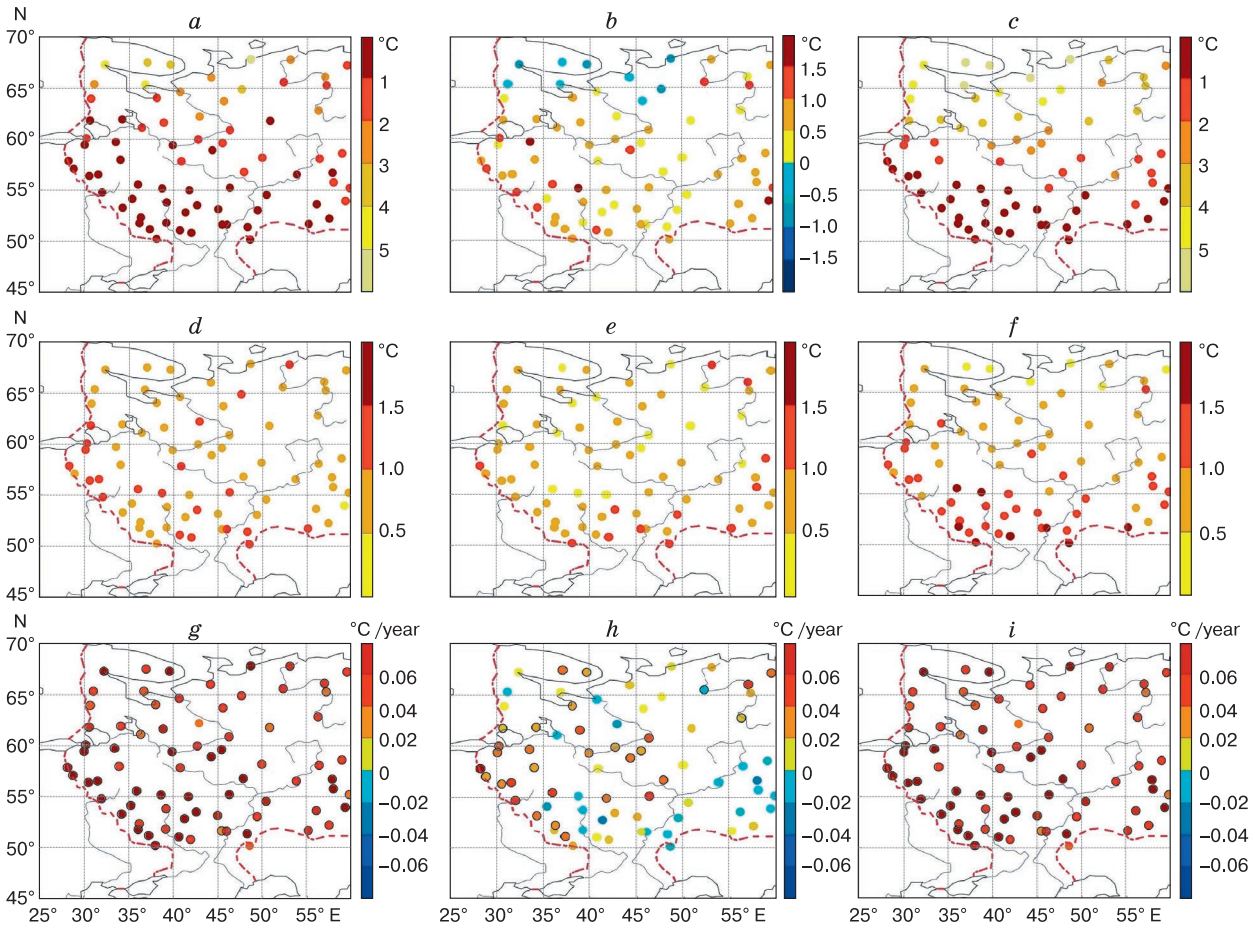

Fig. 2. Spatial distribution of soil temperature characteristics for a depth of 40 cm for the period 1989–2015:

a–c – average values in October–November (*a*), in December–March (*b*), in April–May (*c*); *d–f* – standard deviation in October–November (*d*), in December–March (*e*), in April–May (*f*); *g–i* – coefficient of the linear trend in October–November (*g*), in December–March (*h*), in April–May (*i*).

times) range of spatial changes in soil temperature in autumn and spring (Fig. 2). A small range of regional spatial changes in soil temperature during a period with stable snow cover occurs against the background of noticeable, mainly zonal, changes in the thickness of snow cover (from 15 to 60 cm) and surface air temperature (from –15 to –30 °C).

LONG-TERM VARIABILITY OF SOIL TEMPERATURE, SNOW COVER AND SURFACE AIR TEMPERATURE

Public availability of observational data from 1989 to 2015 allows us to evaluate not only seasonal, but also long-term pattern of changes in the studied characteristics. Figure 2 shows that the standard deviation of the long-term variation in soil temperature during the period with stable snow cover is lower than the standard deviation of the pre-winter and spring. The territory-averaged standard deviation of soil temperature during the period with stable snow cover at depths of 20, 40, and 80 cm has the values of 0.73, 0.71, and 0.53 °C with a standard deviation of surface air temperature of 2.5 °C. In the pre-winter and spring little-snowy periods, the standard deviation of soil temperature is 0.93, 0.89 and 1.36 °C and 1.1, 0.92 and 1.03 °C, respectively, and the surface air temperature is 1.9–1.6 °C. Consequently, stable snow cover determines, among other things, a small interannual variability in soil temperature of the snow period, 3–5 times lesser variability of surface air temperature and 1.3–2.5 times lesser variability of soil temperature in the pre-winter and spring periods. Those results correspond, in particular, to the conclusion of A.V. Pavlov on the variability of the temperature of seasonally frozen soils at the beginning of the snow period [*Pavlov, 2008*].

As can be seen from Figure 2, in comparison with the autumn and spring periods, long-term tendencies in soil temperature in winter with snow cover are insignificant (with a difference of 2–6.5 times) (Fig. 2),

which coincides with the conclusions of B.G. Sherstyukov [*Sherstyukov, 2008*]. The mean long-term soil temperature values for the depths of 20, 40, and 80 cm differ correspondingly by seasons as follows: in autumn, 0.062, 0.070 and 0.056 °C/year; in winter, –0.009, 0.035 and 0.048 °C/year; in spring, 0.022, 0.061 and 0.049 °C/year.

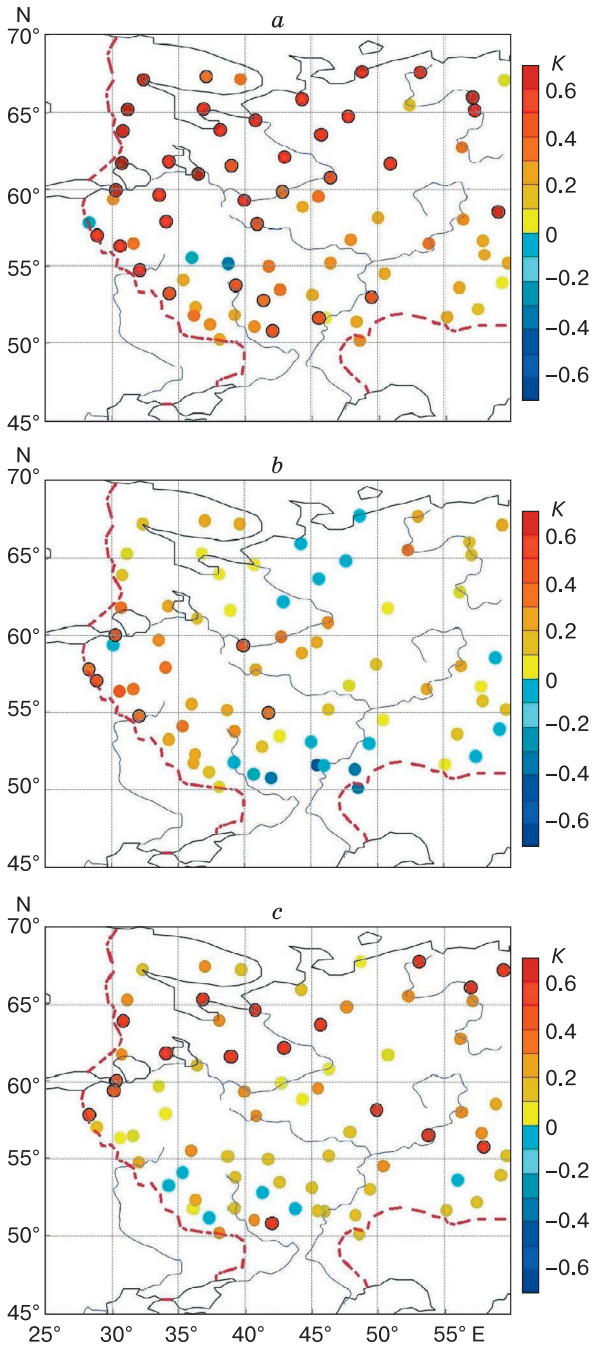

Fig. 3. Spatial distribution the correlation coefficients (K) of long-term variation of surface air temperature and soil temperature at depths of 40 cm in October–November (a), December–March (b), April–May (c).

The circles indicate significant coefficients.

For each meteorological station, the correlation coefficients of the long-term variation (1989–2015) in soil temperature and surface air temperature (average ones for October–November, December–March, April–May) have been calculated. As an example, Figure 3 demonstrates the spatial distribution of temperature correlation coefficients at a depth of 40 cm. The correlation of long-term temperature variations in the absence of snow in autumn and spring is significant in the positive range of correlation coefficients (0.49–0.88), primarily in the northwest of the East European Plain. It can be assumed that latitudinal differences in the tightness of connections can be associated with the difference in the water-physical properties of the soil, in particular, with the dynamics of soil moisture. The relationship of inter-annual temperature variability in the period from December to March is insignificant almost everywhere, because of the extremely low variability of soil temperature during the period with snow cover due to the insulating properties of the snow cover.

CONCLUSIONS

Based on the analysis of observational data from 75 meteorological stations in the period of 1989–2015, a quantitative assessment of the relationship between the local and regional variability of the soil temperature regime, thickness of the snow cover and the surface air temperature in the East European Plain conditions has been carried out.

The phases of seasonal variation in soil temperature in the conditions of seasonal variability of the snow cover thickness and the surface air temperature have been revealed. The rate of decrease in air and soil temperatures during the period of snow cover formation in autumn is lower than the rate of temperature increase during the destruction of snow cover in spring. The limits of soil temperature changes during the period with stable snow cover have been determined: minor fluctuations in soil temperature occur within the range of 2.0–3.0 °C in the area of near-zero values, while the range itself within its limits becomes insignificantly (by the first degrees) displaced from a negative temperature region to a positive one, against the background of significant latitudinal changes in surface air temperature and snow thickness.

In general, for the region, the range of spatial differences in soil temperature during the snow period is small, for the depths up to 40 cm it varies from –1.5 to +1.5 °C, at a depth of 80 cm it changes from 0.5 to 2.0 °C, being significantly less than the corresponding values in autumn and spring. The standard deviation of the long-term variation of soil temperature in the little-snowy periods, pre-winter and spring, is everywhere greater than the standard deviation of the soil

temperature during the period with a stable snow cover. The appearance of snow determines the decrease in the inter-annual variability of soil temperature by 3–5 times relative to the variability of surface air temperature, and by 1.3–2.5 times relative to the variability of soil temperature in the pre-winter and spring periods. Thus, the stable snow cover largely levels the generally accepted relationship between air temperature and soil temperature.

Long-term tendencies of changes in soil temperature during the period with stable snow cover are insignificant, being quite homogeneous in spatial distribution and having linear trend coefficients 2–6.5 times lesser than the coefficients of autumn and spring periods.

The relationship between the inter-annual variability of soil temperature and climate variability in the period from October to May is also ambiguous. Significant correlation coefficients of the long-term variation in soil temperature at a depth of 40 cm and surface air temperature are typical only for autumn and spring (0.49–0.55), being mostly insignificant throughout the entire territory of the East European Plain during the snowy period, with a generally small or insignificant correlation with the course of changes in the snow thickness.

Thus, the setting of stable snow cover in the cold season determines the dynamics for the soil temperature within a narrow range of near-zero values, small or insignificant coefficients of the linear trend, small seasonal and interannual variability, the absence of statistical relationships with the snow thickness and surface air temperature, both locally, and at the regional levels of the East European Plain.

Acknowledgements. *The work has been supported by the Russian Foundation for Basic Research, Project No. 20-55-00007 (collection, processing and primary analysis of initial information) and theme 0148-2019-0009 "Climate changes and their consequences for the environment and livelihoods of the population in Russia" of the Program of fundamental scientific research of state academies of sciences (interpretation of analysis results).*

References

Aalstad, K., Westermann, S., Schuler, T.V., et al., 2018. Ensemble-based assimilation of fractional snow-covered area satellite retrievals to estimate the snow distribution at Arctic sites. The Cryosphere, No. 12, 247–270.

Kitaev, L.M., Ableeva, V.A., Asainova, Z.H., et. al., 2017. Seasonal dynamics of air temperature, snow and soil freezing in the Central part of the East European plain. Led i Sneg [Ice and Snow], 57 (4), 518–526 (in Russian).

Kitaev, L.M., Boyarskiy, D.A., Titkova, T.B., Komarova, N.Yu., 2012. Snow cover of the East European plain according to multi-frequency microwave satellite radiometry. Sovremenniye Problemi Zondirovaniya Zemli iz Kosmosa [Modern Problems of Remote Sensing of the Earth from the Space], 9 (1), 249–258 (in Russian).

Kudryavtsev, V.A., 1954. The temperature of the upper layers of permafrost in the USSR. Publishing House of the AS USSR, Moscow, 182 pp. (in Russian).

Lvovich, M.I., 1963. Man and Water. Geografizdat, Moscow, 568 pp. (in Russian).

Lvovich, M.I., 1986. Water and Life. Mysl', Moscow, 253 pp. (in Russian).

Manual for hydrometeorological stations and posts, Issue 3, Part 1. Gidrometizdat, Leningrad, 299 pp. (in Russian).

Nikolaev, A.N., Skachkov, Yu.B., 2012. Effect of snow cover and temperature of permafrost soils in the radial growth of trees in Central Yakutia. Zhurnal Sibirskogo federal'nogo universiteta, seriya Biologiya [Journal of Siberian Federal University, Biology series], No. 5, 43–51 (in Russian).

Osokin, N.I., Sosnovsky, A.V., 2015. Effect of air temperature and snow depth dynamics on frost depth. Earth's Cryosphere XIX (1), 88–93.

Pavlov, A.V., 2008. Monitoring of the Cryolithozone. Academic Publishing House "Geo", Novosibirsk, 230 pp. (in Russian).

Sherstyukov, A.B., 2008. Correlation of soil temperature, air temperature and snow cover depth in Russia. Kriosfera Zemli [Earth's Cryosphere], XII (1), 79–87 (in Russian).

Sleptsov, V.I., Mordovskoi, S.D., Petrov, E.E., 2012. Calculating the number of freeze-thaw cycles of the rock mass conditions for the Central Yakutia on horizontal surfaces. Gornyj informacionno-analiticheskij byulleten [Mining information-analytical bulletin], No. 9, 101–105 (in Russian).

Sokratov, S.A., Barry, R.G., 2002. Intraseasonal variation in the thermoinsulation effect of snow cover on soil temperatures and energy balance. J. Geophysical Research, vol. 107, D9-D10, pp. 13-1–13-6.

Sokratov, S.A., Golubev, V.N., Barri, R.G., 2002. The influence of climatic variations on the thermoinsulation effect of snow cover and the temperature regime in the underlying soil. Kriosfera Zemli [Earth's Cryosphere], V (2), 83–91 (in Russian).

Vaganov, E.A., Shiyatov, S.G., Mazepa, V.S., 1996. Dendroclimatologic Studies in the Ural-Siberian Subarctic. Nauka, Novosibirsk, 246 pp. (in Russian).

Voeikov, A.I., 1957. Selected Works. Gidrometeoizdat, Leningrad, 259 pp. (in Russian).

URL: www.meteo.ru (last visited: 15.01.2020).

Received April 20, 2020
Revised version received January 15, 2021
Accepted January 25, 2021

Kriosfera Zemli, 2021, vol. XXV, No. 3, pp. 43–51

CALCULATION OF THE HEAT BALANCE COMPONENTS OF THE ALDEGONDA GLACIER (WESTERN SPITSBERGEN) DURING THE ABLATION PERIOD ACCORDING TO THE OBSERVATIONS OF 2019

U.V. Prokhorova[1], A.V. Terekhov[1], B.V. Ivanov[1,2], S.R. Verkulich[1]

[1] *Arctic and Antarctic Research Institute, Bering str. 38, Saint Petersburg, 199397, Russia; uliana@niersc.spb.ru*
[2] *Saint Petersburg State University, Universitetskaya emb. 7/9, Saint Petersburg, 199011, Russia*

Surface heat balance components have been calculated for the mountain valley Aldegonda Glacier (West Spitsbergen Island) based on a physical model with distributed parameters. The meteorological and actinometric observations on the glacier during the ablation period of 2019, a digital elevation model, as well as the remote sensing data needed for assessment of the reflective characteristics of the surface have been used as the input data. As a result of modeling, a spatial distribution of the values of the heat flux spent on melting with a resolution of one day has been obtained. According to the calculations, the average radiation balance for the period has been 89 W/m^2, which is approximately an order of magnitude higher than the heat inflow from turbulent flows (11 W/m^2). The obtained results have been verified using data on the glaciological mass balance monitoring based on ablation stakes. Predicted thickness of melted ice layer is in good agreement with the measurements on ablation stakes. The model systematically overestimates the magnitude of ice melt, but the glacier-average value remains within the confidence interval of the observed value.

Key words: *Svalbard, mountain glacier, glacier ablation, heat balance, physical modelling.*

INTRODUCTION

Over the last decades a steady warming is observed in the Svalbard Archipelago area. Rates of warming are higher than the world average due to the 'Arctic amplification' effect [*Nordli et al., 2014; Gjelten et al., 2016; Isaksen et al., 2016*]. The amount of atmospheric precipitation also tends to increase, but to a much lesser extent [*Førland et al., 2020*], as a result the winter snow accumulation on the archipelago glaciers is not able to compensate summer melting. Therefore, the total mass balance of the Svalbard Archipelago glaciers demonstrates a negative trend and, according to the latest estimate, is -7 ± 4 billion tons/year (excluding the icebergs calving from outlet glaciers) [*Schuler et al., 2020*]. In light of these facts, monitoring and forecasting the mass-balance characteristics of the archipelago glaciers are undoubtedly relevant scientific issues.

At present, the models based on empirical dependence of melting on air temperature are mainly used to assess the ablation of Arctic glaciers [*Krenke, Khodakov, 1966; Ohmura, 2001; Hock, 2003; Chernov et al., 2019*] and providing an integral estimate of ablation over the entire glacier, and the models based on the glacier heat balance equation [*Hock, 2005*]. The latter require a large number of spatially distributed parameters and are used less often due to the smaller number of actinometric observations carried out on glaciers, as well as because of the difficulties in assessing the turbulent flows and reflective characteristics of the surface. Nevertheless, heat-balance models for seasonal and interannual estimates of mass balance were applied, demonstrating good results for glaciers in northern Canada [*Wheler, Flowers, 2011*], in the Swiss Alps [*Klok, Oerlemans, 2002*], in the Caucasus [*Voloshina, 1966, 2001; Retz et al., 2011; Toropov et al., 2018*] and in the Western Spitsbergen [*Arnold et al., 2006; Svyaschennikov, Ragulina, 2010; Van Pelt, 2012; Karner et al., 2013*].

Heat-balance ablation models based on the thermodynamic approach allow to characterize quantitatively the contribution of a particular meteorological parameter to melting on the glacier surface and to reveal the mechanisms of interaction between elements of the climate system (cryosphere–atmosphere).

This paper presents the results of assessing the components of the heat balance of the Aldegonda Glacier surface, based on data from field experiments in August 2019. The heat balance has been calculated using daily time-step heat balance model. The spatial distribution of ablation obtained by simulation was compared with the data of glaciological measurements using ablation stakes for the same period. The Aldegonda Glacier is typical in size and altitude range of the West Spitsbergen central part, where glaciation is decreasing most rapidly, so obtained results can be extrapolated to the entire mountain-glacial system of the archipelago.

OBJECT OF STUDY

The mountain-valley Aldegonda Glacier (in Norwegian, *Aldegondabreen*) is located on the western coast of the Grønfjorden Bay, West Spitsbergen Island (Fig. 1). Almost the entire glacier surface is located in the altitude interval from about 120 to 450 m above sea level; its maximum elevation reaches 600 m. The glacier surface is rather homogeneous in terms of relief and is weakly dissected, mainly by se-

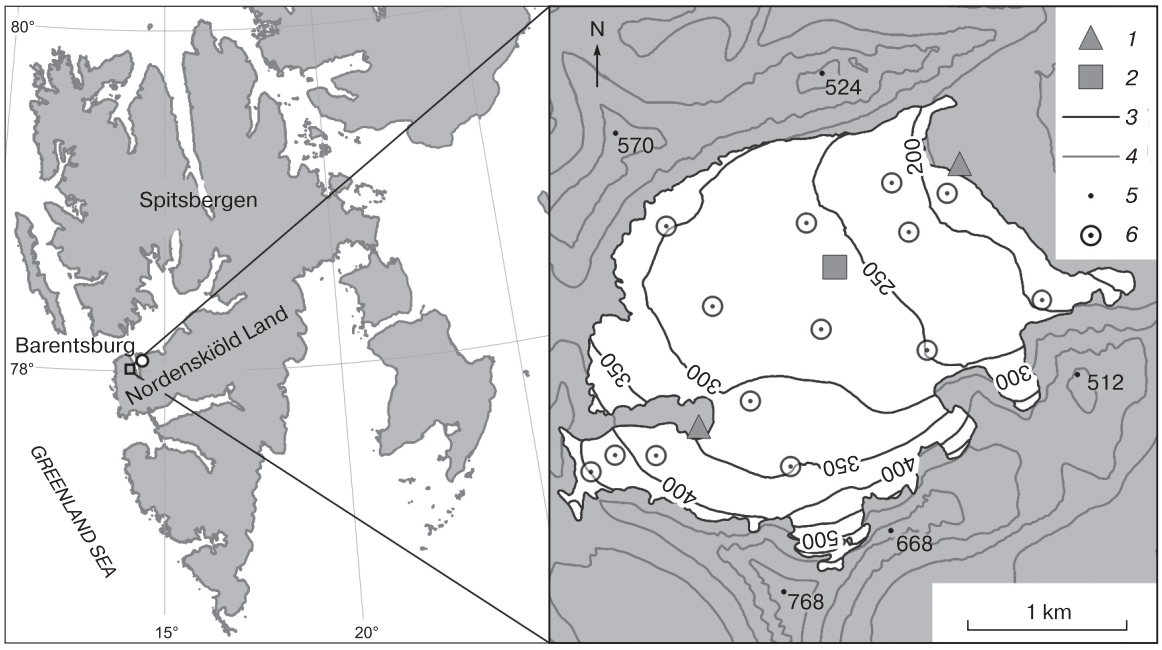

Fig. 1. Aldegonda Glacier and the observation network on it:

1 – permanent automatic weather stations; *2* – heat balance mast in August 2019; *3* – isohypses of the glacier surface; *4*, *5* – isohypses and altitudes of the surrounding topography (heights are given from sea level according to the ArcticDEM for 2013); *6* – ablation stakes.

veral longitudinal streams. There are no icefalls or sharp slope changes expect several crevasses in the very upper reaches. According to the authors' observations, there are no signs of intense ice movement. The small area of the glacier (5.54 ± 0.28 km^2 at the time of the study) and the proximity to Barentsburg settlement, where the logistics base of the Russian Scientific Center on the archipelago is located, predetermined its choice as an object of annual mass balance monitoring based on measurements using ablation stakes. The latter makes it possible to verify the simulation results presented in this work. The altitude range of the glacier is conventionally divided into fifty-meter intervals; fourteen ablation stakes are placed on the glacier surface so that at least one of them falls into each of the intervals (Fig. 1). In the largest by area altitudinal intervals, several stakes are installed in order to take into account possible uneven shading by rocky framing and uneven topography. That makes it possible to analyze not only the dependence of the melting layer thickness on altitude, but also the features of its spatial distribution.

According to the Roshydromet weather station located in Barentsburg, in recent decades the mean surface air temperature in the summer and early autumn (June–September) is positive. Around the same period, active melting of glaciers also occurs in the area of Grønfjorden Bay. On the Aldegonda glacier, the snow cover disappears almost completely by the third decade of July, the entire ice surface is below the snow line by the end of summer.

MATERIALS AND METHODS

The assessment of the heat balance components and the ablation values on the surface of the Aldegonda Glacier in August 2019 has been carried out on the basis of a physical model with spatially distributed parameters. The input meteorological data were obtained during field observations performed by the authors in the Russian Scientific Arctic Expedition on the Svalbard Archipelago (RAE-S), of the State Scientific Center of the Russian Federation 'Arctic and Antarctic Research Institute' (SSC RF 'AARI') in August 2019.

Field data and their interpolation. Heat balance observations were carried out in August in the absence of snow cover on the surface.

The bulk of the input data for modeling has been obtained using a heat balance mast (HBM) installed in the central part of the glacier, at an altitude of about 260 m above sea level for the period from 2 to 26 August 2019. The site had been considered as representative because the glacier surface is as homogeneous as possible, relatively flat and not shaded by slopes (Fig. 1). The HBM was equipped with actinometric sensors to assess the shortwave and longwave components of the surface radiation balance. Those

include: Yanishevsky pyranometers M-80, which record the total (incoming) and reflected solar radiation within the spectral range of 330–2800 nm, as well as APOGEE infrared radiometers, which measure the temperature (°C) of the glacier surface and air; on the basis of the latter, the downwelling longwave radiation of the atmosphere has been calculated. To assess the turbulent heat transfer between the glacier surface and the atmosphere, the HBM was equipped with the air temperature, atmospheric pressure, relative humidity and wind speed sensors from the HOBO automatic weather station kit. The data were recorded by LICOR-1400 and Campbell Scientific loggers each 5 minutes.

Extrapolation of data on air temperature, relative humidity and atmospheric pressure to the entire glacier surface was carried out using the ArcticDEM digital elevation model (DEM) for 2013, covering without gaps the entire glacier surface area and adjacent valley sides, as well as using the values of the vertical gradients of the indicated meteorological parameters. Vertical gradients were estimated using two HOBO automatic weather stations (Fig. 1) installed on moraine-covered rock outcrops in the lower part of the glacier and in its uppermost part. The weather stations were equipped with the temperature, relative humidity, wind speed and direction, atmospheric pressure sensors. The stations operate year-round, with hourly measurements.

One of the few meteorological parameters that is entered into the model as lumped, that is, non-distributed over the entire surface of the glacier, is the near-surface wind speed (modeling the wind field over the glacier surface is an independent and extremely difficult task). The temperature of the melting glacier surface, due to its insignificant changes (from –0.4 to +0.3 °C) according to measurements on the HBM (Fig. 2), was taken constant and equal to 0 °C. The partial pressure was also taken as a constant, equal to 6.11 hPa.

Model-based calculation of melting values. To estimate the values of melting, the equation of the surface heat balance is used. The heat losses on melting are estimated as the residual term of the equation:

$$A = Q(1 - \alpha) + I + P + LE + G, \qquad (1)$$

where: A is heat losses for melting; Q is incoming shortwave radiation; α is albedo of the underlying surface; I is longwave radiation balance; P and LE are vertical turbulent fluxes of sensible and latent heat; G is heat flux directed into the glacier. The simulation time step is equal to one day, so all the flows in the equation (1) are calculated as daily-average ones. The calculation of each of the components is described below.

The shortwave balance, represented in the equation (1) by the $Q(1 - \alpha)$ term, is determined by the flow of incoming shortwave radiation (Q) and the reflective characteristics of the surface (α). To spread the values of the incoming flow (Q) obtained at the HBM installation point to the entire glacier surface, it is necessary to take into account the effects of shading and morphometry (slope and exposure). The authors used the 'Potential Incoming Solar Radiation' algorithm, implemented in the GIS SAGA, which makes it possible to estimate the illuminance of the surface depending on astronomical factors (zenith and hour angle of the Sun, the time of sunrise and sunset) and topography itself (slope, exposure and shading by the surrounding terrain) [*Böhner, Antonić, 2009*]. A 15-minutes time-step was used. The Q value measured on the glacier surface was compared with that obtained at the corresponding point of the model, the scale factor was calculated, and on its basis the model field was corrected. The obtained spatial distribution of the average daily flux of shortwave radiation was used in further calculations.

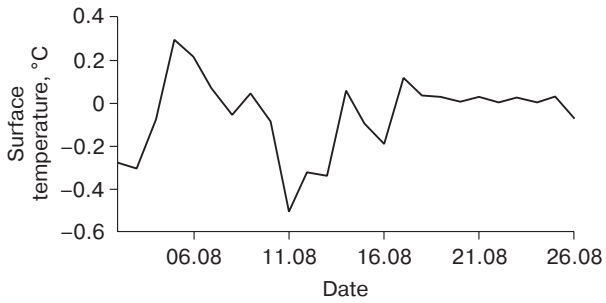

Fig. 2. Day-to-day variability of the surface temperature of the Aldegonda Glacier during 2019 observation period at the point of HBM installation.

The glacier surface albedo (α) is extremely heterogeneous in space and it can vary significantly over time depending on the presence or absence of fresh snow, as well as on the natural pollution of the glacier surface [*Ivanov, Svyashchennikov, 2015*]. Therefore, the point or route measurements on the glacier surface do not allow us to correctly assess these features. A logical solution is to estimate the spatial distribution of the albedo values using satellite data. For that purpose, cloudless images from Landsat-8 Level 2 collection with a spatial resolution of 30 m have been used. The set of images for each date contains data from seven spectral channels of the optical range, converted into the values of surface reflectance (surface spectral brightness coefficients, in Russian) by eliminating atmospheric effects and the difference in illuminance.

To obtain an integral value through the values of the surface spectral albedo in individual wave ranges, the formula proposed in [*Liang, 2001*] and adapted for the Landsat-8 satellite [*Naegeli et al., 2017*] had been used. The formula is a multiple linear regression

equation in which five of the seven Landsat-8 spectral bands are predictors:

$$\alpha = 0.356b_2 + 0.130b_4 + 0.373b_5 + \\ +0.085b_6 + 0.072b_7 - 0.0018, \quad (2)$$

where b_i is the value of surface reflectance in the i-th spectral channel of Landsat-8. It has been revealed in [*Naegeli et al., 2019*] that such a calculation allows to obtain reliable value of mountain-glacier surface albedo. The integral albedo values for the periods between imagery acquisition were obtained by linear interpolation of the images closest in time.

The longwave budget (I) or effective radiation of the earth's surface – the difference between the upward and downward longwave radiation – was calculated using the method described in [*König-Langlo, Augsteine, 1994*]. In accordance with that approach, the longwave budget of the underlying surface is:

$$I = \varepsilon\sigma T_s^4 - \varepsilon_a(n,T,e)\sigma T^4, \quad (3)$$

where T_s is surface temperature (K); ε – radiant emissivity of the surface, taken for ice equal to 0.98; σ is the Stefan-Boltzmann constant equal to $5.669 \cdot 10^{-8}$ W/(m^2·K^4).

However, since during the melting period the glacier surface temperature in the used model is 0 °C according to the observation data (Fig. 2), the upwelling radiation (the first term in the equation (3)) has assumed to be constant and equal to 316 W/m^2.

The second term in the equation (3) is the atmospheric downwelling radiation, where ε_a is the radiant emissivity of the atmosphere, which is a function of the cloud cover (n), air temperature (T), and water-vapor pressure (e) at a 2 m height. A comprehensive review of existing approaches to assessing the atmosphere radiant emissivity is given in [*König-Langlo, Augsteine, 1994*]. We used an empirical relationship adapted by the authors to the conditions of Svalbard Archipelago:

$$\varepsilon_a = a_k + b_k n,$$

where n is the total cloud cover (in unit fractions) according to visual observations; a_k and b_k are empirical coefficients ($a_k = 0.765$, $b_k = 0.22$). To interpolate the values over the entire glacier surface, the vertical air temperature gradient was also taken into account, which was calculated using the AMS data recorded in the upper and lower parts of the glacier (Fig. 1). The upper AMS is installed at a small moraine, and the lower AMS is located in close proximity to the glacier, so there is every reason to assume that the measured temperature gradient is the same as that above the ice.

To calculate the turbulent fluxes of sensible (P) and latent (LE) heat, the method described in [*Munro, 1990*], based on the Monin–Obukhov semi-empirical theory of turbulence, was used. That approach has been successfully applied to simulate the melting of mountain glaciers, and the results are presented in a number of publications [*Hock, 2005; Wheler, Flowers, 2011*]. To estimate the P and LE values, aerodynamic formulas are used, which include the wind speed, temperature and relative humidity of air values at the same height above the surface (z) and the values of meteorological characteristics on the surface (s):

$$P = C_H c_p \rho_a u_z (T_z - T_s),$$

$$LE = C_E L_v \rho_a u_z \left(\frac{0.622}{p}\right)(e_z - e_s),$$

where C_H and C_E are the coefficients of turbulent heat transfer; ρ_a is the air density calculated on the basis of its temperature and pressure; $c_p = 1010$ J/(kg·K) is the air specific heat capacity; $L_v = 2.514 \cdot 10^6$ J/kg is the latent heat of vaporization. The wind speed (u_z), the air temperature (T_z) and the pressure (p) have been measured at a height of $z = 1.6$ m. T_s and e_s are correspondingly the temperatures of the melting surface and the water-vapor pressure near it. The partial pressure of water vapor at height of z is calculated on the base of measured relative humidity.

Turbulent heat transfer coefficients are calculated by the following formulas [*Hock, Holmgren, 1996*]:

$$C_{H,E} = \\ = \frac{k^2}{\left[\ln(z/z_M) - \Psi_M(z/L)\right]\left[\ln(z/z_{H,E}) - \Psi_{H,E}(z/L)\right]}, \quad (4)$$

where $k = 0.4$ is Karman constant; z_M and $z_{H,E}$ are the surface roughness for wind, heat and water vapor; Ψ_M, and $\Psi_{H,E}$ are universal functions; L is the Monin–Obukhov parameter. The roughness values are given by the authors as $z_M = 10$ mm, $z_{H,E} = z_M/100$. These values have been chosen by the authors based on a review of similar calculations performed for the surface conditions of other glaciers [*Wheler, Flowers, 2011*].

The Ψ_M and $\Psi_{H,E}$ function values have been calculated in accordance with the work [*Beljaars, Holtslag, 1991*] and characterize the conditions of stable stratification of near-surface air layer prevailing over the glacier surface in the summer season:

$$-\Psi_M = \frac{az}{L} + b\left(\frac{z}{L} - \frac{c}{d}\right)\exp\left(-d\frac{z}{L}\right) + \frac{bc}{d},$$

$$-\Psi_{H,E} = \left(1 + \frac{2az}{3L}\right)^{1.5} + b\left(\frac{z}{L} - \frac{c}{d}\right)\exp\left(-d\frac{z}{L}\right) + \frac{bc}{d} - 1,$$

where a, b, c, d are empirical coefficients equal to 0.7, 0.75, 5.0, 0.35, respectively. Wheler and Flowers [*2011*] have demonstrated that these values of the universality functions give an acceptable result in ablation simulations.

Calculations using the formulas above require the value of the Monin–Obukhov parameter (L),

which has been determined using the following expressions:

$$L = \frac{\rho c_p u_*^3 T_z}{kgP}; \quad (5)$$

$$u_* = \frac{ku_z}{\ln(z/z_M) - \Psi_M}, \quad (6)$$

where u_* is dynamic velocity.

Thus, the calculation of the Monin–Obukhov parameter requires a fixed value of the unknown sensible heat flux. In such cases, an iterative procedure is used. At the first step, the ratio z/L (stability function) is assumed to be zero, which simplifies the formula (4). Based on that, an approximate value of the sensible heat flux is calculated, which is then substituted into the formulas (5), (6) to obtain the value of the Monin–Obukhov parameter. At the next iteration, the L value is substituted into the formula (4), and the calculations are being repeated until the calculated value of P flux differs from the value obtained at the previous step by 0.1 W/m^2.

The work [*Svyaschennikov, Ragulina, 2010*] analyzes the isothermality found in the upper layer of the Aldegonda Glacier during the ablation period; its thickness is 40–50 cm. The isothermal layer temperature corresponds to the melting point of ice. That makes it possible to determine the thickness of the ice layer melted during a day (in units of water equivalent) based on the heat flux spent on melting:

$$A_i = \frac{N_i \rho_i \Delta h_i}{\Delta t_i},$$

where A_i is the heat flux spent on melting, W/m^2; N_i is specific heat of ice melting, taken as $3.33 \cdot 10^5$ J/kg; ρ_i is ice density, taken equal to 916.7 kg/m^3; Δh_i is thickness of melted ice, mm w.e.; Δt_i is time interval, s.

Glaciological data. To verify modeling results, surface melting field observations data obtained on fourteen ablation stakes [*The study..., 2019*] evenly distributed over the glacier surface in almost all of its altitude range (Fig. 1), have been used. The surface melting values averaged over the glacier area have been calculated based on the ablation altitude profile obtained by linear approximation of melting values on individual stakes. The average values in fifty-meter altitude intervals are multiplied by the fraction of that altitudinal zone area in the total glacier area and summed up.

To calculate the error of ice ablation averaged over the glacier, we used the technique described in detail in the well-known work [*Klug et al., 2018*]. It includes two criteria: the standard deviation of the linear vertical dependence of ablation relative to field measurements, as well as the accuracy and representativeness of readings on the stakes. The error in ice density estimation is not taken into account.

RESULTS AND DISCUSSION

Quantitative evaluation of the heat balance and ice ablation components. As follows from Fig. 3, *a*, *b*, the average daily positive values of the surface heat balance components (shortwave budget (*2*) and turbulent heat transfer (*4*)) tend to decrease in their absolute values, which is associated with a decrease in the daylight hours duration and air temperature. The longwave budget of the surface does not have such a tendency (Fig. 3, *b*, *3*), since it is largely determined by the cloud cover value. Changes in the absolute value of the energy spent on ice melting (Fig. 3, *a*, *1*) generally repeat the fluctuations in the value of the shortwave budget of the surface, which clearly demonstrates its decisive role in melting on the glacier surface.

The spatial distribution of the radiation balance components (monthly mean values) during the period of maximum ablation is shown in Fig. 4. The shortwave balance, which is determined by the magnitude of incoming shortwave radiation (Fig. 4, *a*) and the albedo (Fig. 4, *b*), indicates that the greatest influx of solar radiation falls on to the northeastern part of the glacier. That is due to the azimuth and steepness of the glacier surface, as well as the greater, compared to other areas, shading of its southern part, and the minimum albedo at the glacier tongue and along the entire northern flank.

The longwave budget of the glacier surface during the ablation period is entirely determined by the atmospheric counter-radiation magnitude, since the longwave radiation from the surface directed upward

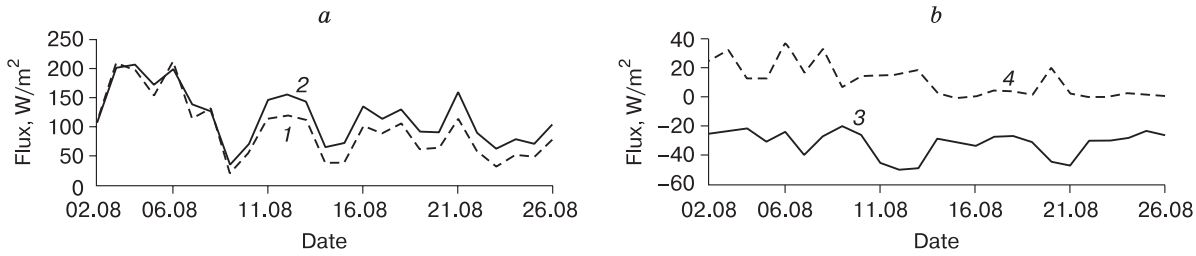

Fig. 3. Day-to-day variability of the heat balance components for the period from August 2 to 26, 2019.

a: heat consumption for ice melting (*1*), shortwave balance (*2*); *b*: longwave balance (*3*), turbulent heat exchange between the atmosphere and the underlying surface (*4*).

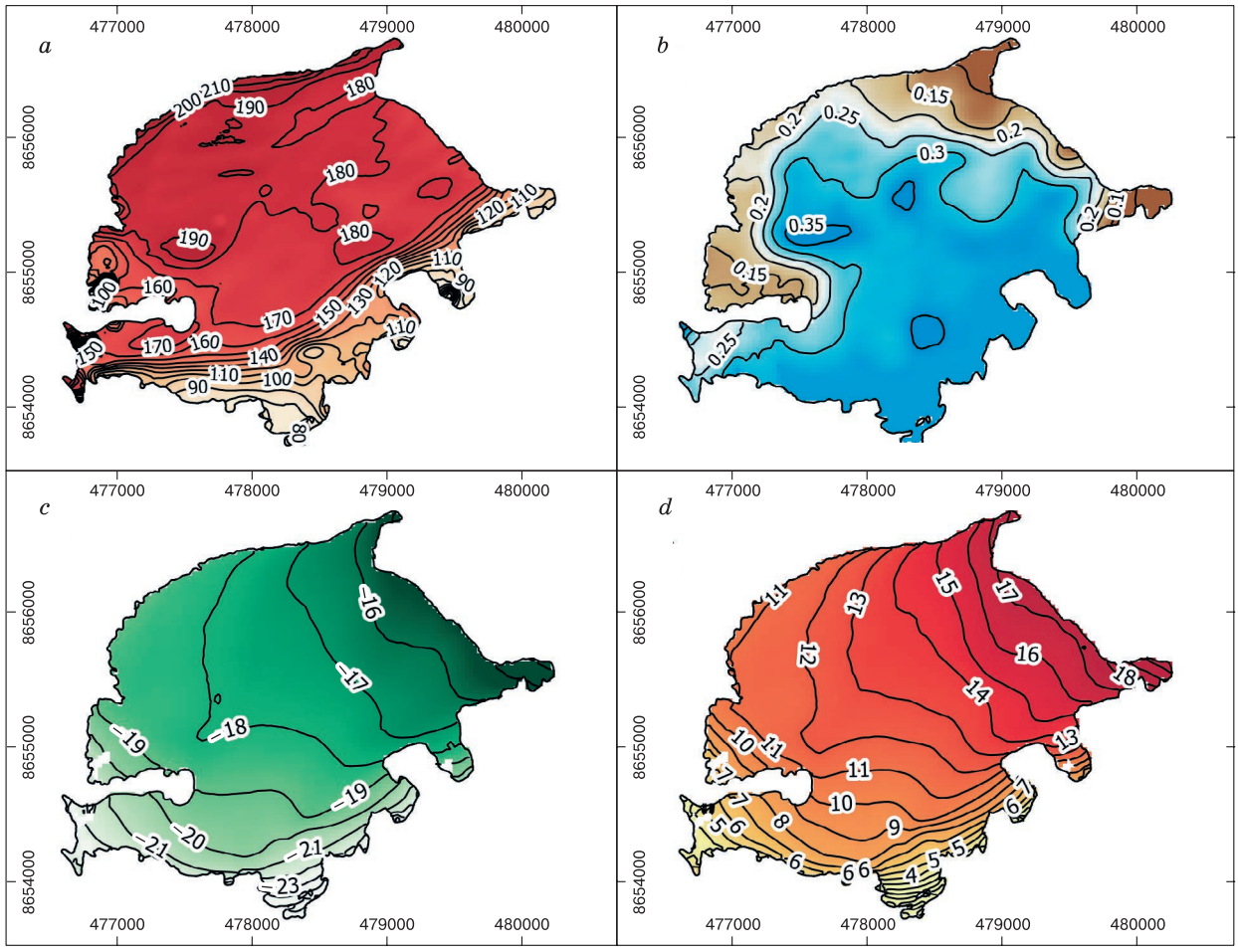

Fig. 4. Average monthly values of the heat balance components of the Aldegonda Glacier surface in August 2019.

a – incoming shortwave radiation (W/m^2); *b* – albedo of the underlying surface, in unit fractions; *c* – longwave balance of the surface (W/m^2); *d* – turbulent heat exchange between the underlying surface and the atmosphere (W/m^2). Coordinates are given in the UTM projection, Zone 33 on the WGS84 ellipsoid.

is assumed to be unchanged due to the constancy of measured melting-ice temperature. It follows from Fig. 4, *c* that the atmospheric counter-radiation decreases with the decreasing of the glacier surface altitude.

The maximum and minimum values of melting according to model calculations were correspondingly 1000–1200 mm w.e. per month, and 200–300 mm w.e. per month. According to our calculations, the main factor determining the spatial pattern of melting is the shortwave radiation balance of the glacier surface, since it is most variable in space. That is why the spatial distribution of surface melting (Fig. 5, *a*) largely repeats the spatial pattern of the albedo and incoming solar radiation distribution (Fig. 4, *a*, *b*).

There are several ways to assess the quantitative ratio of the heat balance components, depending on which value is taken as 100 %. The first method (used, for example, in [*Ohmura, 2001*]) is to find the share of each positive balance components of their sum. The ratio of components calculated in that way is shown in Table 1. In another approach [*Toropov et al., 2018*], the total radiation balance is considered as a separate component, and turbulent fluxes are considered as the other two. In comparison with the previous method, the share of turbulent fluxes greatly increases, since the radiation balance contains a negative component, – longwave radiation from the surface. The ratio of components calculated in this way is shown in Table 2.

In any case, turbulent heat transfer (Fig. 4, *d*, Table 1, 2) makes the smallest contribution, estimated at 3 % or 11 %, depending on the calculation method, which is almost an order of magnitude less than the radiation balance contribution. N.S. Arnold with

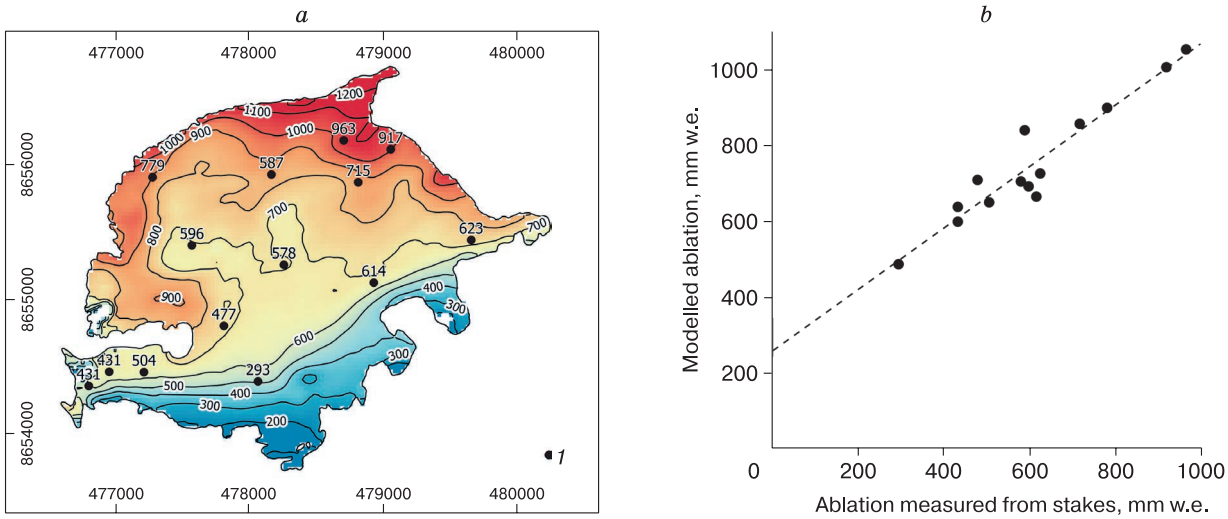

Fig. 5. Comparison of values of melting on the Aldegonda Glacier surface in August 2019 according to model and field data:

a – spatial distribution of melting (mm w.e.); *1* – ablation values measured from stakes (coordinates are given in the UTM projection zone 33 on the WGS84 ellipsoid); *b* – deviations of the simulation results from the actually measured values.

coauthors [*Arnold et al., 2006*] came to a similar conclusion for the Midtre Lovénbreen Glacier, located near Ny-Alesund (about one hundred kilometers to the north of Barentsburg) and comparable in size and altitude range to the Aldegonda Glacier.

Model verification. To assess the accuracy of the used model of the glacier surface heat balance, let us compare simulated and measured values of melting at the points of installation of the ablation stakes. In addition, we will calculate the average melting over the glacier surface, since this indicator is one of the main characteristics of the mass balance.

Figure 5, *b* is a scatter plot illustrating the relationship between the simulated and measured melting values for ablation stakes. The linear regression equation has the form of $y = 0.81x + 257.97$, the coefficients are significant ($p = 0.05$). The correlation coefficient is 0.95, the determination coefficient (R^2) is 0.90. On average, the ablation value at the glacier surface, obtained on the basis of the heat balance model, is 698 mm w.e./month, on stakes it is 615 ± 150 mm w.e./month. Thus, the model estimates of the average melting over the entire glacier surface fall within the confidence interval of the average value calculated based on field observations.

Possible sources of errors in model calculations. The absolute values of the differences between the calculated and measured values of melting, according to the authors, are not informative enough for analyzing the sources of errors, since both values are multiplied by a conversion factor equal to ice to water density ratio for conversion to water equivalent units. Here the ice was taken as the maximum possible (916.7 kg/m^3), although, in general the ice on the glacier surface is less dense due to the inclusion of air bubbles. Using a different ice density value will proportionally reduce those differences. Therefore, the authors tried to estimate the errors of the model in the heat flux values, but not in the melted layer thickness, thereby excluding the ice density as an additional factor introducing the error. Based on measured ablation values, the heat amount necessary to ensure that melting bas been calculated (Fig. 6).

It follows from Fig. 6, *a* that, despite the high value of correlation coefficient, the model systematically overestimates the heat losses for ice melting relative to those measured using ablation stakes, and that difference changes with glacier surface altitude (Fig. 6, *b*). In our case, the difference increases from about 10 to 30 W/m^2. Several factors can explain

Table 1. **The ratio of the heat balance components of the Aldegonda Glacier, calculated in accordance with [*Ohmura et al., 2001*]**

Absorbed shortwave radiation		Downwelling longwave radiation		The sum of turbulent fluxes	
W/m^2	%	W/m^2	%	W/m^2	%
121	29	278	68	11	3

Table 2. **The ratio of the heat balance components of the Aldegonda Glacier, calculated in accordance with [*Toropov et al., 2018*]**

Radiation balance		Sensible heat flux		Latent heat flux	
W/m^2	%	W/m^2	%	W/m^2	%
89	89	10	10	1	1

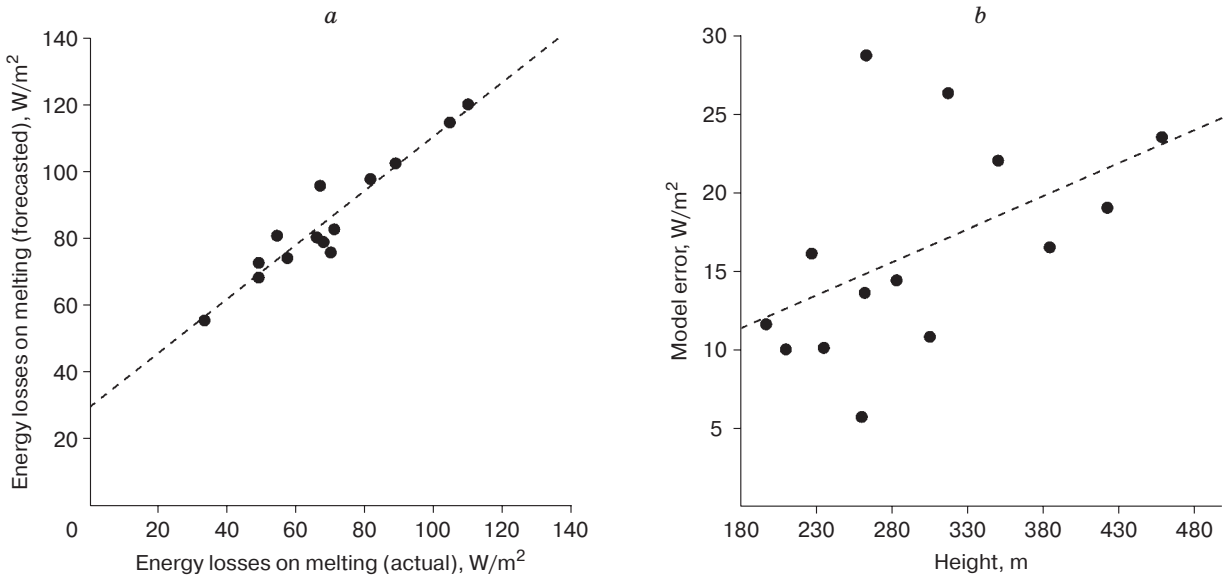

Fig. 6. Model error in the units of heat flux:

a – deviations of simulation results from measured values; *b* – their altitude dependence.

that. Since the largest positive part of the heat balance components is the incoming shortwave solar radiation, the model becomes most sensitive to errors in estimating this component. In particular, the underestimated albedo can introduce a significant part of the error. Because of the peculiarities of the glacier's exposure and the configuration of surrounding terrain, the shaded area at this season increases with altitude. It is known [*Liang, 2001*] that the surface reflectivity values obtained from satellite data can be underestimated in areas with low illuminance. Nevertheless, it is not entirely correct to associate model errors only with inaccuracy in determining the albedo. With the value of incoming shortwave radiation average for the observation period equal to about 250 W/m^2, the systematic error in calculating the albedo should be, averaged over the glacier surface, at least 10 %, which is unrealistically high.

The next possible source of errors is the structure of the surface ice layer which is not taken into account in a model. First, the heat flux from the isothermal layer into the underlying glacier layers is not taken into account due to its thermal conductivity. However, the magnitude of such a flux during the period of maximum ablation is no more than –5 W/m^2 for a mountain glacier located in similar climatic conditions [*Hock, Holmgren, 1996*], but can amount only to some part of model error. Second, the model does not take into account the penetration of shortwave radiation into the ice (into the radiation active layer). A significant part of solar energy, primarily in the ultraviolet and near infrared parts of the spectrum, is absorbed directly below the surface of the glacier, since the penetration of energy into the stratum rapidly decreases exponentially with depth in accordance with the Bouguer–Lambert law. However, some part of the shortwave radiation penetrates below the isothermal layer, which introduces a systematic positive error into the model, revealed based on field data.

Thus, the authors associate the further development of the heat balance model of glacier melting with a more detailed description (parameterization) of the processes associated with heat transfer deep into the glacier, and with a more realistic description of surface ice layer density and structure.

CONCLUSION

The modeled estimates of the spatial distribution of ablation values were compared with the results of field measurements using ablation stakes for the same period. The correlation coefficient was 0.95, and the determination coefficient (R^2) was 0.90. The magnitude of the glacier surface ablation, obtained based on the heat balance model, averaged 698 mm w.e./month. A similar value obtained from the stakes is 615 ± 150 mm w.e./month. Thus, the model estimates do not go beyond the confidence interval of estimates obtained based on field observations.

According to the authors' calculations, the main factor determining melting is the radiation balance of the glacier surface, and the turbulent heat transfer makes an order of magnitude smaller contribution to melting (3 % to 11 %, depending on the method of estimating the component ratio). A similar result has been obtained in a number of other works [*Arnold et al., 2006; Van As, 2011; Jakobs et al., 2019*]. The pat-

tern of melting spatial distribution largely repeats that of the albedo and incoming solar radiation distribution, since it is those values that have the greatest variability on the glacier surface.

Acknowledgments. *The authors are grateful to the participants and the leadership of the "Spitsbergen-2019" RAE-S expedition for help in organizing and performing seasonal field work.*

The work was performed within the framework of theme 5.1.4 of the R&D plan of the Roshydromet.

References

Arnold, N.S., Rees, W.G., Hodson, A.J., Kohler, J., 2006. Topographic controls on the surface energy balance of a high Arctic valley glacier. J. Geophys. Res.: Earth Surface, vol. 111, No. F2.

Beljaars, A.C.M., Holtslag, A.A.M., 1991. Flux parameterization over land surfaces for atmospheric models. J. Appl. Meteor. 30, 327–341.

Böhner, J., Antonić O., 2009. Land surface parameters specific to topo-climatology. Developm. Soil Sciences 33, 195–226.

Chernov, R.A., Kudikov, A.V., Vshivtseva, T.V., Osokin, N.I., 2019. Estimation of the surface ablation and mass balance of Eustre Grønfjordbreen (Spitsbergen). Led i Sneg [Ice and Snow], 59 (1), 59–66 (in Russian).

Førland, E.J., Isaksen, K., Lutz, J., et al., 2020. Measured and modeled historical precipitation trends for Svalbard. J. Hydrometeor. 21, 1279–1296.

Gjelten, H.M., Nordli, Ø., Isaksen, K., et al., 2016. Air temperature variations and gradients along the coast and fjords of western Spitsbergen. Polar Research 35, p. 29878.

Hock, R., 2003. Temperature index melt modelling in mountain areas. J. Hydrol. 282, 104–115.

Hock, R., 2005. Glacier melt: a review of processes and their modelling. Progress in Phys. Geography 29 (3), 362–391.

Hock, R., Holmgren, B., 1996. Some aspects of energy balance and ablation of Storglaciaren, northern Sweden. Geografiska Ann.: Ser A, Physical Geography 78 (2–3), 121–131.

Isaksen, K., Nordli, Ø., Førland, E.J., et al., 2016. Recent warming on Spitsbergen – Influence of atmospheric circulation and sea ice cover. J. Geophys. Res. Atmos. 121 (11), 913–931.

Ivanov, B.V., Svyashchennikov, P.N., 2015. Albedo of the snow-glacier surface of Svalbard. Izvestiya, Atmospheric and Oceanic Phys. 51 (9), 943–948.

Jakobs, C.L., Reijmer, C.H., Kuipers Munneke, P., et al., 2019. Quantifying the snowmelt-albedo feedback at Neumayer Station, East Antarctica. The Cryosphere 13 (5), 1473–1485.

Karner, F., Obleitner, F., Krismer, T., et al., 2013. A decade of energy and mass balance investigations on the glacier Kongsvegen, Svalbard. J. Geophys. Res.: Atmospheres 118 (10), 3986–4000.

Klok, E., Oerlemans, J., 2002. Model study of the spatial distribution of the energy and mass balance of Morteratschgletscher, Switzerland. J. Glaciol. 48 (163), 505–518.

Klug, C., Bollmann, E., Galos, S.P., et al., 2018. Geodetic reanalysis of annual glaciological mass balances (2001–2011) of Hintereisferner, Austria. The Cryosphere, 12, 833–849.

König-Langlo, G., Augsteine, E., 1994. Parameterization of the downward long-wave radiation at the Earth's surface in polar regions. Meteorologische zeitschrift 3 (6), 343–347.

Krenke, A.N., Khodakov, V.G., 1966. On the connection between surface melting of glaciers and air temperature. Materialy Glyatsiologicheskikh Issledovaniy [Data of Glaciological Studies], No. 12, 153–164 (in Russian).

Liang, S., 2001. Narrowband to broadband conversions of land surface albedo I: Algorithms. Remote Sens. Environ. 76, 213–238.

Munro, D.S., 1990. Comparisons of melt energy computations and ablatometer measurements on melting ice and snow. Arct. Alp. Res. 22 (2), 153–162.

Naegeli, K., Damm, A., Huss, M., et al., 2017. Cross-Comparison of albedo products for glacier surfaces derived from airborne and satellite (Sentinel-2 and Landsat 8) optical data. Remote Sens. 9 (2), article 110.

Naegeli, K., Huss, M., Hoelzle, M., 2019. Change detection of bare-ice albedo in the Swiss Alps. The Cryosphere 13, 397–412.

Nordli, Ø., Przybylak, R., Ogilvie, A.E.G., Isaksen, K., 2014. Long-term temperature trends and variability on Spitsbergen: the extended Svalbard Airport temperature series, 1898–2012. Polar Res. 33 (1), p. 21349.

Ohmura, A., 2001. Physical basis for the temperature-based melt-index method. J. Appl. Meteorol. 40, 753–761.

Rets, E.P., Frolova, N.L., Popovnin, V.V., 2011. Modelling of surface ablation of a mountain glacier. Led i Sneg [Ice and Snow], 51 (4), 24–31 (in Russian).

Schuler, T.V., Kohler, J., Elagina, N., et al., 2020. Reconciling Svalbard glacier mass balance. Frontiers in Earth Sci., vol. 8, article 156.

Svyaschennikov, P.N., Ragulina, G.A., 2010. Estimation of surface ablation of Aldegonda glacier, Svalbard archipelago. In: Nature of shelves and archipelagos of the European Arctic. Comprehensive studies of Svalbard nature. GEOS, Moscow, pp. 469–474 (in Russian).

The study of present-day state and the analysis of past changes of characteristics of Svalbard archipelago environment: Scientific report (final report), 2019. In: Scientific Report. Arctic and Antarctic Research Institute Repository ID No. P-6596. Saint Petersburg, 247 pp. (in Russian).

Toropov, P.A., Shestakova, A.A., Smirnov, A.M., Popovnin, V.V., 2018. Evaluation of the components of the heat balance of the Djankuat glacier (Central Caucasus) during the period of ablation in 2007–2015. Earth's Cryosphere XXII (4), 37–48.

Van As, D., 2011. Warming, glacier melt and surface energy budget from weather station observations in the Melville Bay region of northwest Greenland. J. Glaciol. 57 (202), 208–220.

Van Pelt, W.J.J., Oerlemans, J., Reijmer, C.H., et al., 2012. Simulating melt, runoff and refreezing on Nordenskiöldbreen, Svalbard, using a coupled snow and energy balance model. The Cryosphere 6, 641–659.

Voloshina, A.P., 1966. Heat balance of a surface of high-mountain glaciers during summer period: case study of Elbrus. Nauka, Moscow, 150 pp. (in Russian).

Voloshina, A.P., 2001. Meteorology of the mountain glaciers. Materialy Glyatsiologicheskikh Issledovaniy [Data of Glaciological Studies], No. 92, 3–138 (in Russian).

Wheler, B.A., Flowers, G.E., 2011. Glacier subsurface heat-flux characterizations for energy-balance modelling in the Donjek Range, southwest Yukon, Canada. J. Glaciol. 57 (201), 121–133.

Received September 22, 2020
Revised version received January 17, 2021
Accepted January 19, 2021

EARTH'S CRYOSPHERE
SCIENTIFIC JOURNAL

Kriosfera Zemli, 2021, vol. XXV, No. 3, pp. 52–53

CHRONICLE

MARINA OSKAROVNA LEIBMAN
(*on the 70th anniversary*)

A.I. Kizyakov[1], I.D. Streletskaya[1], A.V. Khomutov[2]

[1] *Lomonosov Moscow State University, Faculty of Geography, Department of Cryolithology and Glaciology, Leninskie Gory 1, Moscow, 119991, Russia; akizyakov@mail.ru*
[2] *Earth Cryosphere Institute, Tyumen Scientific Centre SB RAS, Malygina str. 86, Tyumen, 625026, Russia; akhomutov@gmail.com*

On the 22 of June, 2021 famous scientist, Doctor of Science in geology and mineralogy, M.O. Leibman has celebrated her 70th anniversary. Marina Oskarovna combines a fundamental scientific approach with active field research, managing to cover a wide range of tasks for the study of permafrost and cryogenic processes. She has become an attentive scientific consultant and scientific advisor for many young researchers.

Key words: *cryogenic processes, permafrost, ground ice.*

On June 22, 2021, Marina Oskarovna Leibman, Doctor of Geological and Mineralogical Sciences (post-doctorate degree in Russia), leading researcher of the Earth Cryosphere Institute (ECI), Tyumen Scientific Center SB RAS, turns 70.

Marina Leibman was born in 1951 in Moscow. After graduating from school in 1968, she entered the Faculty of Geology, Lomonosov Moscow State University. While studying at the Department of Permafrost Science, Marina Oskarovna became interested in harsh nature of the North, participated in an expedition to the Yana River.

After graduating from university in 1973, M.O. Leibman worked at PNIIIS (Industrial and Research Institute for Engineering Surveys in Construction). At that time, she studied permafrost in Eastern Siberia. In 1983 based on the collected field data Marina defended her Ph.D. thesis "Ground temperature formation regularities in mountainous countries (on the example of the BAM test site)" under the scientific supervision of Dr. S.M. Fotiev. Further, the area of Marina's research expanded to the north of Western Siberia, where she participated in field work along the projected Obskaya-Bovanenkovo railway on the Yamal Peninsula. In this region, Marina Leibman is actively continuing her research at the present time.

Since 1994, Marina Oskarovna worked at the Federal Center for Geoecological Systems of the Ministry of Natural Resources of Russia. From 1996 to the present, she has been working at the ECI, where she now holds the position of leading researcher.

In 2005 Marina Leibman defended her doctoral dissertation "Cryogenic slope processes and their geoecological consequences under the conditions of tabular ground ice development", summarizing sig-

nificant experience accumulated in the study of cryogenic relief-forming processes in the permafrost zone. Marina Oskarovna is a member of the dissertation councils of the ECI and the Faculty of Geography of the Lomonosov Moscow State University.

Marina Oskarovna's scientific interests are extremely broad. Among them the state of permafrost in the north of Western Siberia, the conditions and mechanisms for the development of cryogenic slope processes, thermal erosion, the gas emission craters formation conditions; dynamics of the seasonally thawing layer; geochemical and isotopic characteristics of ground ice. Every year she participates in expeditions to various regions of the permafrost zone.

M.O. Leibman is the founder and scientific advisor of the Vaskiny Dachi geocryological research station at Central Yamal. The station was founded in 1988 and since then a comprehensive study of the Arctic geosystems has been conducted there. Over the years, a wide range of research was performed – geocryological, cryolithological, geomorphological, geobotanical, landscape, hydrological, etc. Monitoring observations of active-layer thickness and permafrost temperature are carried out (currently in frames international programs Circumpolar Active Layer Monitoring – CALM and Thermal State of Permafrost – TSP). The studies of thermal erosion, cryogenic slope processes, frost heave, development of thermocirques, studies of the physical and mechanical properties of permafrost, geochemical characteristics of the seasonally thawed layer are conducted. Thanks to the energy of Marina Oskarovna and development of her scientific ideas, publications and scientific reports, this research station has become widely known both among domestic and foreign colleagues. Marina Oskarovna supervises the work of graduate students who successfully defend their Ph.D. theses. For many years she has been working with students-cryolithologists, whom she takes with her to field practices, including the Vaskiny Dachi research station, and helps to master the skills of expeditionary studies of permafrost and cryogenic processes.

Results of Marina's research are published in over than 130 scientific papers, she is a co-author of two monographs, a participant in leading Russian and foreign conferences on permafrost-related topics.

Since the foundation of the "Earth's Cryosphere" journal (1997) M.O. Leibman actively participates in its work as an author and reviewer.

Marina Oskarovna sets an example of high professionalism, hard work, dedication, creative activity and adherence to principles in science and life. She is well known and respected scientist both in Russia and abroad.

Colleagues, students and friends sincerely congratulate Marina Oskarovna and wish her longevity, good health and new scientific achievements!

Received May 11, 2021